JOINT TRANSPORTATION
RESEARCH PROGRAM
INDIANA DEPARTMENT OF TRANSPORTATION
AND PURDUE UNIVERSITY

Evaluating Reserve Strength of Girder Bridges Due to Bridge Rail Load Shedding

Yao Wang, Mirela D. Tumbeva, Ashley P. Thrall

SPR-4311 • Report Number: FHWA/IN/JTRP-2021/08 • DOI: 10.5703/1288284317308

RECOMMENDED CITATION

Wang, Y., Tumbeva, M. D., & Thrall, A. P. (2021). *Evaluating reserve strength of girder bridges due to bridge rail load shedding* (Joint Transportation Research Program Publication No. FHWA/IN/JTRP-2021/08). West Lafayette, IN: Purdue University. https://doi.org/10.5703/1288284317308

AUTHORS

Yao Wang
Mirela D. Tumbeva
Graduate Students
Department of Civil & Environmental Engineering & Earth Sciences
University of Notre Dame

Ashley P. Thrall
Myron & Rosemary Noble Associate Professor of Structural Engineering
Department of Civil & Environmental Engineering & Earth Sciences
University of Notre Dame
(574) 631-2533
athrall@nd.edu
Corresponding Author

ACKNOWLEDGEMENTS

This work was supported by the Joint Transportation Research Program administered by the Indiana Department of Transportation (INDOT) and Purdue University. The support of Business Owner Stephanie Wagner, Project Advisor Prince Baah, and Study Advisory Committee Members Jose Ortiz, Nathaniel Pfeiffer, Randy Strain, and Tim Wells. The authors are grateful to INDOT maintenance and bridge inspection crews of Fort Wayne and Seymour Districts, as well as Tim Koster and Steve Fernandez of Superior Construction, for their support of the field monitoring. Graduate student Sara Cardona is gratefully acknowledged for her field work in monitoring the bridges. The authors are grateful to Brett Commander of BDI for training the research team and taking part in monitoring of Asset 020-20-07229. The authors also appreciate the assistance of Laboratory Technician Tina Mitchell in carrying out the field work for Asset 331-71-08732. Undergraduate students Claire Gasser and Camila Gonzalez Flores are also gratefully acknowledged for their contributions to the literature review. The authors greatly appreciate the guidance provided by Ted Zoli of HNTB Corporation. Research Assistant Rebecca Fitzmaurice is acknowledged for her contributions to formatting and editing the report. The contents of this report reflect the views of the authors, who are responsible for the facts and accuracy of the data presented herein, and do not necessarily reflect the official views or policies of the sponsoring organizations. These contents do not constitute a standard, specification, or regulation.

JOINT TRANSPORTATION RESEARCH PROGRAM

The Joint Transportation Research Program serves as a vehicle for INDOT collaboration with higher education institutions and industry in Indiana to facilitate innovation that results in continuous improvement in the planning, design, construction, operation, management and economic efficiency of the Indiana transportation infrastructure. https://engineering.purdue.edu/JTRP/index_html

Published reports of the Joint Transportation Research Program are available at http://docs.lib.purdue.edu/jtrp/.

NOTICE

TECHNICAL REPORT DOCUMENTATION PAGE

1. Report No. FHWA/IN/JTRP-2021/08	**2. Government Accession No.**	**3. Recipient's Catalog No.**
4. Title and Subtitle Evaluating Reserve Strength of Girder Bridges Due to Bridge Rail Load Shedding		**5. Report Date** February 2021
		6. Performing Organization Code
7. Author(s) Yao Wang, Mirela D. Tumbeva, and Ashley P. Thrall		**8. Performing Organization Report No.** FHWA/IN/JTRP-2021/08
9. Performing Organization Name and Address Joint Transportation Research Program Hall for Discovery and Learning Research (DLR), Suite 204 207 S. Martin Jischke Drive West Lafayette, IN 47907		**10. Work Unit No.**
		11. Contract or Grant No. SPR-4311
12. Sponsoring Agency Name and Address Indiana Department of Transportation (SPR) State Office Building 100 North Senate Avenue Indianapolis, IN 46204		**13. Type of Report and Period Covered** Final Report
		14. Sponsoring Agency Code

15. Supplementary Notes
Conducted in cooperation with the U.S. Department of Transportation, Federal Highway Administration.

16. Abstract
This research experimentally and numerically evaluated the reserve strength of girder bridges due to bridge rail load shedding. The investigation included: (1) performing non-destructive field testing on two steel girder bridges and one prestressed concrete girder bridge, (2) developing validated finite element numerical models, and (3) performing parametric numerical investigations using the validated numerical modeling approach. Measured data indicated that intact, integral, reinforced concrete rails participate in carrying live load. Research results culminated in recommendations to evaluate the reserve strength of girder bridges due to the participation of the rail, as well as recommendations for bridge inspectors for evaluating steel girder bridges subjected to vehicular collision.

17. Key Words bridge railings, girder bridges, structural health monitoring, strain gauges, digital image correlation, finite element method	**18. Distribution Statement** No restrictions. This document is available through the National Technical Information Service, Springfield, VA 22161.

19. Security Classif. (of this report) Unclassified	**20. Security Classif. (of this page)** Unclassified	**21. No. of Pages** 71 including appendices	**22. Price**

EXECUTIVE SUMMARY

Introduction

The aim of this research was to evaluate the participation of intact, integral, reinforced concrete bridge rails, experimentally and numerically, in carrying live load. Steel and prestressed concrete multi-girder bridges are designed conservatively, resulting in reserve strength. One source of this reserve strength, which is not permitted to be considered when evaluating strength and extreme event limit states per current bridge design code, is load shedding to bridge rails. The specific research objectives of this project were to investigate this reserve strength through (1) performing non-destructive field testing, (2) developing validated finite element numerical models, and (3) performing parametric numerical investigations using the validated numerical modeling approach. The focus was on multi-girder steel and prestressed concrete bridges with intact, integral, reinforced concrete rail (specifically Indiana Department of Transportation (INDOT) FC, FT, PS-1, and PS-2 rail types (INDOT, 2020)). One steel girder bridge (two-span continuous) and one prestressed concrete girder bridge (six-span continuous), as well as a steel girder bridge damaged by vehicular collision (two-span continuous) were monitored. Research results culminated in recommendations to evaluate the reserve strength of girder bridges due to the participation of the rail, as well as recommendations for bridge inspectors for evaluating steel girder bridges subjected to vehicular collision.

Findings

The main research findings are as follows.

Findings from Measured Data

1. Generally, both FC and PS-1 rail types participate in carrying live load.
2. Neutral axis locations indicate that full composite behavior can be achieved between the girder, deck, and rail.
3. Strains in an exterior girder increase when there is a gap in the rail in the positive moment region (where positive moment refers to compression in the top of a section and tension in the bottom).
4. Near abutments, full composite behavior between the girder and deck may not yet developed.
5. When an exterior girder is subjected to Category T damage (i.e., torsion about the longitudinal direction (Avent, 2008)) from a vehicular collision, the shear connection between the deck and girder may be damaged. Live load amplification factors may also be higher due to the damage.

Findings from Numerical Modeling of Monitored Bridges

1. FE numerical models, with the following features, are able to accurately capture rail participation for steel and prestressed concrete girder bridges for which there are no damaged girders.
    a. Components modeled with the following element types:
        i. Rail: Thick shell elements, with changing thickness based on the geometry
        ii. Deck: Thick shell elements
        iii. Girders: Frame elements representing the top and bottom flanges, thin shell elements representing the webs for steel girders, thick shell elements representing the webs for prestressed concrete girders.
    b. Composite behavior—implemented by constraining all translational and rotational degrees of freedom of the nodes between the components (i.e., nodes that share the same longitudinal coordinates)—modeled between the rail and deck, as well as the deck and the top flange of the girders.
2. For steel girder bridges where an exterior girder is subjected to Category T damage (i.e., torsion about the longitudinal direction (Avent, 2008)) from a vehicular collision, FE models that remove the composite behavior between the girder and the deck in the region of the damage (by removing the translational and rotational constraints between the top flange of the girder and the deck) can accurately capture behavior. The damaged profile of the girder should be considered.

Findings from Numerical Parametric Investigation

1. When fully composite behavior between the rail, deck, and girder is assumed, the curvature is reduced in the positive moment region, meaning strains in the deck and girder are reduced, as compared to a comparable system where only the deck and girder are composite. The vertical location of the neutral axis is increased (measured from the bottom flange) in the positive moment region as compared to a comparable system where only the deck and girder are composite.
2. FT, FC, PS-1, and PS-2 rail types all contribute to the above-mentioned reduction in curvature. The greatest benefit was observed when using the FT rail, with decreasing benefit corresponding to the rail types that result in composite sections with decreasing moment of inertia.
3. Rail discontinuity at piers has negligible impact on the behavior of the exterior girders in the positive moment region.
4. Skew (up to 30 degrees) has negligible impact on the behavior of the exterior girders in the positive moment region.

Other Findings

1. Through comparisons between measured digital image correlation (DIC) and strain gauge data, DIC is further validated as a technique for field monitoring of bridges.

Implementation

Research culminated in *Recommendations for Evaluating the Reserve Strength of Girder Bridges Due to Rail Participation* (Appendix A). Based on findings from this study, as well as findings from SPR-4119: *Assessment of Bridges Subjected to Vehicular Collision* (Wang & Thrall, 2019), a *Recommendations for Bridge Inspectors for Evaluating Steel Girder Bridges Subjected to Vehicular Damage* document has been developed (Appendix B). The latter document will be included in the Indiana Department of Transportation (INDOT) *Bridge Inspection Manual*. Findings and recommendations will be presented at the 2021 Purdue Road School. A journal paper is currently in preparation and will be submitted for publication. The final report will be posted on the Purdue e-Pubs website and will be freely available to the public.

CONTENTS

LIST OF TABLES

LIST OF FIGURES

1. INTRODUCTION

The aim of this research was to evaluate the participation of intact, integral, reinforced concrete bridge rails, experimentally and numerically, in carrying live load. Steel and prestressed concrete multi-girder bridges are designed conservatively, resulting in reserve strength. Experimental studies have demonstrated that multi-girder bridges have greater capacity and stiffness than predicted by design code (e.g., Bakht & Csagoly, 1979; Barker, 2001; Burdette & Goodpasture, 1973; Eom & Nowak, 2001; Fu et al., 1996; Goodpasture et al., 1973; Kim & Nowak, 1997). One source of this additional strength and stiffness—which is not permitted to be considered when evaluating strength and extreme event limit states per current bridge design code (AASHTO, 2020)—is the participation of the rails in carrying load. The primary function of bridge rails is to protect pedestrians and vehicular traffic. Their design is governed by the goal of containing and redirecting traffic (AASHTO, 2020), with performance in the U.S. evaluated per the American Association of State Highway and Transportation Officials (AASHTO) *Manual for Assessing Safety Hardware* (AASHTO, 2016) or National Cooperative Highway Research Program (NCHRP) *Report 350: Recommended Procedures for the Safety Performance Evaluation of Highway Features* (Ross et al., 1993). The design parameters for bridge rail are selected based on resistance to crash loadings.

Existing numerical research (to be reviewed in Section 2) indicates that including bridge rails in a finite element (FE) numerical model increases the load capacity of girder bridges. A prior Indiana Department of Transportation (INDOT) project SPR-4119: *Assessment of Bridges Subjected to Vehicular Collision* (Wang & Thrall, 2019), found that loads are generally redistributed away from damaged steel girders, potentially to adjacent girders and/or the rail. However, there is almost no measured data on the strains induced in bridge rails under live load. Thus, there is a major research gap in understanding the behavior of bridge rails. Further, there are no existing guidelines or recommendations for evaluating the reserve strength of girder bridges due to bridge rail load shedding.

To address these research needs and knowledge gaps, the specific objectives of this project included the following:

1. Non-destructively test the behavior of steel and prestressed concrete multi-girder bridges with varying railing types.
2. Develop validated numerical models and perform parametric numerical investigations.
3. Develop assessment guidelines that quantify the reserve strength from load shed to bridge rails.

The focus is on multi-girder steel and prestressed concrete bridges, as the relative stiffness of the bridge rail can impact the load being carried by exterior and adjacent interior girders. Specifically, field monitoring was performed one steel girder bridge (two-span continuous), one steel girder bridge damaged by vehicular collision (two-span continuous), and one prestressed concrete girder bridge (six-span continuous), as shown in Figure 1.1. The study was limited to intact, reinforced concrete bridge rails that are integral to the deck. Specifically, the behavior of four integral, reinforced concrete INDOT rail types was considered (INDOT, 2020): FC, FT, PS-1, and PS-2 (Figure 1.2). Research culminates in *Recommendations for Evaluating the Reserve Strength of Girder Bridges due to Rail Participation* (Appendix A). Based on findings from this study, as well as findings from SPR-4119: *Assessment of Bridges Subjected to Vehicular Collision*

Figure 1.1 Monitored bridges.

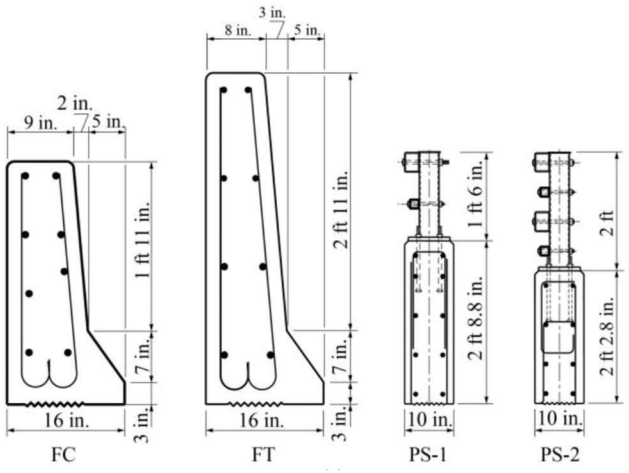

Figure 1.2 Integral reinforced concrete INDOT rail types: FC, FT, PS-1, and PS-2 (adapted from INDOT, 2020).

(Wang & Thrall, 2019), a *Recommendations for Bridge Inspectors for Evaluating Steel Girder Bridges Subjected to Vehicular Damage* document has been developed (Appendix B).

2. BACKGROUND

Existing research in the behavior of the rail of multi-girder steel and prestressed concrete bridges can be categorized as studies that (1) measured strains in field tests and performed numerical FE analyses that considered bridge rails, and (2) investigated bridge rail participation through numerical modeling exclusively. Table 2.1 summarizes these studies, including the type of study conducted, the type of bridge studied, and the number of bridges investigated.

2.1 Field Tests and Finite Element Numerical Studies

An Indiana Department of Transportation (INDOT) project SPR-2793: *Long-Term Effects of Super Heavy-Weight Vehicles on Bridges* (Wood et al., 2007) numerically investigated the effect of continuous and discontinuous concrete bridge rails for two steel girder and two prestressed concrete girder bridges. The focus of the project was on understanding the long-term effects of superload trucks on girder bridges, but found interesting results related to rail participation. Specifically, the study monitored one prestressed concrete girder bridge (two-span continuous under live load, single-spans under dead load, with spans of 121 ft. and 119 ft.) and one steel girder bridge (118.1-ft. single-span), measuring both strains and deflections, during a live load test and over a six-month period. Three-dimensional (3D) FE analyses of these bridges, as well as an additional prestressed concrete girder (three-span continuous under live load, single-spans under dead load, with spans of 41.5 ft., 53 ft., and 41.5 ft.) and steel girder bridge (five-span continuous, with spans of 92 ft., 108 ft., 94 ft., 101 ft., and 92 ft.), were performed. The additional five-span continuous steel girder bridge had previously been monitored by Canna and Bowman (2001), with strains in the girders (flanges and webs) and diaphragms measured by strain gauges and displacements measured by rulers. Most relevant for this report, this INDOT project numerically investigated the influence of bridge rails on the behavior of these four studied bridges, culminating also in a journal paper on the topic (Akinci et al., 2008). Wood et al. (2007) and Akinci et al. (2008) conclude from these numerical investigations that rails contribute to the bridge stiffness and that, as a result, girder distribution factors (GDF) in exterior girders can be reduced by 30% if continuous reinforced concrete rails are included. Wood et al. (2007) and Akinci et al. (2008) also found that discontinuities in the rail in the positive moment region can result in higher stresses in the girders. Discontinuities in the rail in the negative moment region can increase the stress in the deck, as compared to a fully continuous rail.

Wood et al. (2007) also reported that four foil strain gauges were applied to the reinforced concrete rail of the monitored single-span steel girder bridge. Unfortunately, two of the gauges malfunctioned due to problems with installation. Wood et al. (2007) indicated that the accuracy of the other two gauges was limited, but report that the measurements demonstrate that the rail participated in carrying the applied load and that FE predictions agreed well with the measured results. This is the only measured data on the behavior of bridge rails in the literature.

The reader is also referred to Wood et al. (2007) for a literature review on this topic, including a brief

TABLE 2.1
Summary of existing literature

	Type of Research Performed		Type of Bridge Investigated, with Number of Bridges Studied	
Author (Year)	**Field Testing**	**Numerical Modeling**	**Prestressed Concrete Girder**	**Steel Girder**
Wood et al. (2007), Akinci et al. (2008), Canna & Bowman (2001)[1]	✓	✓	2	2
Barker et al. (1999), Barker (2001)	✓			1
Billing (1984)[2]	✓		4	10
Chung et al. (2006)[3]		✓		36
Conner & Huo (2006)[4]		✓	20	
Eamon & Nowak (2002)		✓	120	120
Mabsout et al. (1997)		✓		120
Roddenberry et al. (2011)	✓	✓	2	
Smith & Mikelsteins (1988)[5]		✓	18	18
Stallings & Yoo (1993)	✓			3

[1]Two steel girder and one prestressed concrete girder bridge were monitored during field testing. FE analyses of an additional prestressed concrete girder bridge was performed.
[2]A total of 27 bridges were tested. The numbers here indicate only the number of I-girder type bridges tested.
[3]Additional studies were performed on 10 steel girder bridges investigating the impact of preexisting cracks. These are not reviewed here.
[4]A total of 34 analyses were performed. 20 of these related to the rail study.
[5]Prestressed concrete voided slab decks were also studied.

discussion of many of the articles that are further reviewed in this report.

Roddenberry et al. (2011) investigated the effect of secondary bridge elements (i.e., barriers, curbs, and diaphragms) on the behavior of two prestressed concrete girder bridges, by measuring the longitudinal surface strains in the bottom flanges of girders and comparing the measured results to FE numerical predictions. Specifically, the behavior of a Florida Bulb T-girder bridge with a continuous slab was monitored before the barrier was constructed and after it was constructed. The behavior of a simply supported AASHTO Type IV girder bridge was monitored only after the barrier was in place. The bridges were loaded incrementally with varying amounts of 2-ton blocks and with a Florida Department of Transportation test vehicle to measure the maximum longitudinal strains in the bottom flanges of the girders due to bending at midspan. Measured results were compared with the FE predictions, culminating in validated models. Roddenberry et al. (2011) discusses these field tests, but only presents FE results. By comparing FE models of the two studied bridges featuring no barriers and barriers, they found that barriers decrease the strain in the exterior girders as well as interior girders, with the greatest reduction being in the exterior girders. Barrier joints can locally increase the strain in exterior girders.

Stallings and Yoo (1993) monitored the behavior of three simply-supported steel girder bridges, with spans of 44 ft., 77 ft., and 49 ft., under static and dynamic truck loads. Strains in the top and bottom flanges of girders were measured, as well as midspan deflections. Girder strains were used to calculate the bending moments, assuming section moduli. The paper explicitly acknowledges that bridge rails and curbs stiffen the deck edges and contribute to carrying moment. However, the assumed section modulus of the exterior girder neglects the contribution of the rail and only considers the curb as part of the exterior girder's effective flange. The moments calculated using the measured strains and the assumed section moduli are smaller than the applied moment. Stallings and Yoo (1993) attribute this difference primarily to restraining moments at the bridge bearings due to friction.

Barker (2001) and Barker et al. (1999) developed field testing procedures which quantify various factors that contribute to bridge strength and stiffness, but which may not be accurately captured using load rating methods including: "(1) actual impact factor, (2) actual section dimensions, (3) unaccounted system stiffness such as curbs and railings, (4) actual lateral load distribution, (5) bearing restraint effects, (6) actual longitudinal live load distribution, and (7) unintended or additional composite action." Their procedures are applied to the field testing of a three-span continuous steel girder bridge (spans of 60 ft., 90 ft., and 60 ft.), with behavior monitored by strain gauges on the steel girders. When comparing measured data to analytical predictions, they found contributions from the additional stiffness of the rails, curbs, and noncomposite slab on the order of 1.04 to 1.28.

Billing (1984) performed field testing on 27 bridges of varying types and spans, with ten of these being steel I-girder bridges and four being prestressed concrete I-girder bridges. The focus was on understanding dynamic live loading, with each bridge instrumented with accelerometers, pressure sensors, strain gauges, and displacement transducers. Measurements of bridge deflections with a rail under static truck loads compared to deflections of a bridge without a rail, indicate that rails and curbs contribute to the structural stiffness of a bridge.

2.2 Numerical Studies

Additional studies have further investigated the effect of rail on bridge behavior using numerical modeling.

Smith and Mikelsteins (1988) performed grillage analyses to investigate the edge stiffening effects from curbs, sidewalks, and rails. Single-span prestressed concrete and steel girder bridges were studied, with varying span lengths (49.2 ft., 98.4 ft., and 148 ft.) and edge conditions. Specifically, six edge conditions were varied: (1) no edge, (2) curb, (3) sidewalk (4) curb with rail, (5) sidewalk with rail, and (6) rail only. Smith and Mikelsteins (1988) found that including edge components increased the bending moment carried by exterior girders, but these exterior girders also deflect less due to the additional stiffness provided. This effect is greatest for the smallest span considered, regardless of bridge type. Generally, increases in bending moment of the exterior girders was associated with increased moment of inertia from the type of edge condition considered.

Mabsout et al. (1997) performed FE numerical analyses on single-span, two-lane, steel girder bridges, to understand the effect of bridge rail and sidewalks on wheel load distribution. A total of 120 analyses were performed, with varying span length (56 ft., 77 ft., 98 ft., and 119 ft.) and girder spacing (6 ft., 8 ft., and 12 ft.). A 50 inch-wide, 7.5 inch-thick, reinforced concrete sidewalk and an 8 inch-thick, 30 inch-high, reinforced concrete rail were also considered, with varying locations (left, right, or both sides of the bridge) and combinations (e.g., sidewalk alone, rail alone, and both combined). They found that including sidewalks and bridge rails in their models increased the capacity of the bridge by 5% to 30%. Specifically, when a bridge rail is included, the combined deck and rail participate in carrying 45% of the total bending of the exterior girder, compared to just 4% when only the deck is present. With both the sidewalk and rail, this increases to 52%. Mabsout et al. (1997) also made comparisons between their FE results and AASHTO and National Cooperative Highway Research Program (NCHRP) analytical predictions for wheel load distribution factors, finding both predictive methods conservative except for short spans.

Eamon and Nowak (2002) numerically investigated the effect of bridge rails, as well as other secondary

elements including sidewalks and diaphragms, on bridge capacity for simple-span, two-lane steel and prestressed concrete girder bridges. A total of 240 FE analyses were performed, varying span length (32.8 ft., 98.4 ft., and 164 ft.), girder type (steel or prestressed concrete), girder spacing (6.56 ft., 9.84 ft., and 13.1 ft.), secondary elements (i.e., sidewalk, barrier, and diaphragm), and concrete deck thickness (5.91 in., 9.06 in., and 11.8 in.). They found that secondary bridge elements decrease the GDFs by 10% to 40% in the elastic range and an additional 5% to 20% in the plastic range. Specifically, elastic analyses demonstrated that the maximum girder moment is reduced by the following amounts for each secondary element considered individually (maximum value, followed by the average in parentheses): diaphragms—13% (4%), rails—32% (10%), sidewalks—35% (20%). Diaphragms were found to be more effective at reducing GDFs for wider girder spacings and longer spans, with rails and sidewalks being more effective for smaller girder spacings and longer spans. Generally, the effect of secondary elements is more significant in steel girder bridges, as these are less stiff in comparison to prestressed concrete girder bridges. Eamon and Nowak (2002) specifically note that further experimental data supporting these conclusions is needed.

Conner and Huo (2006) focused on two-span continuous prestressed concrete girder bridges (each span is 76 ft.), numerically investigating the effect of rail and bridge aspect ratio (i.e., ratio of span length to bridge width) on live load moment distribution. Varied parameters for the 20 analyses in the rail study included: skew (0 or 45 degrees) and overhang length (0 to 4.5 ft., in increments of 6 in.). Scenarios with a reinforced concrete and without a rail were compared. In all cases investigated (except for zero overhang), the GDF for the exterior girder was greatly reduced when the rail was modeled (average 31% reduction for 0-degree skew bridges; average 28% reduction for 45-degree skew bridges). The zero overhang cases showed increased load being carried by the exterior girders, as the rail increases the stiffness of the exterior girder when it is directly on top of it. Comparisons were also made with AASHTO analytical predictions, finding these predictions (which ignore the contribution of the rail) to be conservative when compared with FE models that incorporate the rail.

Chung et al. (2006) performed FE numerical analyses to investigate the effect of secondary elements (i.e., rail and lateral bracing) on wheel load distribution factors (LDF) for nine steel girder bridges based on the INDOT inventory, with different span lengths and lateral bracing types. For each bridge, four FE models were built as follows: (1) "as is" with the rail and bracing elements, (2) rail only, (3) lateral bracing only, and (4) primary members (girders, deck, and bearing) only. When comparing the FE predictions, Chung et al. (2006) found that the presence of the rail alone decreases the peak LDF by up to 25%, while the presence of lateral bracing alone decreases the peak LDF by up to 11%. The "as is" models decrease the peak LDFs by 17 to 38%. The presence of the rail can change the location of the peak LDF, for example from first interior girder to the second interior girder. They also found that their FE models predicted lower LDFs than the code predictions.

2.3 Summary

This prior research provides valuable data on the behavior of steel and prestressed concrete girder bridges, incorporating the effect of bridge rails. These experimental and numerical studies indicate the participation of bridge rails and other secondary members in carrying load. However, the field testing studies (with the exception of one study which provided limited data), do not directly measure the strains in the bridge rail. The numerical FE studies include the bridge rails and other secondary members but rely on idealized models which do not necessarily capture the full behavior of the system (e.g., relative contribution of secondary members, sidewalk, and rails to behavior). There is a major research gap in measured data on rail performance (i.e., measured strains in the rail under live load).

3. FIELD MONITORING AND NUMERICAL MODELING

3.1 Field Monitoring Approach

Field monitoring was performed on two steel girder bridges and one prestressed concrete girder bridge with varying rail types, as shown in Figure 1.1 and summarized in Table 3.1.

Note that Asset 037-55-05265 was selected for monitoring as it has been damaged by vehicular collision and was previously studied in SPR-4119: *Assessment of Bridges Subjected to Vehicular Collision* (Wang & Thrall, 2019). This prior study had indicated that girders damaged by vehicular collision resulting in Category T damage (i.e., torsion about the longitudinal direction (Avent, 2008), Figure 3.1) may shed load to

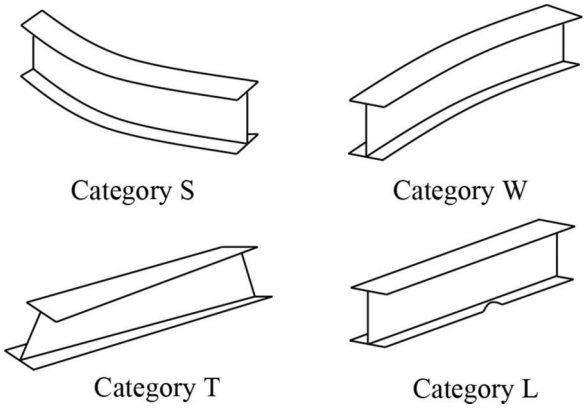

Figure 3.1 Categories of damage (adapted from Avent, 2008 and reprinted from Wang & Thrall, 2019), where Category S refers to strong axis bending, Category W refers to weak axis bending, Category T refers to torsion about the longitudinal axis, and Category L refers to local damage (shown for a flange deformation as an example).

TABLE 3.1
Field monitoring program

Asset No.	Girder Material	Span Arrangement	Rail Type	Load Tests
020-20-07229	Steel	Two-span continuous	FC	**Static: Two trucks at peak positive moment, 1 ft. from rail.** **Crawl: One truck traveling at ~ 5 mph, 1 ft. from rail.** Crawl: One truck traveling at ~ 5 mph, in center of lane adjacent to rail. **Speed: One truck traveling at ~ 45 mph, in center of lane adjacent to rail.**
037-55-05265	Steel[1]	Two-span continuous	FC	*Static: Two trucks at peak positive moment, 1 ft. from rail.* *Static: Two trucks positioned to induce peak positive moment in damaged region, 1 ft. from rail.* *Crawl: One truck traveling at ~ 5 mph, 1 ft. from rail.* *Crawl: One truck traveling at ~ 5 mph, in center of lane adjacent to rail.* *Speed: One truck traveling at ~ 20 mph, in center of lane adjacent to rail.*[1]
331-71-08732	Prestressed concrete	Six-span continuous	FC, PS-1	Static (FC-side): Two trucks at peak positive moment, 1 ft. from rail. Crawl (FC-side): One truck traveling at ~ 5 mph, 1 ft. from rail. **Crawl (FC-side): One truck traveling at ~ 5 mph, in center of lane adjacent to rail.**[2] Speed (FC-side): One truck traveling at ~ 30 mph, in center of lane adjacent to rail. Static (PS-1-side): Two trucks at peak positive moment, 1 ft. from rail. Crawl (PS-1-side): One truck traveling at ~ 5 mph, in center of lane adjacent to rail. Speed (PS-1-side): One truck traveling at ~ 30 mph, in center of lane adjacent to rail.

Note:
Bold text indicates a load test was performed twice for repeatability.
Italicized text indicates the load test was performed on both the damaged side and the undamaged side for comparison.
[1]This load test was performed three times on the undamaged side, only once on the damaged side.
[2]Bridge was damaged by vehicular collision.

adjacent girders or the bridge rail, and it was the impetus for the current research. However, there was no data measured on the rail behavior in this prior study and so Asset 037-55-05265 was re-monitored in the current study.

While the research proposal planned to monitor six bridges, only three were monitored due to complications related to COVID-19. The Business Owner, Principal Investigator, Project Advisor, Study Advisory Committee agreed that sufficient data had been obtained from the three monitored bridges.

3.1.1 Loading

The behavior of the three bridges was monitored under truck loads (i.e., heavily loaded dump trucks) as summarized in Table 3.1. Static load tests were performed in which two trucks were positioned to induce the peak positive moment (where positive moment refers to compression in the top of a section and tension in the bottom) in the bridge overall. The positions of the trucks to induce this peak positive moment were found using influence lines. Table 3.2 summarizes the locations of the trucks, and truck weights and axle spacing for each bridge. The trucks were positioned approximately 1 ft. away from the interior of the rail transversely with some variations for each bridge. In this report, positive moment refers to compression on the top of a section and tension on the bottom. For Asset 037-55-05265, additional static load tests were performed in which the two trucks were positioned to induce peak positive moment in the damaged region and the symmetric region on the undamaged side. Crawl and speed tests were also performed using a single heavily loaded truck.

3.1.2 Strain Gauge Sensors

The behavior of the girders and rail in each bridge was monitored using an array of ST350 strain transducers (BDI, 2018) with the STS4 data acquisition system (BDI, 2014) provided by BDI. The ST350 strain transducers have a gauge length of 3 in. The gauge length was extended to 1 ft. to monitor the surface strains on the rail in Asset 020-20-07229 and Asset 037-55-05265. The strain transducers were adhered to the bridge components by Loctite 410 epoxy and were removed when testing was completed. Figure 3.2 shows the researchers adhering a gauge to the bottom flange of a steel girder in Asset 020-20-07229. For the steel girder bridges, the paint was removed prior to adhering the gauge. All gauges were aligned to measure longitudinal strains.

As Asset 331-71-08732 was new construction, four model 3911 resistance type rebar strain meters (sister bar, Geokon, 2019) were inserted in the deck and the rail to monitor the internal strains in these components. Figure 3.3 shows researchers installing a sister bar

TABLE 3.2
Truck weights, locations, and axle spacing for static test

Asset No.	Girder Lines Loaded[1]	Axle Weights (kip) / Distances[2] (ft.) / Transverse Wheel Spacing (ft.)					
020-20-07229	G1/G2	17.8/	21.8/	21.8/	12.8/	18.9/	18.9/
		24.3/	38.5/	43.1/	57.2/	70.8/	75.2/
		7.04	6.08	6.08	7.04	6.06	6.06
037-55-05265	G1/G2	15.4/	25.2/	23.7/	10.6/	26.4/	25.7/
		8.50/	22.7/	27.0/	40.8/	55.6/	60.2/
		7.08	6.00	6.00	7.08	6.17	6.17
	G5/G6	15.4/	25.2/	23.7/	10.6/	26.4/	25.7/
		28.0/	42.2/	46.5/	60.3/	75.1/	79.7/
		7.08	6.00	6.00	7.08	6.17	6.17
331-71-08732	G1/G2/	10.3/	20.5/	20.5/	10.3/	20.7/	20.7/
	G3/G4	37.5/	23.9/	19.5/	69.3/	55.2/	50.5/
		6.96	5.88	5.88	7.04	5.92	5.92

[1]Indicates the girder lines that were loaded (see Figure 3.9, Figure 3.19, and Figure 3.27).
[2]Longitudinal distances measured from reference points in Figure 3.9, Figure 3.19, and Figure 3.27.

Figure 3.2 Researchers adhering a strain gauge to the bottom flange of Asset 020-20-07229 (left) and an adhered gauge (right).

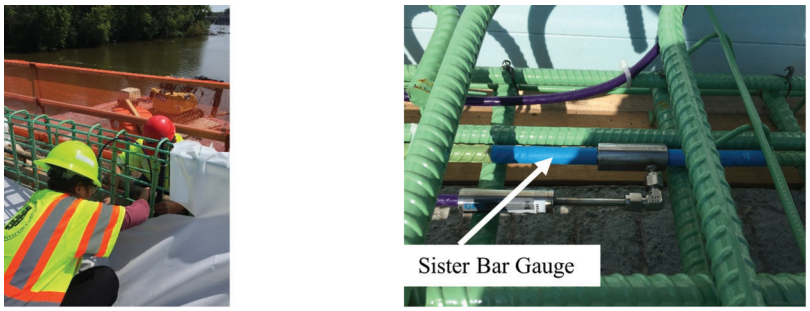

Figure 3.3 Researchers installing a sister bar gauge in Asset 331-71-08732 (left) and the installed gauge (right).

gauge in Asset 331-71-08732 by attaching it to rebar via zip ties prior to concrete casting.

3.1.3 Digital Image Correlation

In the prior study, SPR-4119: *Assessment of Bridges Subjected to Vehicular Collision* (Wang & Thrall, 2019), the behavior of the bottom flanges of Asset 037-55-05265 were monitored using the photographic measurement technique digital image correlation (DIC). This study monitors this bridge using both strain gauges and DIC, providing valuable data that further validates DIC as a technique for field monitoring bridges.

The three-dimensional (3D) DIC system used in this project consisted of two cameras (2,448 × 2,050 pixels, 0.472-in. lenses). A 6-foot long DIC pattern was applied to the full-width of the bottom flange of the monitored girders using pressure-activated adhesive tape (Wang et al., 2019; Wang & Thrall, 2019). This rapid approach to DIC pattern application is especially important when access time is limited (e.g., Wang et al., 2021).

The ARAMIS (2017) software package was used to calculate strains, using a gauge length of 2.97 in. To reduce the noise in the measured DIC data, both spatial filter (median filter of 7) and temporal filter (binomial filter of 5) were used. Area averaging (performed over

the area of the DIC pattern while excluding 0.5 in. from the edges to eliminate the development length of the pattern (Wang et al., 2019; Wang & Thrall, 2019)) was used to further reduce the noise.

3.2 Numerical Modeling Approach

3E FE models of the monitored bridges were built in CSiBridge (2020) and ABAQUS (2016) to understand the behavior of bridge rail. The CSiBridge models were made for the two-span continuous steel girder bridge (Asset 020-20-07229) and the six-span continuous prestressed concrete girder bridge (Asset 331-71-08732). ABAQUS was used for the two-span continuous bridge that was damaged by vehicular collision (Asset 037-55-05265) because of its capabilities to handle the complex geometry of the damaged girder.

3.2.1 General Modeling Assumptions

This section summarizes modeling assumptions that are used in both the CSiBridge and ABAQUS models. Specific features for each software are included in the following subsections.

The analyses were performed under the measured loads of the trucks used for each field monitoring test. Each truck is approximated as six-point loads, with magnitudes as indicated in Table 3.2. Self-weight was not considered.

In each relevant section, plan drawings indicate the boundary conditions for each monitored bridge. A "pin" boundary condition is implemented in the models as free rotation in the transverse direction and fixed translation in all directions. A "roller" boundary condition is implemented in the models as free rotation in the transverse direction and free translation in longitudinal direction. For the semi-integral abutments in Asset 331-71-08732, versions of the model where the boundary condition at the abutments are both pinned and one is pin and the other roller are considered. The boundary conditions above the piers are all assumed to be rollers for this bridge.

Linear material models were assumed for steel, reinforced concrete, and prestressed concrete. The materials in all models remain in the elastic material range. Steel is assumed to have a Young's modulus of 29,000 ksi and a Poisson's ratio of 0.3. For 3 ksi and 4 ksi compressive strength concrete rails and deck, a Young's modulus of 3,592 ksi and 3,950 ksi, respectively (calculated per Equation C5.4.2.4-1 of AASHTO, 2020) and Poisson's ratio of 0.2 is assumed. For 8 ksi compressive strength prestressed concrete, a Young's modulus of 4,965 ksi (calculated per Equation C5.4.2.4-1 of AASHTO, 2020) and Poisson's ratio of 0.2 is assumed.

The concrete deck and rail were modeled as thick shell elements. The rail was comprised of a series of stacked thick shell elements, with centers aligned vertically (Figure 3.4). Each shell element was given the appropriate thickness for that height of the rail. On each side of the bridge, in the transverse direction, the rail

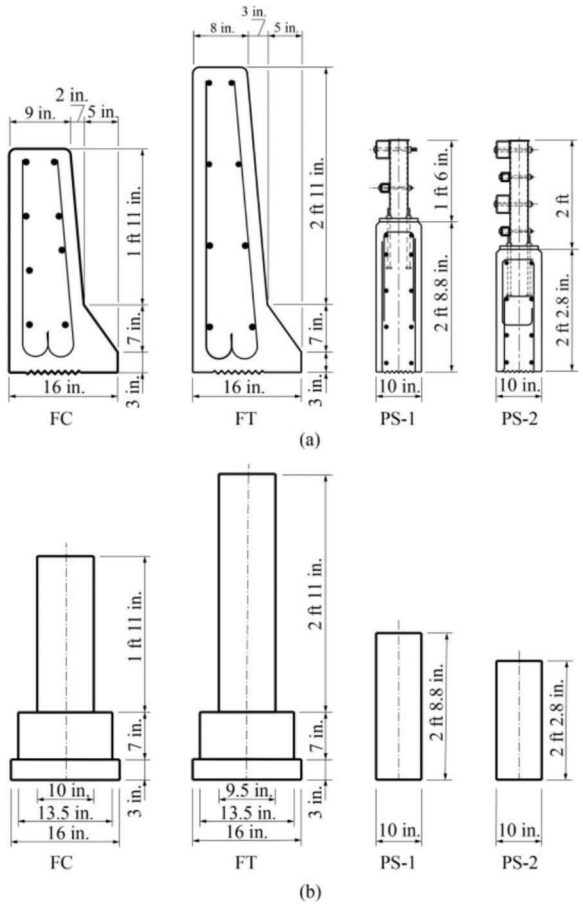

Figure 3.4 Rail types: (a) actual geometry (adapted from INDOT, 2020) and (b) assumed geometry in FE models.

was positioned at a distance half of the largest thickness of the rail, measured from the edge of the deck. The presented rail strain data is the average of the interior and exterior faces of the shell elements. In the FE models, trucks were positioned 1 ft. away from the interior of the rail for all the bridges.

The boundary conditions were applied at the intersection of the web and the bottom flange of the modeled girders. Any transverse slope of the deck is ignored.

3.2.2 Finite Element Models in CSiBridge

3D FE models were built in CSiBridge, assuming linear geometry (Figure 3.5). For all components in both bridge types, a mesh size of 6 in. was used.

For the steel girder bridge (Figure 3.5a), the webs of the girders were modeled as thin shell elements. The flanges were modeled as frame elements. The diaphragms were modeled in the same way.

For the prestressed concrete girder bridge (Figure 3.5b), only the gross concrete area of the girders was modeled. The webs of the girders were modeled as thick shell elements and the flanges were modeled as frame elements. The prestressing tendons were not modeled, as the measured strains were only induced by the truck

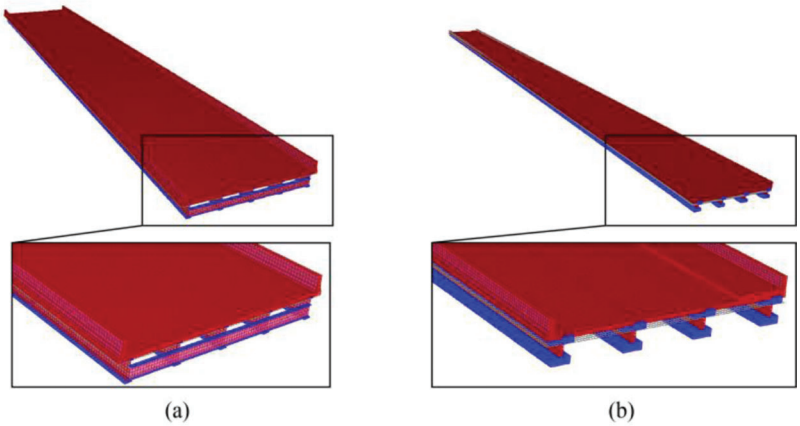

Figure 3.5 3D FE numerical models in CSiBridge: (a) two-span continuous steel girder bridge, Asset 020-20-07229 and (b) six-span continuous prestressed girder bridge, Asset 331-71-08732.

loads and the prestressing tendons had negligible effect on the cross-section properties. The diaphragms were modeled as frame elements.

In both bridges, composite behavior between girders and deck and between deck and rail was assumed. To approximate composite behavior between the girders and deck, the deck was geometrically positioned at the top of the web. As deck and girders are meshed, common nodes are created at the interface which represents the connection between elements. To place the deck at the correct elevation above the girders, the deck was offset by a distance equal to the summation of the thickness of the flange and half of the deck thickness. To approximate composite behavior between the deck and the rail, the body joint constraint available in CSiBridge was used. A pair consisting of the nodes of the bottom of the rail and nodes of the deck with close coordinates in longitudinal and transverse directions was created. Each pair of nodes is constrained in all degrees of freedom, meaning that there is no relative translation and rotation between components.

For both bridges, strains at the nodes were considered. As the webs, deck, and rails were modeled as shell elements, strains were exported at the nodes in each element directly from CSiBridge and then averaged. Because the flanges of the girders were modeled as frame elements, the strains were calculated following Hooke's law and using the cross-sectional properties and Young's modulus. For the steel girder bridges, only the axial force in the frame elements was used. For the prestressed concrete bridge, both axial force and bending moment were considered. Strains at each node were averaged across the two elements sharing the node.

3.2.3 Finite Element Model of Damaged Bridge in ABAQUS

A 3D FE model of the two-span continuous bridge that was damaged by vehicular collision (Asset 037-55-05265) was built in ABAQUS using the approach developed in Wang and Thrall (2019) (Figure 3.6). Specifically, geometric nonlinearity was incorporated. S4R shell elements were used for all components. The concrete deck and rail (Figure 3.7) were modeled as shell elements with a mesh size of 3 in.

As a vehicular collision may damage the shear connection between girders and the deck (Wang & Thrall, 2019), models were made that considered both composite behavior and non-composite behavior. Composite behavior with the rail (i.e., the girders are composite with the deck and the rail) is also investigated. Composite behavior is achieved by tying nodes of components together, meaning that there is no relative translation between components. When non-composite behavior is modeled between the girders and the deck, surface to surface contact was used. The coefficient of friction between the concrete and steel was assumed to be 0.65 (Rabbat & Russel, 1985). To prevent penetration between components, hard contact in the normal direction is implemented. The diaphragms are tied to the girder webs and it was assumed that they are centered vertically on the girder webs.

The geometry of the damaged exterior girder was approximated by a web rotation angle (α = 13.95 degrees) and deformed shape of the bottom flange that was approximated using a 5th order polynomial with the following boundary conditions: (1) start point (coordinates: 0,0,0), peak point (coordinates: x $d\sin\alpha$, $d(1-\cos\alpha)$), and end point (coordinates: l_s, 0, 0), and (2) the 1st order derivative at the start, peak, and end of the damage was required to be zero. Here d is the height of the web (d = 34.81 in.), and l_s is the length of the damage (l_s = 325.25 in.) (Figure 3.8). The start of the damaged region, D was 70 ft. from the west pier. See Wang and Thrall (2019) for more information regarding these measurements for Asset 037-55-05265. While it is acknowledged that the plastic deformation from a vehicular collision would change the steel material properties, these changes were ignored in this model. This is a conservative assumption as any plastic deformation of the steel would result in an increase in yield and ultimate strength.

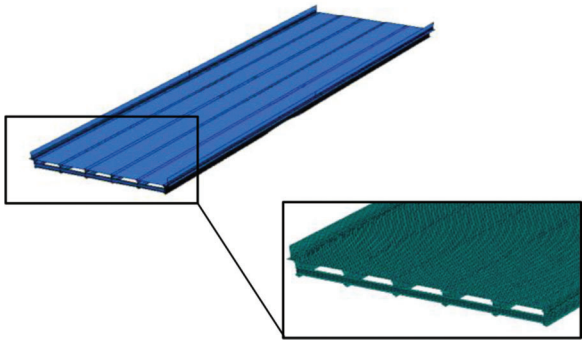

Figure 3.6 3D FE numerical model in ABAQUS, Asset 037-55-05265.

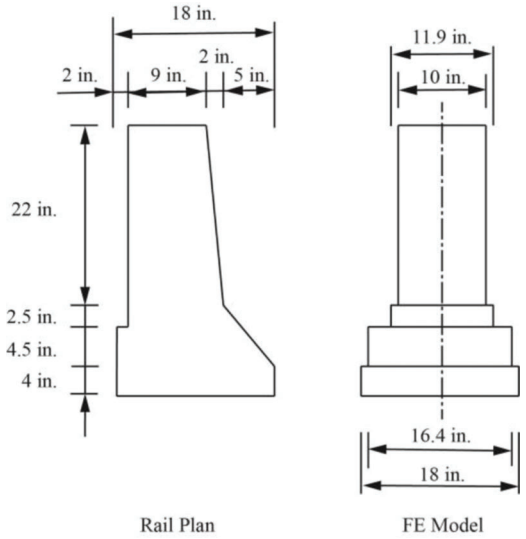

Figure 3.7 FE model and plan of rail for Asset 037-55-05265.

Strains at the nodes are exported directly from ABAQUS.

3.3 Two-Span Continuous Steel Girder Bridge: Asset 020-20-07229 (Fort Wayne District)

Asset 020-20-07229 (Figure 3.9) is a two-span (108 ft. and 101 ft. spans) continuous, composite, steel girder bridge that was built in Elkhart, IN in 1991. It features FC rail that has discontinuities at every 30 ft. along the span length.

Field monitoring focused on the behavior of the exterior Girder 1 and the adjacent FC rail, as the bridge was symmetric. Loads were applied on this side of the bridge, as described in Table 3.1.

Figure 3.9 shows the longitudinal positions of the strain gauges. Gauges were positioned at the location where peak positive moment is achieved under the load of two trucks (M), where there was a gap in the rail (N), and near the abutment (E). Locations are indicated, here and throughout this report, using the aforementioned letters and a number to indicate the girder line. For example, Location E1 refers to near the abutment for Girder 1 and Location M4 refers to the peak positive moment region of Girder 4.

3.3.1 Behavior Under Static Truck Loads Positioned for Peak Positive Moment

Figure 3.10 shows the measured strains and the FE predictions in the exterior girder near the abutment (Location E1), when the bridge is loaded by two trucks positioned to achieve peak positive moment. In this plot and all similar plots in this report, the vertical position of zero corresponds to the bottom of the bottom flanges. The white region indicates the girder. Medium grey shows the deck region and the darker grey shows the rail region. For bridges with a sidewalk, light grey is used for the sidewalk region. To the right of the plot a cross-section is shown which corresponds to the same vertical locations in the plot for reference. Blue circles on the plot indicate the measured strain gauge data and also the location of the gauges on the cross-section. FE predictions in the plot are indicated by $\times$ markers. Red indicates an FE model where the rail, deck, and girder are fully composite. Green indicates FE predictions when the rail was not included in the model. The lines indicate linear fits of the data in the girder only, with colors corresponding to the relevant data. The dashed black line indicates the analytical prediction for the neutral axis location when it is assumed that the girder, deck, and rail are fully composite (with the rail directly above the girder). The dash-dotted black line indicates the analytical prediction for the neutral axis location when only the girder and deck are composite. These analytical predictions are made by considering the cross-sectional properties of the girder, deck and rail. The assumed material properties discussed in Section 3.2, which are based on the bridge design plans, are used to transform the material properties. For exterior girders, the effective width of the deck is half of the girder spacing plus the length of the overhang. For interior girders, the effective width of the deck is the girder spacing. These analytical predictions can be used as simplified benchmarks indicating composite behavior. A more sophisticated comparison is achieved with the 3D FE models. Throughout the report, positive strain indicates tension and negative indicates compression.

Figure 3.10 shows good agreement between both FE models and the measured data at Location E1. From the FE models, which provide additional data points in the web region, it is clear that shear behavior dominates in this region (i.e., plane sections do not remain plane), as expected near the abutment. Table 3.3 show that the neutral axis—calculated by finding the y-intercept of the best fit line—for the measured data is 15.8% lower than the analytical prediction for composite behavior with the deck only. This indicates that composite behavior between the girder and deck is not fully developed near the abutment. This is also the case in the FE model which shows a neutral axis 11.5% lower than the analytical prediction for composite behavior with the

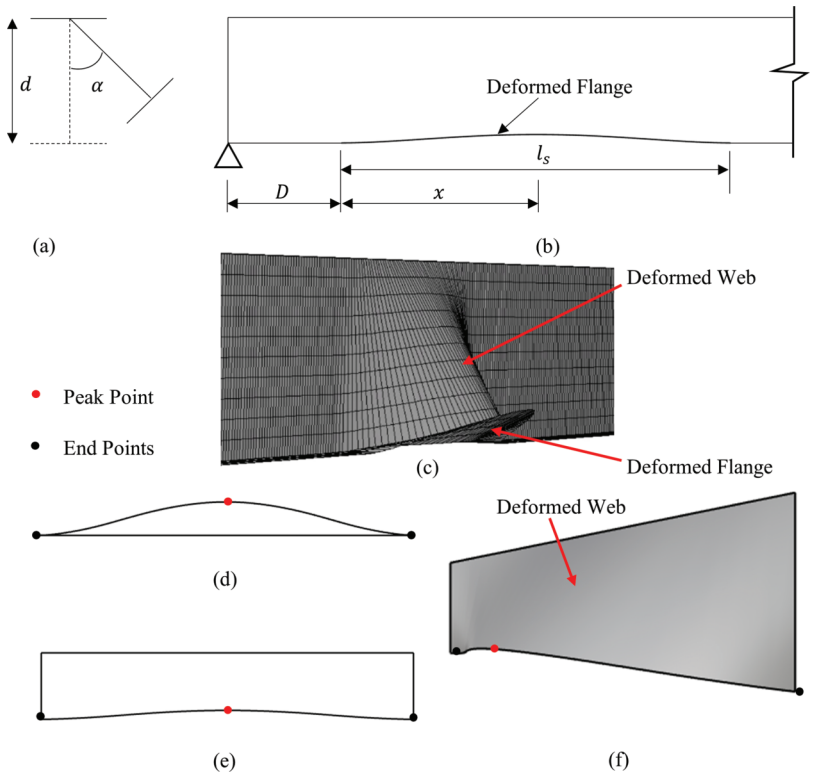

Figure 3.8 Parameters for approximating damage: (a) cross-section, (b) elevation, (c) 3D view, including mesh, (d) plan, (e) elevation, and (f) 3D view of the deformed shape of the center line of bottom flange (reprinted from Wang & Thrall, 2019).

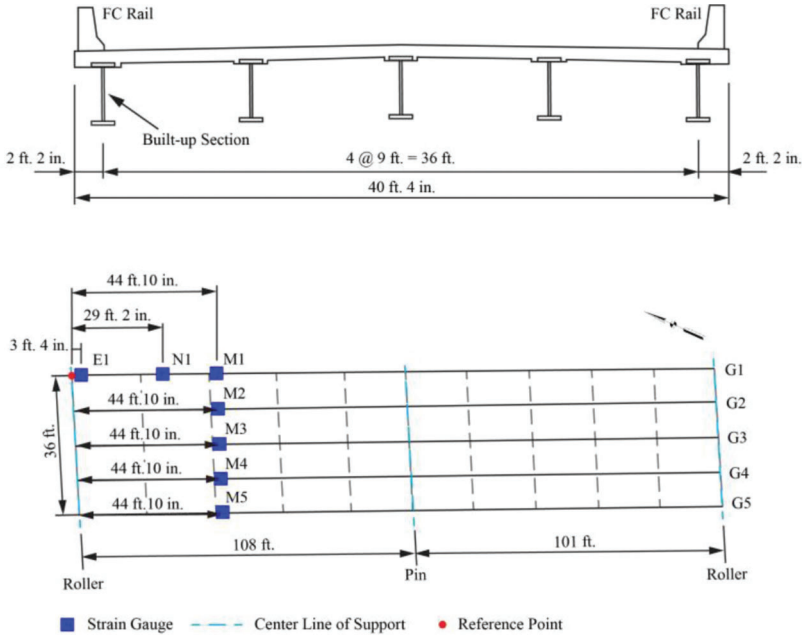

Figure 3.9 Cross-section, frame plan, and strain gauge locations for Asset 020-20-07229.

deck only. When comparing the two FE models, the behavior is very similar below the neutral axis, and varies slightly above the neutral axis, with the FE model that includes the rail indicating lower strains, as expected due to the increased stiffness provided by the rail.

Figure 3.11 shows the measured strains and the FE predictions in the exterior girder at the location of peak positive moment (Location M1), when the bridge is loaded by two trucks positioned to achieve peak positive moment. At this location, strain gauges were also adhered to the surface of the concrete rail (using a

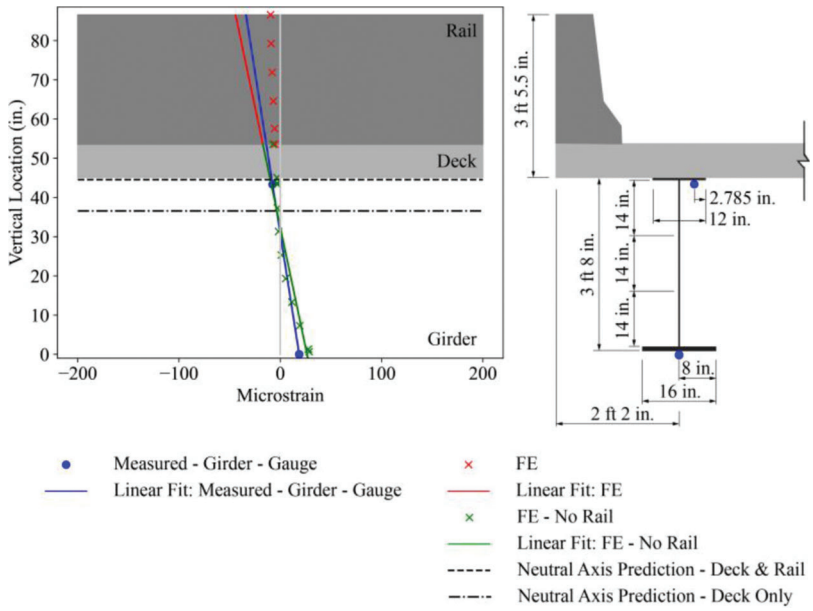

Figure 3.10 Asset 020-20-07229 Location E1: measured and predicted strains under statics load of two trucks positioned to induce peak positive moment.

TABLE 3.3
Asset 020-20-07229 location of the neutral axis, relative to the bottom of the bottom flange of the girder

Location	Measured	FE Prediction	Analytical: Deck	Analytical: Deck + Rail
E1	30.8	32.4[1]	36.6	44.5
M1	46.3	43.6	36.6	44.5
N1	49.1	43.5	36.6	–
M2	42.6	40.4	38.7	–
M3	NA	39.9	38.7	–
M4	NA	39.4	38.7	–
M5	NA	28.6	36.6	44.5

Note:
NA = not available.
[1]FE data is for the model with composite rail.

gauge length of 1 ft.), at the top, interior, and exterior of the rail. These are indicated by blue triangles in the plot, with their locations indicated by the same marker in the cross-section. From the measured data on the exterior of the rail, it is clear that the rail is engaged and carrying live load. The trend of the data is expected, with lower strains in the rail near the deck and higher strains at the top. Overall, there is very close agreement between the FE data and the measured data in the girder, including the neutral axis location (Table 3.3) and the curvature (Table 3.4), where curvature is calculated as the reciprocal of the slope of the best fit line. Note that all curvature shown in this report is an absolute value. The measured neutral axis is just 6.19% higher than the FE neutral axis. The measured curvature is just 7.51% lower than the FE curvature. The close agreement between the FE data, which assumes fully composite behavior between the girder, deck, and rail, indicates that the rail is indeed acting compositely with the section. This is also supported by the analytical predictions for the neutral axis when the rail is included (Table 3.3), which shows that the measured neutral axis is only 4.04% higher than this analytical prediction.

The measured strains on the surface of the rail in Figure 3.11, especially the interior of the rail, exceed both the expected strains based on the best fit line of the measured data in the rail (which represents the assumption that plane sections remain plane) and the FE predictions. This can be attributed to the fact that the interior and top gauges may have been exposed to heat (from both the sun and the nearby trucks) which would cause them to register compressive strains. These compressive strains can be approximated as the difference (Δ) in strain between the measured data in the rail and the data of the measured best fit line for the same vertical location. Given in the following order based on location of the strain gauges in the rail: top, interior top, interior bottom, Δ, given in microstrain is: 230, 250, 100, 51, and 48. The 51 and 48 microstrain

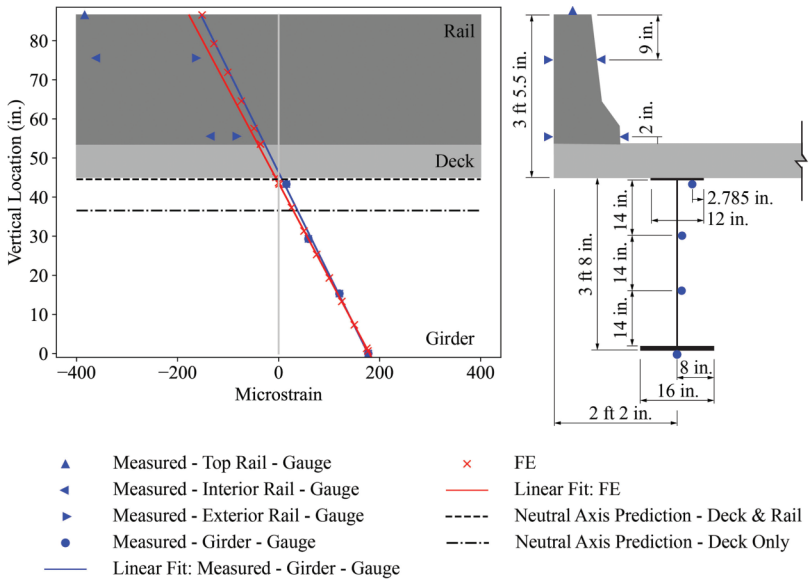

Figure 3.11 Asset 020-20-07229 Location M1: measured and predicted strains under the static load of two trucks positioned to induce peak positive moment.

TABLE 3.4
Asset 020-20-07229 curvature

Location	Measured	FE Prediction
E1	0.61	0.82[1]
M1	3.82	4.13
N1	4.47	4.66
M2	3.14	3.69
M3	NA	2.20
M4	NA	0.93
M5	NA	0.04

Note:
NA = not available.
[1]FE data is for the model with composite rail.

difference at the rail exterior can be attributed to the fact that the rail is not directly above the girder. 3D effects resulting from a truck loading that is eccentric to the rail are likely playing a role. The 100–250 microstrain in the rail interior can be attributed to both 3D effects and the above-mentioned thermal effects. This will be discussed further in Section 3.4.1.

Figure 3.12 shows the measured and FE data for Location N1, which is a positive moment region where there is also a gap in the rail. The gap in the rail is modeled by removing the shell elements of the rail at that location. The measured curvature at Location N1 is 17.0% higher compared to the measured curvature at Location M1. This indicates that the strains in the girder increase where there is a gap in the rail in the positive moment region. Note that according to the moment diagram of the girder the strains at Location N1 should be lower than Location M1. The measured neutral axis at Location N1 is higher than Location M1, which is unexpected and warrants further study. The FE data matches the measured data closely (Figure 3.12, Table 3.3, and Table 3.4). The FE data indicates that the strain in the deck is higher at Location N1 than Location M1. Note that there are two FE data points at the deck-rail interface in Figure 3.12. The high compressive strain is the data corresponding to the deck.

At the adjacent interior girder, Location M2, the measured and FE data generally agree (Figure 3.13, Table 3.3, and Table 3.4). Specifically, the measured neutral axis is just 5.44% higher than the FE value, and the measured curvature is 14.9% lower. The measured neutral axis location is 10.1% higher than the analytical prediction for an interior girder that is composite with the deck. This can be attributed to conservative assumptions on the effective flange width.

The measured and FE data for the other girders at Locations M3, M4, and M5 all show good agreement (Figure 3.14, Figure 3.15, and Figure 3.16). As expected, the strains decrease for the girders farther away from where the load is being applied.

3.3.2 Girder Distribution Factors

Girder distribution factors (GDF) were calculated using the results from the above-mentioned static tests. Unweighted GDFs were calculated as follows:

$$GDF_i = \frac{\varepsilon_i}{\sum_{i=1}^{n} \varepsilon_i} \qquad \text{(Eq. 3.1)}$$

where ε is the strain that occurred in the bottom flange of the girder under the static truck loading, i refers to the girder number, and n is the total number of girders, per the approach described in Ghosn et al. (1986) and Nowak et al. (2003). Weighted GDFs were also

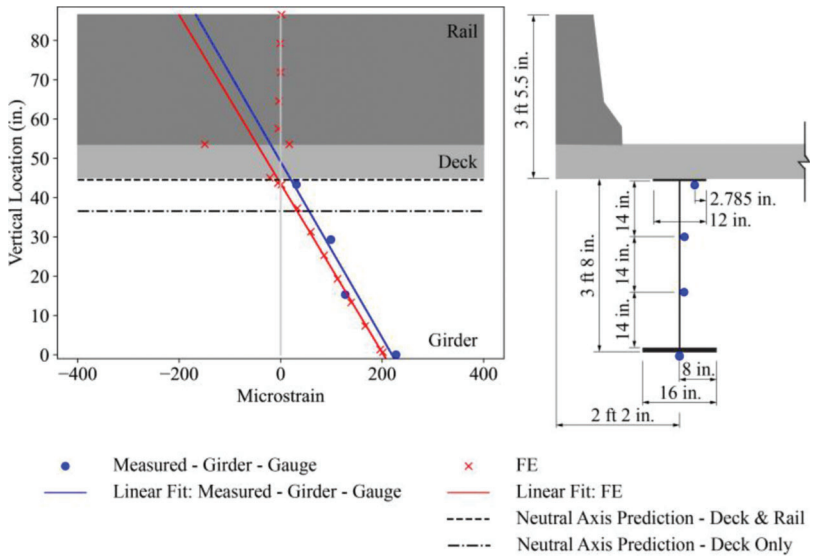

Figure 3.12 Asset 020-20-07229 Location N1: measured and predicted strains under the static load of two trucks positioned to induce peak positive moment.

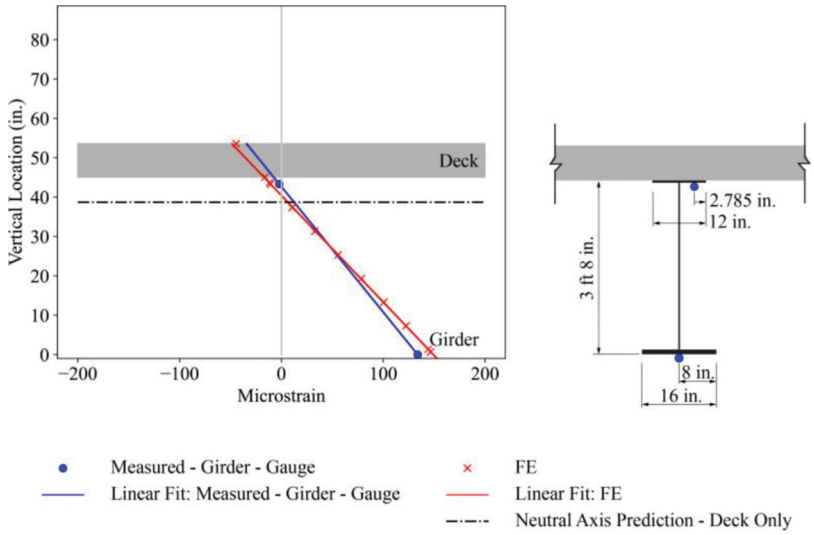

Figure 3.13 Asset 020-20-07229 Location M2: measured and predicted strains under the static load of two trucks positioned to induce peak positive moment.

calculated which take into account the composite behavior with the rail. These were calculated as follows:

$$GDF_i = \frac{\omega_i \varepsilon_i}{\sum_{i=1}^{n} \omega_i \varepsilon_i} \quad \text{(Eq. 3.2)}$$

where ω is the ratio of the section modulus of girder i to the section modulus of an interior girder. Stallings and Yoo (1993) used this approach for calculating GDFs to account for the edge stiffening effect of curbs, but not rails.

Figure 3.17 shows both the weighted and unweighted measured GDFs, also in comparison with the current bridge design code value for an exterior girder using the lever rule (AASHTO, 2020). As expected for the loading condition, the GDF for Girder 1 is highest and almost zero for Girder 5. The weighted GDF for Girder 1 is 22.4% higher than the unweighted version and is an indicator of the additional load that can be attracted into Girder 1 as a result of the rail. Importantly, the measured GDFs are all lower than the design code value, confirming the conservatism of current code even when considering weighted GDFs.

3.3.3 Behavior Under Crawl and Speed Tests

Both crawl (~5 mph) and speed (~45 mph) tests were performed (Table 3.1), with a single truck moving in the center of the lane above Girders 1 and 2. Live load amplification factors (AF) were then calculated as follows:

$$AF = \frac{max\ \varepsilon_{speed}}{max(\varepsilon_{crawl})} \quad \text{(Eq. 3.3)}$$

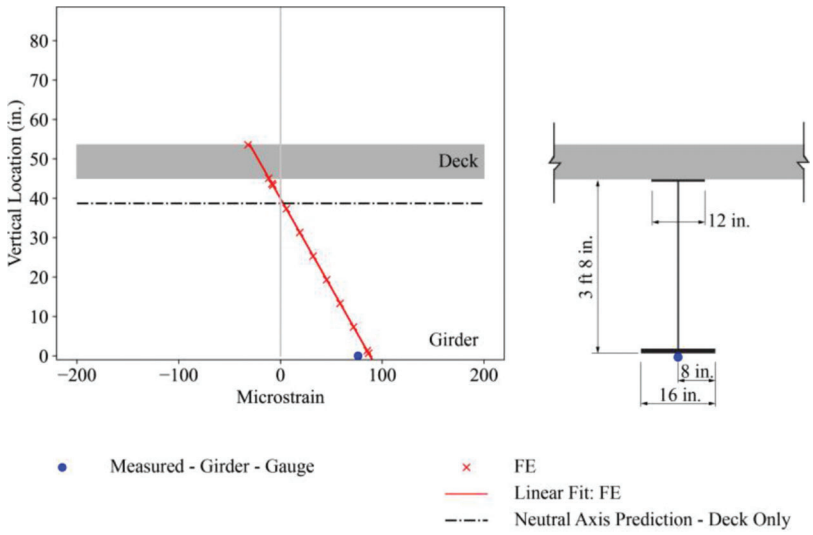

Figure 3.14 Asset 020-20-07229 Location M3: measured and predicted strains under the static load of two trucks positioned to induce peak positive moment.

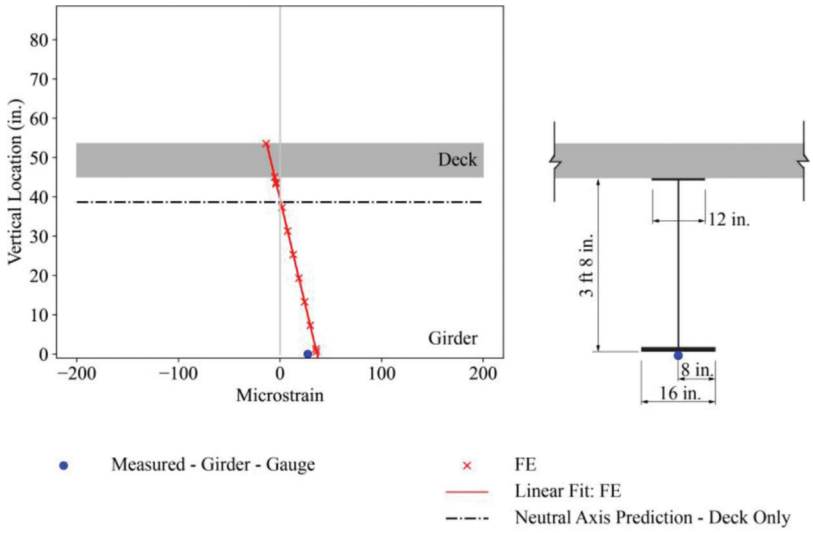

Figure 3.15 Asset 020-20-07229 Location M4: measured and predicted strains under the static load of two trucks positioned to induce peak positive moment.

where ε is the strain that occurred in the bottom flange of the girder at any point during the speed (numerator) or crawl (denominator) test.

Figure 3.18 show the live load amplification factors for each girder line of the bridge, with Girder 1 having the highest value of 1.18. As expected, Girders 1 and 2 had the highest amplification factors. The strain in the other girders was overall low. The highest value in Girder 1 indicates the conservatism of current design code which uses a 33% impact factor (AASHTO, 2020).

3.4 Two-Span Continuous Steel Girder Bridge Damaged by Vehicular Collision: Asset 037-55-05265 (Seymour District)

Asset 037-55-05265 (Figure 3.19) is a two-span (each span is 70 ft.) continuous, composite, steel girder bridge that was built in Martinsville, IN in 1966 and then reconstructed in 1990. It features FC rail, which is discontinuous above the pier.

As noted earlier, the behavior of Asset 037-55-05265 was previously monitored using DIC as a part of SPR-4119: *Assessment of Bridges Subjected to Vehicular Collision* (Wang & Thrall, 2019). In that prior study, only the surface strains of the bottom flanges (specifically the bottom of the cover plates) of the exterior and adjacent interior girders, on both sides of the bridge, were monitored. The current study adds to the knowledge of the behavior of the bridge by also using strain gauges to measure strains in the top and bottom flanges of the same girders, as well as the rails.

Figure 3.19 shows the instrumentation layout for the current project. Note that the designation D refers to the damaged region that occurs on Girder 6. A symmetric region on Girder 1 is also labeled with D.

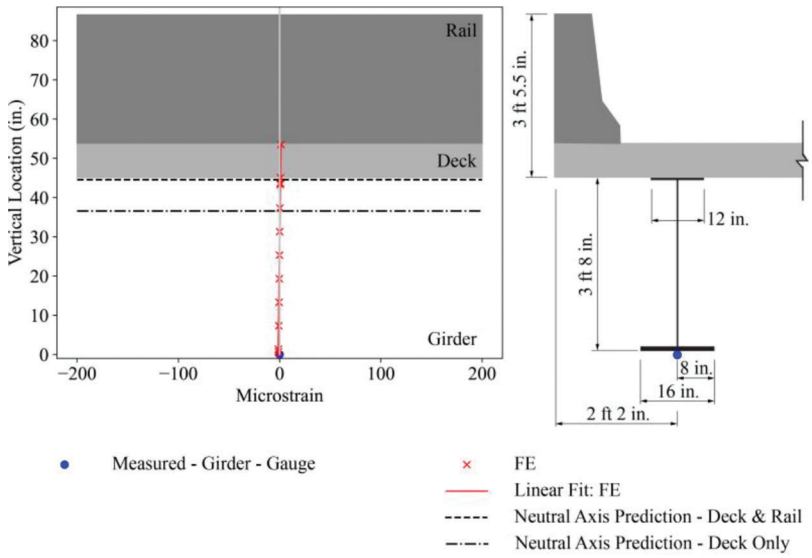

Figure 3.16 Asset 020-20-07229 Location M5: measured and predicted strains under the static load of two trucks positioned to induce peak positive moment.

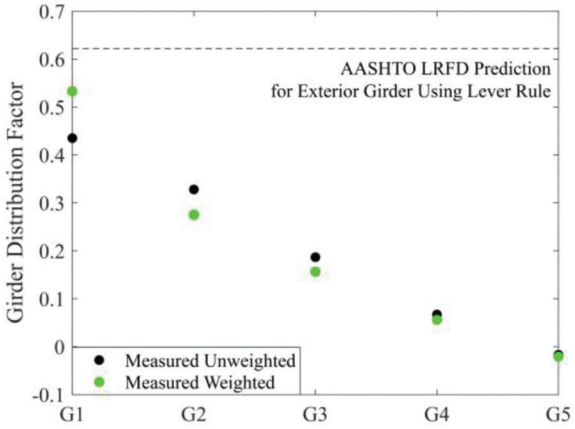

Figure 3.17 Asset 020-20-07229 girder distribution factors.

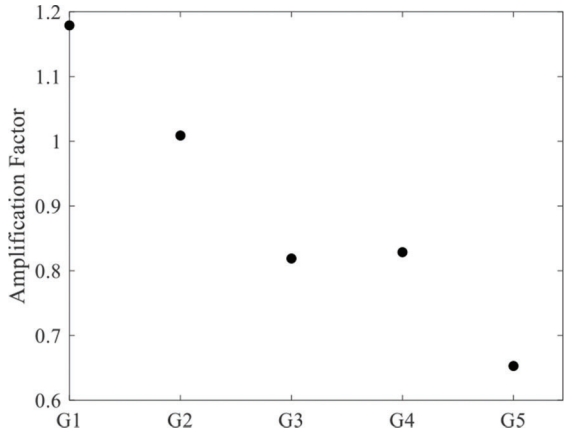

Figure 3.18 Asset 020-20-07229 live load amplification factors.

3.4.1 Behavior Under Static Truck Loads Positioned for Peak Positive Moment

This bridge has been subjected to vehicular collision in 2013 and in 2015, with the 2015 collision resulting in the displacement of the lower flange of Girder 6 in. by 6 in. (Figure 3.19, Figure 1.1). Between the monitoring of this bridge in Wang and Thrall (2019) and the current study, another vehicular collision occurred. Thus, the results of Wang and Thrall (2019) should not be directly compared to the current study as the bridge behavior may have changed.

The monitoring program included placing the two heavily loaded trucks in positions to induce peak positive moment on the damaged side and on the symmetric undamaged side. Data shown for each girder relates to when the trucks were loaded on that side.

Figure 3.20 and Figure 3.21 show the measured and FE numerical data for the exterior girder of the undamaged side. A gauge length of 1 ft. was used for the gauge on the rail. The average of the two gauges on the bottom flange when applicable was presented in the plots. The average value is used here to eliminate any out-of-plane bending of the bottom flange. From the measured strain in both the girder and the rail, it is clear that composite behavior between the girder, deck, and rail is achieved and that rail is participating in carry live load. More specifically, the measured neutral axis at both M1 and D1, exceeds the analytical prediction when considering the deck only by 28.9% and 19.4%, respectively (Table 3.5). The measured neutral axis at M1 and D1 are also just 1.81 % and 9.07%, respectively, below the analytical prediction when considering both the deck and rail in the composite section. The FE predictions shown in Figure 3.20 and Figure 3.21 assume fully composite behavior between the top flange of the girder and the deck, as well as between the deck and the rail. The close agreement between the measured and FE data, as also shown by the neutral axis location

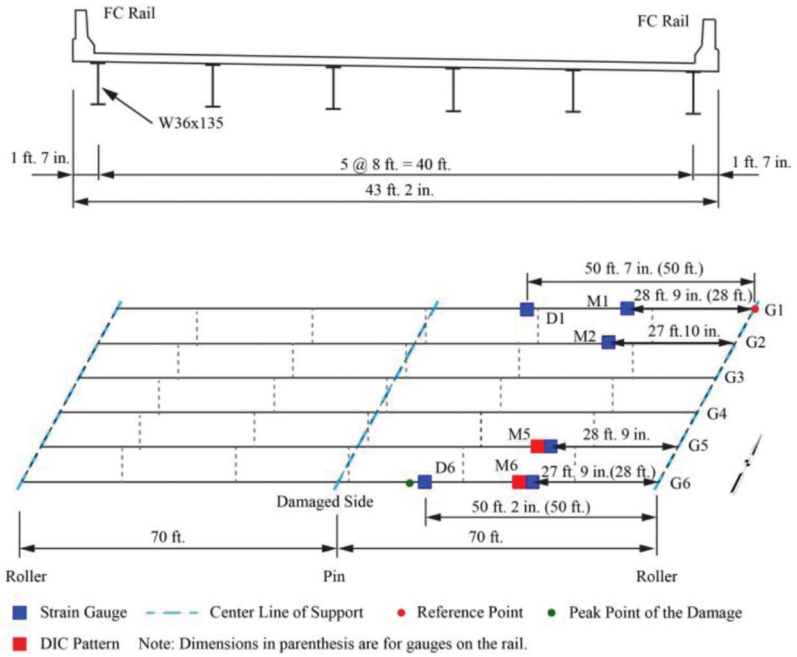

Figure 3.19 Cross-section, frame plan, and pattern locations for Asset 037-55-05265.

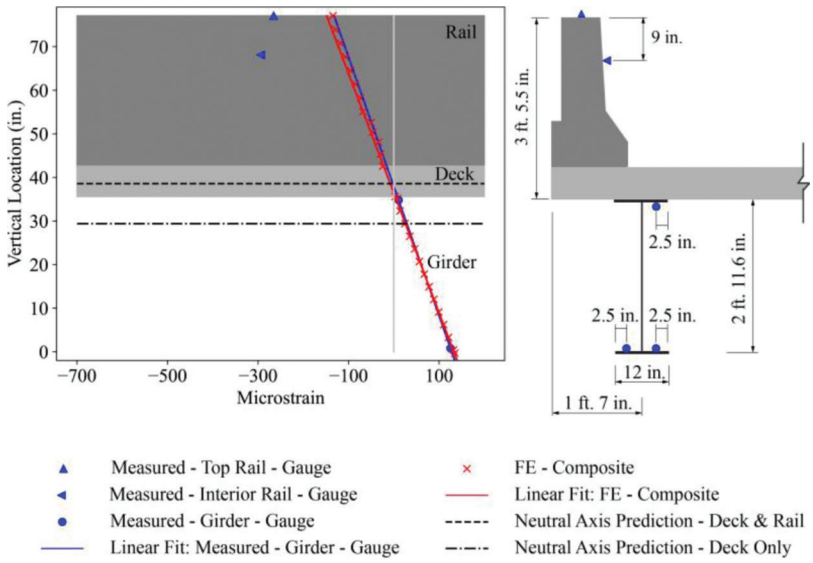

Figure 3.20 Asset 037-55-05265 Location M1: measured and predicted strains under the static load of two trucks positioned to induce peak positive moment.

and curvature in Table 3.5 and Table 3.6, further indicates that full composite behavior including the rail has been achieved. For example, at Location M1, the measured neutral axis is just 4.12% higher than the FE prediction. The measured curvature at the same location is just 7.67% higher than the FE prediction. As expected, the measured and FE prediction for the curvature (Table 3.6) are higher at Location M1 compared to Location D1, as the truck loads were positioned to achieve peak positive moment at Location M1.

The compressive measured strains on the exterior of the rail in Figure 3.20 and Figure 3.21 indicate that the rail is carrying live load. However, the measured strains at both locations are higher than predicted by the FE model and the best fit line of the measured strains on the girder. Further, the strain on the interior of the rail is higher than the top of the rail at Location M1, contrary to what would be expected. These higher compressive strains can be attributed to the strain gauges being subjected to heat radiating from the trucks as discussed in Section 3.3.1. The difference between the measured strains on the rail and the prediction by the best fit line of the measured strains on the girder, Δ can be used to estimate the thermal strain induced in the gauge for

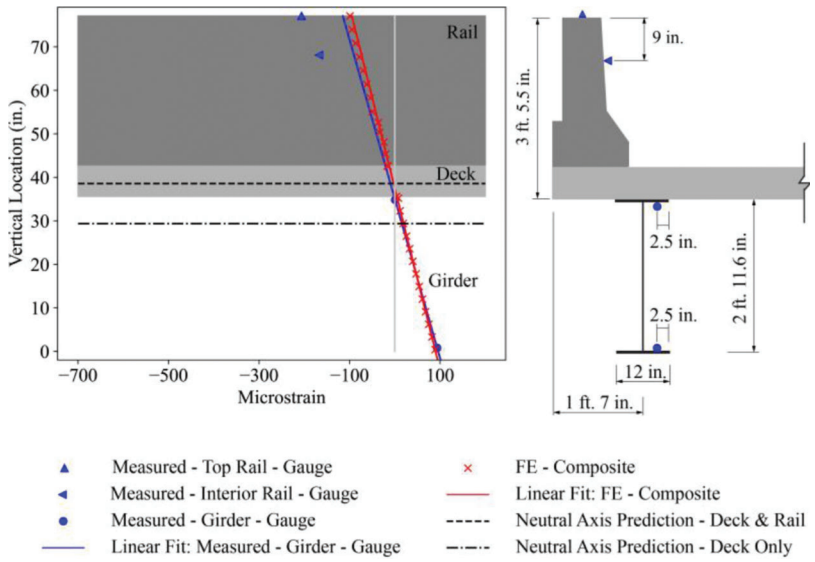

Figure 3.21 Asset 037-55-05265 Location D1: measured and predicted strains under the static load of two trucks positioned to induce peak positive moment.

TABLE 3.5
Asset 037-55-05265 location of the neutral axis, relative to the bottom of the bottom flange of the girder

Location		Measured	FE Composite Prediction	FE Untie DR Prediction	Analytical: Deck	Analytical: Deck + Rail
Undamaged Side	M1	37.9	36.4	–	29.4	38.6
	D1	35.1	37.5	–	29.4	38.6
	M2	35.5	35.1	–	31.3	–
Damaged Side	M5	32.5	33.7	33.9	31.3	–
	M6	40.8	35.5	35.1	29.4	38.6
	D6	18.5	43.7	25.8	29.4	38.6

Note: Analytical predictions do not take into account the shape of the damaged girder.

TABLE 3.6
Asset 037-55-05265 curvature

Location		Measured	FE Composite Prediction	FE Untie DR Prediction
Undamaged Side	M1	3.37	3.65	–
	D1	2.73	2.40	–
	M2	2.91	3.54	–
Damaged Side	M5	3.33	4.14	4.22
	M6	1.91	3.62	3.58
	D6	2.74	1.73	3.19

Location D1 and Location M1 (Table 3.7). The magnitude of Δ for these locations is on the same order as was observed for Asset 020-20-07229.

At the interior girder on the undamaged side, Location M2, there is close agreement between the measured and FE data (Figure 3.22, Table 3.5, and Table 3.6), with measured neutral axis 1.14% higher than the FE prediction. The measured neutral axis is 13.4% higher than the analytical prediction for composite behavior with the deck. This is similar to what was found in Asset 020-20-07229 and is likely related to conservative assumptions on the effective flange width.

Overall, the comparisons at Locations M1, D1, and M2 indicate that the FE models are able to accurately predict the behavior of the bridge on the undamaged side.

Figure 3.23 shows the measured and FE data at the region of greatest damage on the exterior girder (on the damaged side), Location D6. Based on the measured data from the gauges on the flanges, the neutral axis is

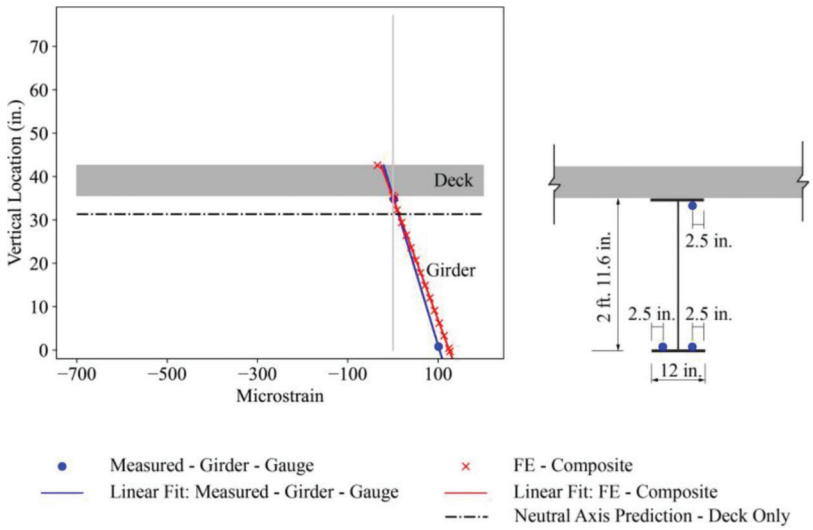

Figure 3.22 Asset 037-55-05265 Location M2: measured and predicted strains under the static load of two trucks positioned to induce peak positive moment.

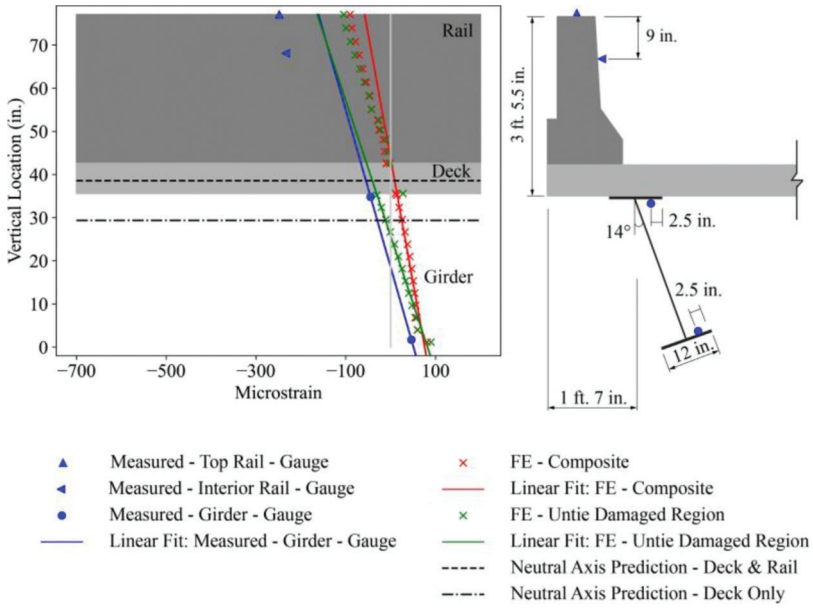

Figure 3.23 Asset 037-55-05265 Location D6: measured and predicted strains under the static load of two trucks positioned to induce peak positive moment.

approximately halfway up the girder (18.5 in. measured from the bottom of the bottom flange of the undamaged section, compared to a total depth of 35.6 in.). This indicates that the girder is no longer composite with the deck and that the shear connection between the top flange of the girder and the deck was damaged during the vehicular collision. Comparing measured data at Location D6 with the symmetric undamaged region (Location D1, Figure 3.21), clearly shows this change in behavior. Indeed, the neutral axis at D1 is 35.1 in., compared to 18.5 in. at D6 (Table 3.5). This is further supported by the FE data. The red data in Figure 3.23 is for an FE model in which the girder, deck, and rail are all fully composite. The green data is for an FE model where the constraints used to implement composite behavior between the top flange of the girder and the deck are released to make the system non-composite in the damaged region, referred to as "Untie Damaged Region." The composite behavior between the rail and deck is maintained in this model. The closer agreement between the "Untie Damaged Region" model and the measured data indicates that the shear connectivity was indeed damaged. Differences between the measured data and the "Untie Damaged Region" FE predictions can be attributed to errors in the assumed geometry of the deformed girder in the FE model, as this geometry was based on limited field data.

TABLE 3.7
Measured strain of the top and interior of the rail (unit: microstrain)

Location		Measured Strain	Predicted Strain	Δ
Undamaged Side	M1–Top	-265	-132	-133
	M1–Interior	-294	-102	-192
	D1–Top	-206	-115	-91.2
	D1–Interior	-167	-90.3	-77.1
Damaged Side	M6–Top	-547	-69.5	-477
	M6–Interior	-468	-52.3	-416
	D6–Top	-248	-161	-87.2
	D6–Interior	-233	-136	-97.0

The measured strains in Figure 3.23 and Table 3.7 do show that that rail is participating in carrying live load. These measured strains are higher than the "Untie Damaged Region" FE model and best fit line of the measured strains on the girder would predict. This can be attributed to the same thermal strains discussed above. Indeed, the Δ for the gauge on the top and interior of the rail is comparable with the values for D1, indicating similar thermal strain induced by the heat radiation from the trucks.

Along the same damaged girder but at the location of peak positive moment (Location M6), Figure 3.24 shows that the composite behavior is intact. Specifically, the measured data on the girder indicates a neutral axis location of 40.8 in., which is 5.70% higher than the analytical prediction for the neutral axis when the rail is considered to act composite. The measured data is also close to the FE model where full composite behavior is assumed. The differences can again be attributed to errors in approximating the shape of the damaged girder. Notably, the FE model for the "Untie Damaged Region" predicts almost the same strains as the FE model with full composite behavior. Thus, the damage to the shear connection in the damaged region does not have an impact on the behavior on the positive moment region of the girder.

The measured strains of the rail in Figure 3.24 and Table 3.7 show that the rail is participating in carrying live load. The measured strains, however, are far higher in magnitude than the FE predictions and predictions from the best fit line of the measured strains on the girder. While there could be thermal strains, similar to what was found at Location M1 and D1, the measured strains at Location M6 far exceed these. The difference between the Δ values between M6 and M1 are -344 microstrain for the gauge on the top of the rail and -224 microstrain for the gauge on the interior of the rail. Likely, the bridge rail is picking up higher load in this region as the load is redistributed away from the damaged region. This is an area for future research.

When comparing Location M6 on the damaged girder (Figure 3.24) to Location M1 on the symmetric undamaged girder (Figure 3.20), the measured data indicates that the damaged girder is carrying less load while the rail is carrying more load. Specifically, the measured curvature at Location M1 is 3.37 compared to 1.91 at Location M6. This indicates that load redistribution is occurring, away from the damaged girder. The FE models are not able to fully capture this redistribution.

At Location M5 in the adjacent interior girder (Figure 3.25) the strains are very similar to the symmetric interior girder on the undamaged side at Location M2 (Figure 3.22). The measured curvature at Location M5 is 3.33 compared to 2.91 at Location M2. This indicates that the damaged exterior girder is not impacting the behavior of the adjacent interior girder. However, the agreement between the FE and numerical data at Location M5 is not as good as was observed at the symmetric interior girder, Location M2. This is likely due to the assumptions made in modeling the damaged girder is influencing the adjacent girder in the FE model. There is negligible difference between the two FE models at Location M5, indicating that the loss of shear connectivity in the damaged region does not impact the behavior of the peak positive moment region of the adjacent interior girder.

Figure 3.24 and Figure 3.25 feature both strain gauge data and data measured via DIC, indicated by magenta squares. DIC measures the behavior of the bottom of the cover plate while the strain gauge measures the behavior of the top of the flange. At Location M6, the strain measured by DIC is 3.95% higher than the measurement of strain gauge. At Location M5, the strain measured by DIC is 37.7% lower than the measurement of strain gauge. It is clear that the DIC and strain gauge data generally agree, given that they are also measuring strain at different vertical locations on the cross-section. Thus, this report can also conclude that DIC is further validated as a strategy for field monitoring of bridges.

3.4.2 Behavior Under Crawl and Speed Tests

Crawl (~5 mph) and speed (~20 mph) tests were performed on both the damaged side of the bridge and the undamaged side of the bridge (Table 3.1), with a single truck moving in the center of the lane.

Figure 3.26 shows the amplification factors, calculated per Equation 3.3, on both the undamaged (left) and damaged (right) side of the bridges. Both girders on the damaged side have significantly higher amplification

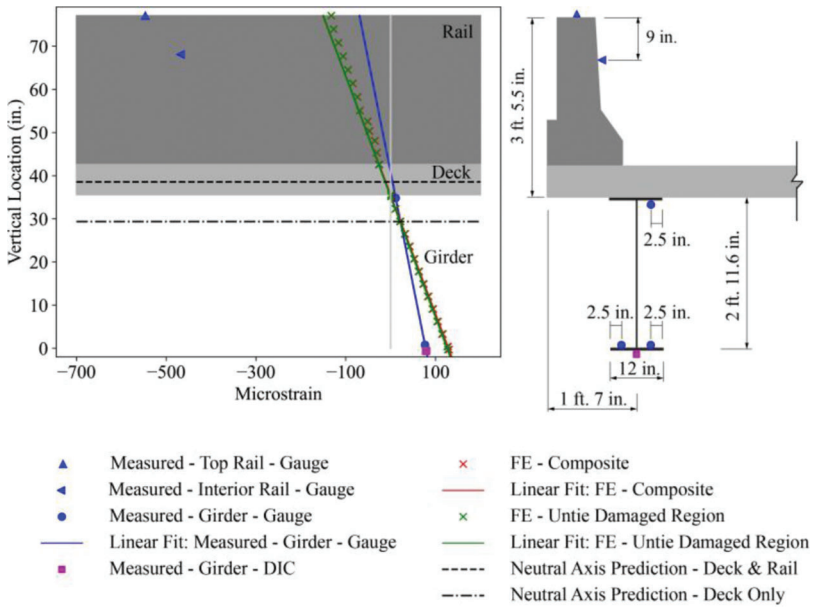

Figure 3.24 Asset 037-55-05265 Location M6: measured and predicted strains under the static load of two trucks positioned to induce peak positive moment.

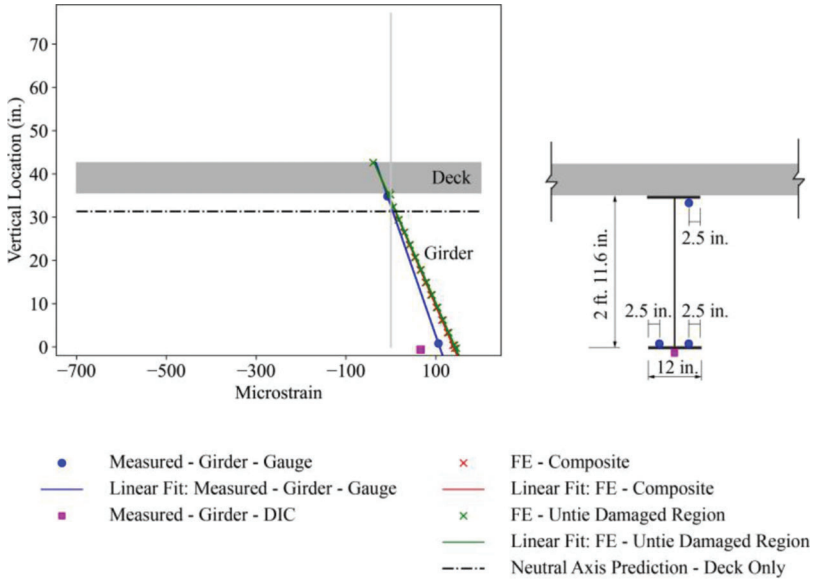

Figure 3.25 Asset 037-55-05265 Location M5: measured and predicted strains under the static load of two trucks positioned to induce peak positive moment.

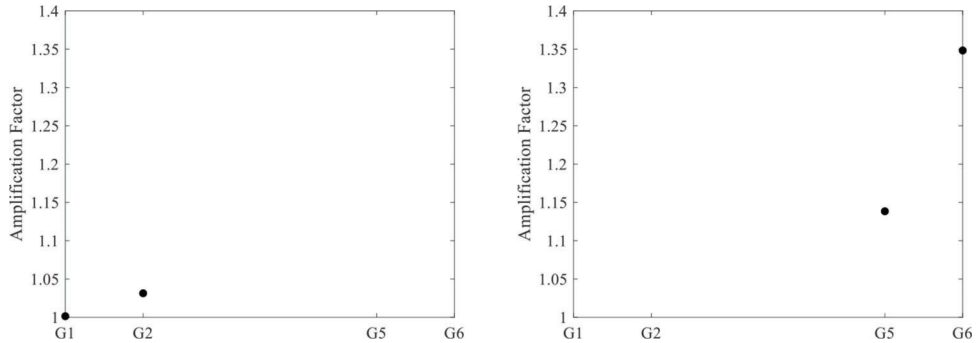

Figure 3.26 Asset 037-55-05265 live load amplification factors: left plot shows the amplification factor when trucks were driving on the undamaged side and the right plots shows the amplification factor when trucks were driving on the damaged side.

factors than the symmetric undamaged girders. The damaged girder (G6) had the highest overall amplification factor. On the undamaged side, the interior girder had the higher amplification factor compared to the exterior girder. This was opposite to what occurred on the damaged side. Note that the truck drivers did their best to maintain consistent crawl and speed tests on each side of the bridge, but there is inherently some variability in actual speeds driven. Nonetheless, this provides interesting data on how bridge behavior is affected by a vehicular collision.

Notably, the highest amplification factor for Asset 020-20-07229 was 1.18 in the exterior girder which demonstrated conservatism of the 33% impact factor in current design code (Figure 3.18). In comparison, the damaged girder G6 in Asset 037-55-05265 had an amplification factor of 1.35, which exceeds this 33%. While amplification factors could vary based on the surface condition of the structure, the 1.35 amplification factor for damaged girder G6 compared to 1.00 for the symmetric undamaged girder G1 indicates that damage to a girder increases the amplification factor.

3.5 Six-Span Continuous Prestressed Concrete Girder Bridge: Asset 331-71-08732 (La Porte District)

Asset 331-71-08732 (Figure 3.27) is a six-span (two end spans of 95 ft. and four inner spans of 95 ft. 6 in.) continuous, composite, prestressed concrete girder bridge that was built in Mishawaka, IN in 2019. The north-bound bridge was monitored. One side of the bridge features FC rail and the other side PS-1 with a sidewalk. There were no discontinuities in the PS-1 or FC rail. As this was a newly constructed bridge, the researchers were able to place sister bar gauges in both the deck and the rail.

Field monitoring focused on loading each side of the bridge (separately) to be able to study and compare both the FC and PS-1 rail behaviors. Figure 3.27 shows the longitudinal positions of the strain gauges.

3.5.1 Behavior Under Static Truck Loads Positioned for Peak Positive Moment

The monitoring program included placing the two heavily loaded trucks in positions to induce peak positive moment on the FC side and then on PS-1 side. Data shown for each girder relates to when the trucks were loaded on that side. For the PS-1 side, the trucks were driven up on the sidewalk to be able to be positioned as closely as possible to the rail. A gauge length of 3 in. was used for all external strain gauge locations as no cracks were expected in the rail of this newly built bridge.

Figure 3.28 shows that the measured strain near the abutment at Location E1 on the FC side is nearly zero. A challenge in the FE modeling of this bridge was the semi-integral abutments at either end. Thus, two FE models were built. One assumed pin restraints at both abutments and roller restraints above all the piers (for each girder line), referred to as "Pin" and shown in red in Figure 3.28. The other assumed a pin restraint at one abutment and roller constraints at all piers and the other abutment (for each girder line), referred to as "Roller" and shown in green in Figure 3.28. Neither fully captures the behavior of a semi-integral abutment but provide reasonable bounds on behavior for this research. The FE predictions in Figure 3.28 indicate that the "Pin" FE model more closely approximates the measured behavior.

Figure 3.29 shows the measured and FE predictions for the positive moment region, Location M1, on the

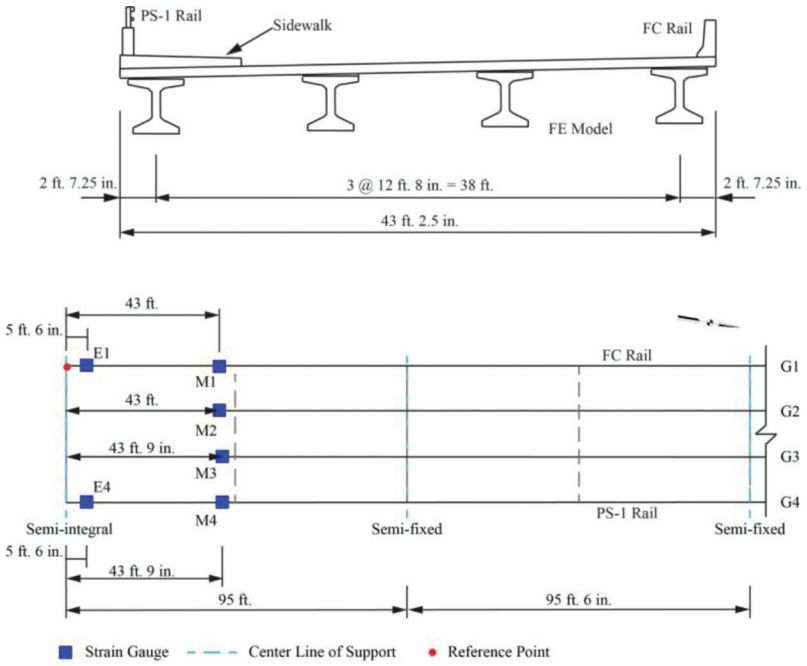

Figure 3.27 Cross-section, frame plan, and strain gauge locations for Asset 331-71-08732.

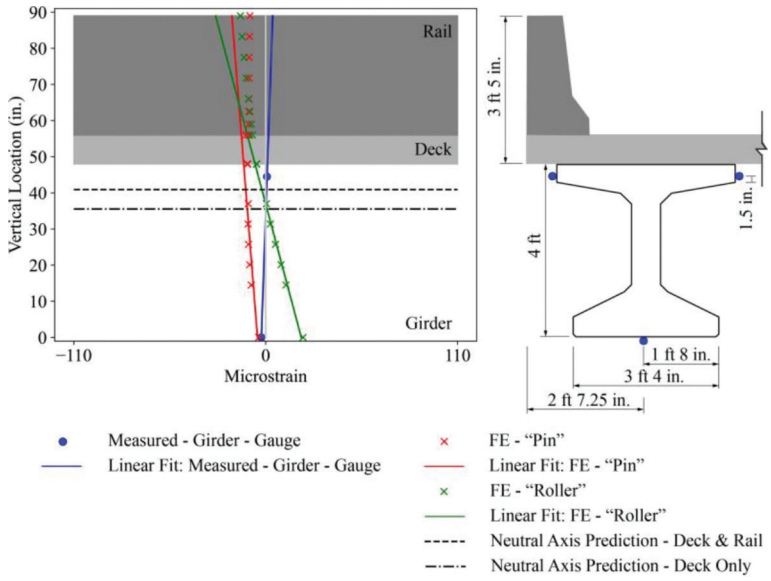

Figure 3.28 Asset 331-71-08732 Location E1: measured and predicted strains under the static load of two trucks positioned to induce peak positive moment.

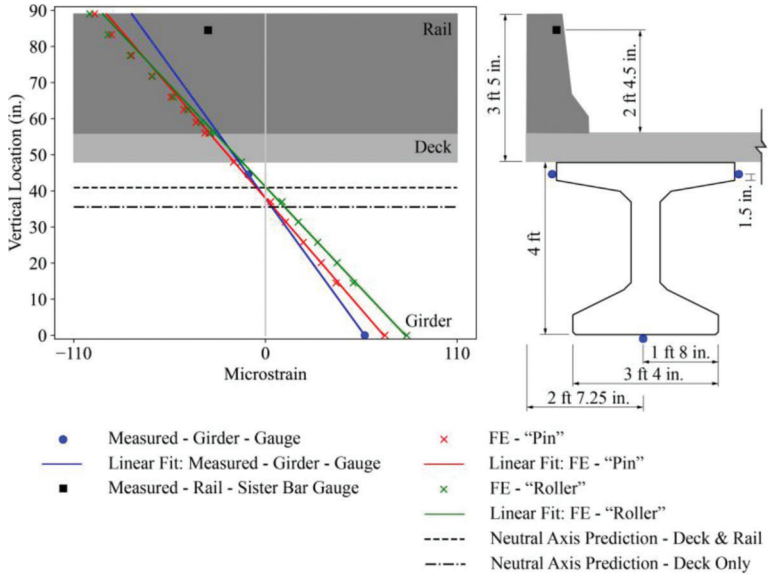

Figure 3.29 Asset 331-71-08732 Location M1: measured and predicted strains under the static load of two trucks positioned to induce peak positive moment.

FC side. As was the case for Location E1, the "Pin" FE model better matches the measured data. Note that due to uncertainties in the material properties of the concrete, it is expected that the FE results do not match the measured data as closely as was found for the steel girder bridges. Specifically, the material properties were based on the design compressive strength of each concrete component. However, it is likely that the concrete of the built structure has much higher compressive strengths as a contractor would want to make sure they achieve the minimum required strengths. The neutral axis of the measured data is just 0.263% lower than the "Pin" FE predictions and the curvature is 16.2% lower (Table 3.8 and Table 3.9). As the FE model assumes full composite behavior including the rail, this verifies that the rail is acting compositely in the built structure. Further, the neutral axis is just 7.33% lower than the analytical prediction including the rail. Unfortunately, a sister bar gauge that was in the deck malfunctioned and no data was retrieved. However, the compressive strain registered in the sister bar of the FC rail indicates that the rail is clearly participating in carrying live load. The magnitude of the strain is lower than what would be expected from the FE model and assuming plane sections remain plane from the measured data on the rail (i.e., following the blue linear fit line). This may be due to errors in the positioning of the sister bar gauge, the afore-mentioned uncertainty in the material pro-

TABLE 3.8
Asset 331-71-08732 location of the neutral axis, relative to the bottom of the bottom flange of the girder

Location	Measured	FE Prediction[1]	Analytical: Deck	Analytical: Deck + Rail
M1	37.9	38.0	35.5	40.9
E1	34.1	-28.3	35.5	40.9
M2	NA	37.4	38.0	–
M3	NA	39.4	38.0	–
M4	45.5	41.8	35.5	45.7
E4	73.3	-28.9	35.5	45.7

Note:
NA = not available.
[1]FE predictions are for the "Pin" model only.

perties assumed in the FE model, or 3D effects in the bridge.

At the interior girder on the FC side, Location M2 (Figure 3.30), the measured and FE data agrees well. There is little difference between the "Pin" and "Roller" FE models at this location, showing the boundary condition has a lesser effect on the interior girder line under this loading.

When the trucks were loaded on the PS-1 side, little strain is measured at the abutment Location E4 (Figure 3.31). Like Location E1, the "Pin" FE model better matches the behavior at the abutment. In Figure 3.31 and the other figures showing data for the PS-1 side, note that the light grey represents the sidewalk, the medium grey the deck, and the dark grey the rail.

Like the FC side, the measured data at the peak positive moment location (Location M4) on the PS-1 side indicates the rail is participating in carrying live load and that full composite behavior is achieved. Specifically, the measured data agrees well with the FE "Pin" model which assumed full composite behavior between the rail, sidewalk, deck, and girder (Figure 3.32, Table 3.8, and Table 3.9). The neutral axis of the measured data is just 8.85% higher than the FE data. Further, the neutral axis of the measured data is also just 0.440% below the analytical prediction when the rail and sidewalk are considered. The sister bar gauges

TABLE 3.9
Asset 331-71-08732 curvature

Location	Measured	FE Prediction[1]
M1	1.50	1.79
E1	0.07	0.17
M2	NA	1.21
M3	NA	1.05
M4	1.15	1.58
E4	0.05	0.17

Note:
NA = not available.
[1]FE predictions are for the "Pin" model only.

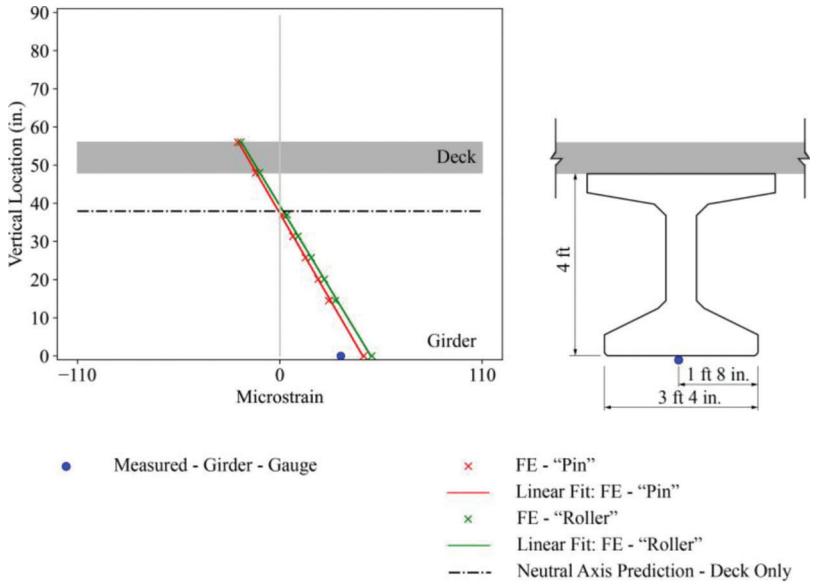

Figure 3.30 Asset 331-71-08732 Location M2: measured and predicted strains under the static load of two trucks positioned to induce peak positive moment.

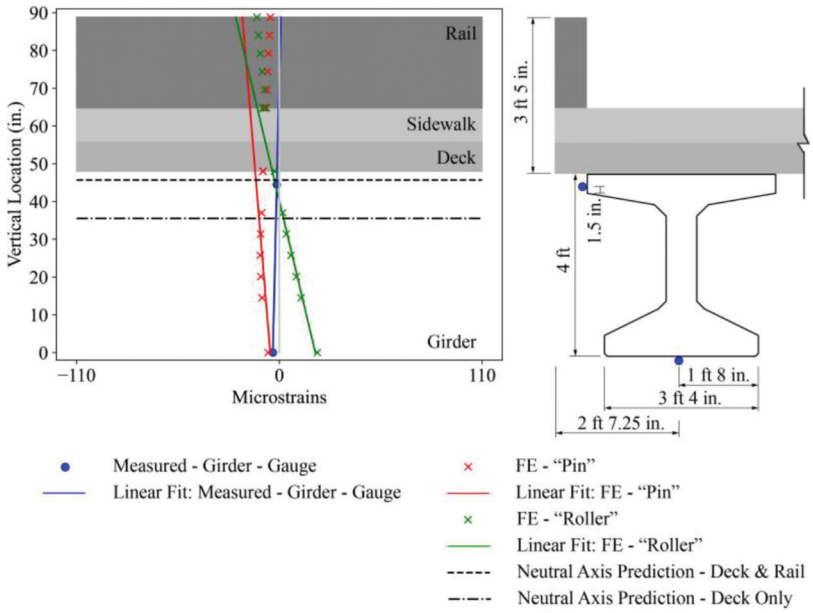

Figure 3.31 Asset 331-71-08732 Location E4: measured and predicted strains under the static load of two trucks positioned to induce peak positive moment.

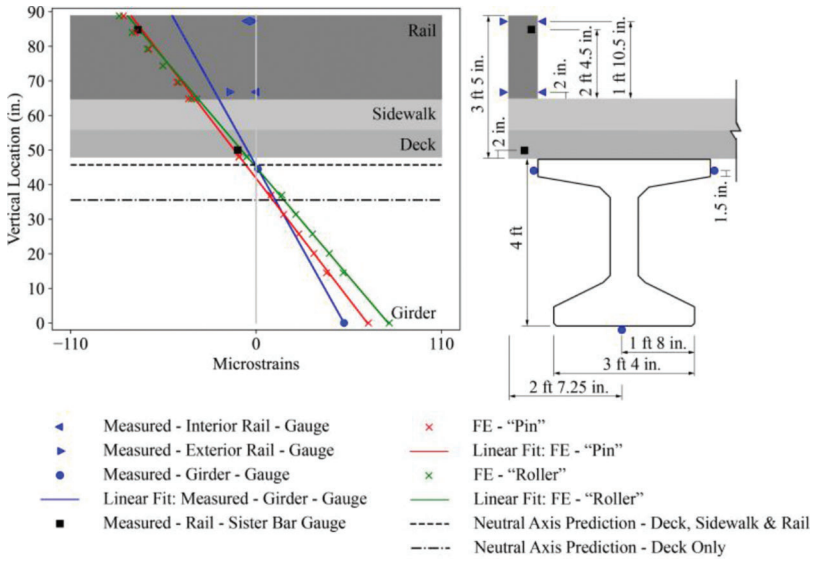

Figure 3.32 Asset 331-71-08732 Location M4: measured and predicted strains under the static load of two trucks positioned to induce peak positive moment.

in both the deck and rail track directly with FE predictions. The measured strains on both the exterior and the interior surface of the rail, however, are quite low. As mentioned before, a gauge length of 3 in. was used for this bridge. Therefore, potential local cracks in the concrete would have a significant effect on the measured strain. The cracks would reduce the surface strains of the concrete but would have less impact on the strain in the rebar.

At the interior girder Location M3, the measure data agrees well with the FE predictions (Figure 3.33). Similar to Location M2, there is little difference between the "Pin" and "Roller" FE models at the interior girder.

3.5.2 Girder Distribution Factors

Figure 3.34 shows the unweighted GDFs (calculated per Equation 3.1) and weighted GDFs (calculated per Equation 3.2, also including the sidewalk) when the trucks are loaded on the PS-1 side (left) and the FC side (right). Comparisons are also made to the design code value for an exterior girder using the lever rule (AASHTO, 2020). As expected and consistent with the

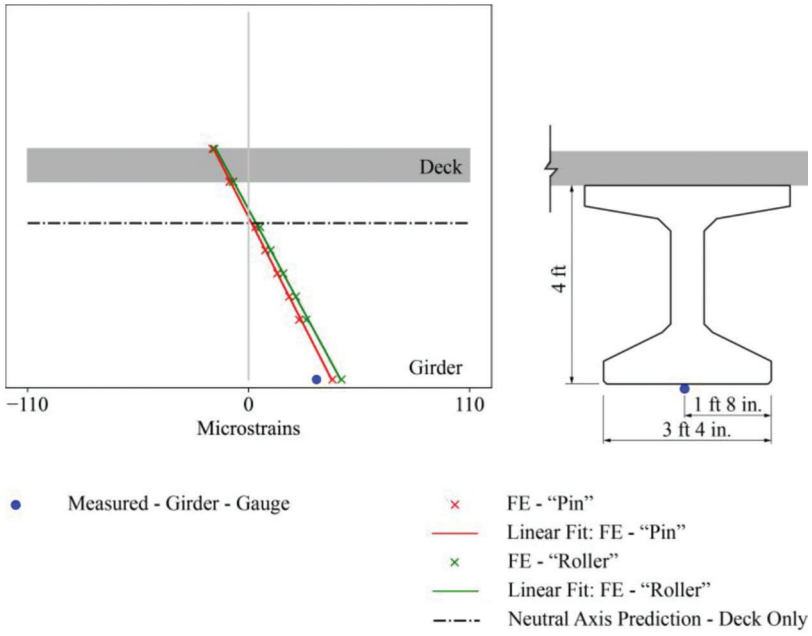

Figure 3.33 Asset 331-71-08732 Location M3: measured and predicted strains under the static load of two trucks positioned to induce peak positive moment.

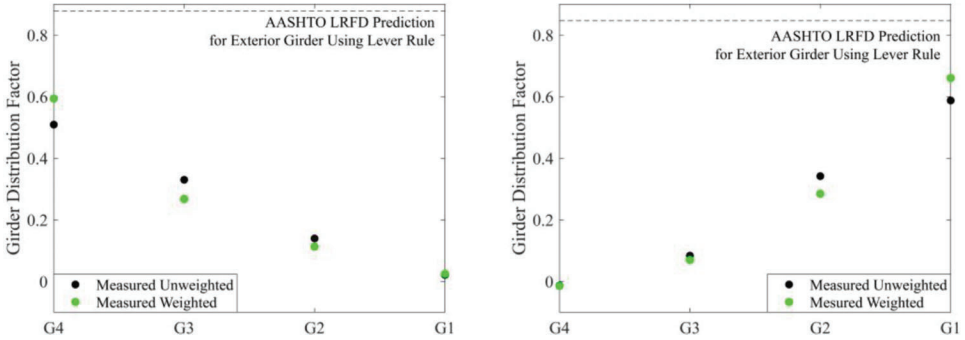

Figure 3.34 Asset 331-71-08732 girder distribution factors: left plot indicates when truck loading was on the PS-1 side (above Girders 3 and 4) and right plot indicates when truck loadings was on the FC side (above Girders 1 and 2).

TABLE 3.10
Summary of behavior of monitored bridges

Asset No.	Research Findings
020-20-07229	Measured strains on surface of FC rail indicate that FC rail carries live load. Composite behavior between the girder and deck not fully developed near abutment. Full composite behavior between the rail, deck, and girder can be achieved. Strains in the exterior girder increase when there is a gap in the rail in the positive moment region. Girder distribution factors and live load amplification factors in current design code are conservative.
037-55-05265	Measured strains on surface of FC rail indicate that FC rail carries live load, on both the damaged and undamaged sides of the bridge. Full composite behavior between the rail, deck, and girder can be achieved. Vehicular collision can damage the shear connection between the top flange of the girder and the deck. Damaged girders have lower strains than symmetric undamaged girders. Load redistribution away from damaged girders to bridge rail likely occurs. Damaged girders and adjacent interior girders have higher live load amplification factors.
331-71-08732	Measured strains of rebar within both FC and PS-1 rails indicates that both of these rail types carry live load. Full composite behavior between the rail, deck, and girder can be achieved. A sidewalk on one side allows a more even distribution of load among girders.

findings for Asset 020-20-07229 (Section 3.3.2), the girders with the highest GDFs correspond to the side that is loaded and the weighted GDFs are about 15% higher than unweighted GDFs for the exterior loaded girder. When comparing the measured GDFs to the design code values, it is clear that the results indicate the conservatism of the design code. In comparing the two sides of the bridge to one another, both the weighted and unweighted GDFs on the PS-1 side are lower than on the FC side (e.g., the weighted GDF for Girder 4 on the left plot is 10.0% lower than for Girder 1 on the right plot). This can be attributed to the sidewalk on the PS-1 side more evenly distributing the load compared to the FC side which does not have a sidewalk.

3.6 Summary

Table 3.10 summarizes the main research findings from each bridge studied. Overall, the strong agreement between the measured data and the FE predictions indicates that validated numerical modeling approaches have been developed for both steel and prestressed concrete girder bridges.

4. NUMERICAL PARAMETRIC INVESTIGATION

4.1 Approach

Using the validated numerical modeling approaches developed in Section 3, numerical parametric investigations were performed on two- and three-span continuous steel and prestressed concrete girder bridges. For each bridge type, a "prototype bridge" was selected from the database of INDOT bridges. The target span for two-span continuous bridges was 110 ft. for each span, and the target span for the three-span continuous bridges was 75 ft. for the midspan, based on the inventory of common bridge spans in Maldonado and Bowman (2019). It was also required that the prototype bridge passed over traffic as the impetus of this study relates to bridges subjected to vehicular collision. Minor modifications of the prototype structures were made for simplicity, as described in the relevant sub-sections.

A parametric, 3D FE model of each modified prototype bridge was built in CSiBridge, using the same modeling assumptions as discussed in Section 3.2. The following parameters were then varied: (1) rail type, with FT, FC, PS-1, PS-2 (Figure 3.4), and no rail configurations evaluated, (2) continuity of the rail at the piers for each of the rail types, and (3) skew angle of the bridge, comparing zero- and 30-degree skew angle. For the studies with the 30-degree skew, the prototype bridges were modified to have the skew. Each bridge was studied under the effect of two lanes of vehicular traffic (0.64 klf per lane, uniformly distributed along a 12-ft. width in the transverse direction measured from the interior of the rail at each side of the deck) across the entire length of the bridge. No design trucks were included. Boundary conditions were as follows: for the two-span continuous steel girder bridges, it was assumed roller at the abutments and pin at the pier; for the three-span continuous steel girder bridges, it was assumed pin at one of the abutments and roller at the other abutment and both piers; for both two- and three-span continuous prestressed girder bridges, it was assumed pin at the abutments and roller at the piers. Results focus on behavior in the positive moment region only.

4.2 Steel Girder Bridge Parametric Study

This study assumed that none of the girders have been damaged and that full composite behavior is developed between the top flange of the girder and the deck as well as between the deck and the rail.

4.2.1 Two-Span Continuous Steel Girder Bridge Behavior

The two-span continuous steel girder prototype bridge structure is based on Asset 020-20-07229. It has been modified as follows: (1) both spans are 108-ft. long, (2) girder section sizes are the same as in the 108-ft. span in the built bridge, and (3) diaphragm spacing is assumed as in the 108-ft. span in the built bridge. Figure 4.1 shows the plan and cross-section of the modified prototype structure, and indicates the location where behavior was studied.

Figure 4.2 and Table 4.1 show the effect of the rail type on behavior, as compared to an FE model where there was no rail modeled. All of the rail types decreased the curvature, meaning reduced the strain in the deck and the girder, compared to the comparable bridge with no rail modeled. Likewise, the neutral axis increased in vertical location. The FT rail provided the greatest benefit, with decreasing benefit from the FC, PS-1, and PS-2 rail types (in order of decreasing benefit). This trend follows with the moment of inertia of the composite section (including the rail), as expected.

Figure 4.3 shows the effect of a discontinuity in the rail at the pier for the two-span continuous steel girder bridge with the FC rail type. Figure C.1, Figure C.2, and Figure C.3 (see Appendix C) show the effect of a discontinuity in the rail at the pier for the two-span continuous steel bridge with the FT, PS-1, and PS-2 rail types, respectively. For all of the rail types, there is negligible difference between the strain profiles at the peak positive moment region.

Figure 4.4 shows the prototype structure with a 30-degree skew and indicates the relative location of the FE data. Figure 4.5 shows the effect of this 30-degree skew angle on the behavior of a two-span continuous steel girder bridge with the FC rail type, as compared to the bridge with no skew. Figure C.4, Figure C.5, and Figure C.6 (see Appendix C) show the effect of this 30-degree skew angle on the behavior of a two-span continuous steel girder bridge with the FT, PS-1, and PS-2 rail types, respectively, as compared to the bridge with no skew. For all rail types, there is negligible difference between the strain profiles of the skew and non-skew bridges in the peak positive moment region.

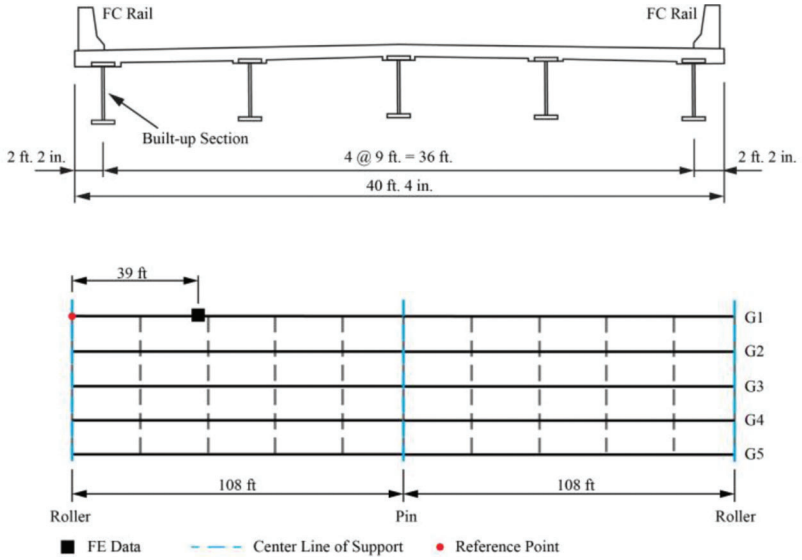

Figure 4.1 Cross-section and frame plan of the modified two-span continuous steel girder bridge.

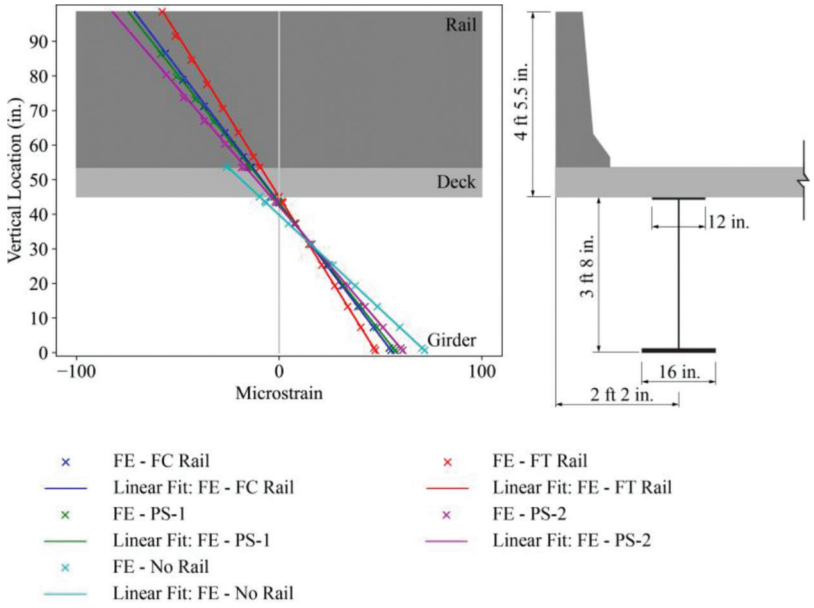

Figure 4.2 Effect of rail type for two-span continuous steel girder bridge: FE predictions for strains at peak positive moment location.

TABLE 4.1
Effect of rail type for two-span continuous steel girder bridge: FE predictions for the curvature and neutral axis location at peak positive moment location

Rail Type	Curvature	% Different from No Rail	Neutral Axis Location	% Different from No Rail
FT	1.07	-41.5	45.0	13.0
FC	1.29	-29.5	43.3	8.79
PS-1	1.34	-26.8	43.2	8.54
PS-2	1.46	-20.2	42.3	6.28
No Rail	1.83	–	39.8	–

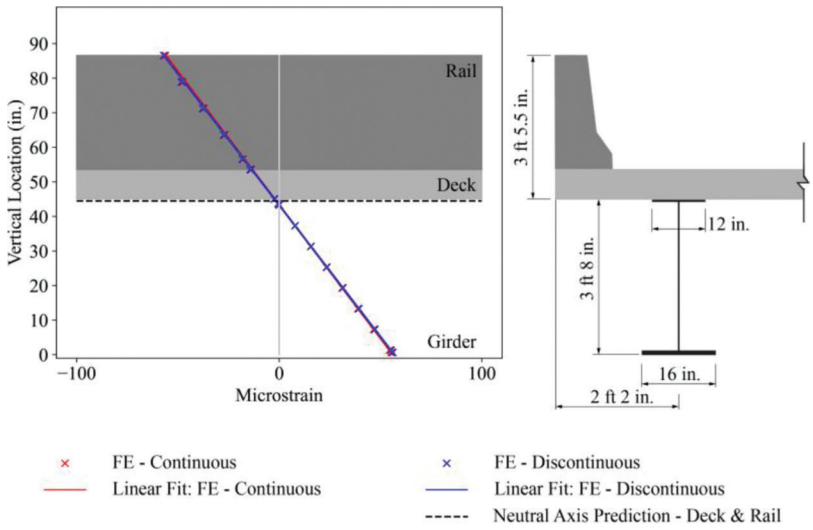

Figure 4.3 Effect of rail discontinuity for two-span continuous steel girder bridge with FC rail: FE predictions for strains at peak positive moment location.

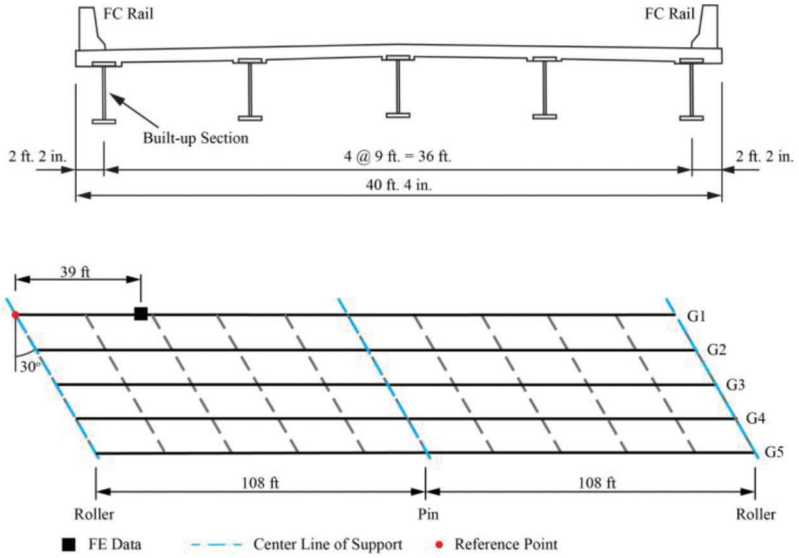

Figure 4.4 Cross-section and frame plan of the modified two-span continuous steel girder bridge with 30-degree skew angle.

4.2.2 Three-Span Continuous Steel Girder Bridge Behavior

The three-span continuous steel girder prototype bridge structure is based on Asset I265-00-05513 B. It has been modified as follows: six girders were modeled instead of seven to achieve an even girder spacing across the width, as well as similar lane and shoulder layout as the other studied bridges. Figure 4.6 shows the plan and cross-section of the modified prototype structure, and indicates the location where behavior was studied.

Figure 4.7 and Table 4.2 show the effect of the rail type on behavior. Similar to the two-span continuous steel girder bridge, all of the rail types decreased the curvature compared to when no rail was modeled. Also, the FT rail provided the greatest benefit, with decreasing benefit from the FC, PS-1, and PS-2 rail types (in order of decreasing benefit). The neutral axis also increased in vertical location with increasing rail height.

Figure 4.8 shows the effect of discontinuity of the rail above the piers for the three-span continuous steel girder bridge with the FC rail type. Figure C.7, Figure C.8, and Figure C.9 (see Appendix C) show the effect of discontinuity of the rail above the piers for the three-span continuous steel girder bridge with the FT, PS-1, and PS-2 rail types, respectively. For each rail type, there is no significant difference between behavior in the positive moment region.

Figure 4.9 shows the prototype structure with a 30-degree skew and indicates the relative location where behavior was studied. Figure 4.10 shows the effect of this 30-degree skew angle on the behavior of a three-span continuous steel girder bridge with the FC rail type, as compared to the bridge with no skew. Figure

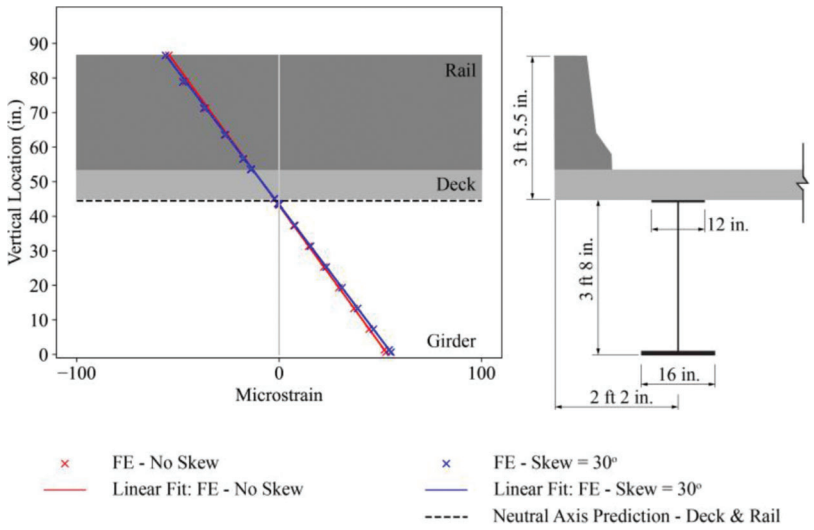

Figure 4.5 Effect of 30-degree skew angle for two-span continuous steel girder bridge with FC rail: FE predictions for strains at peak positive moment location.

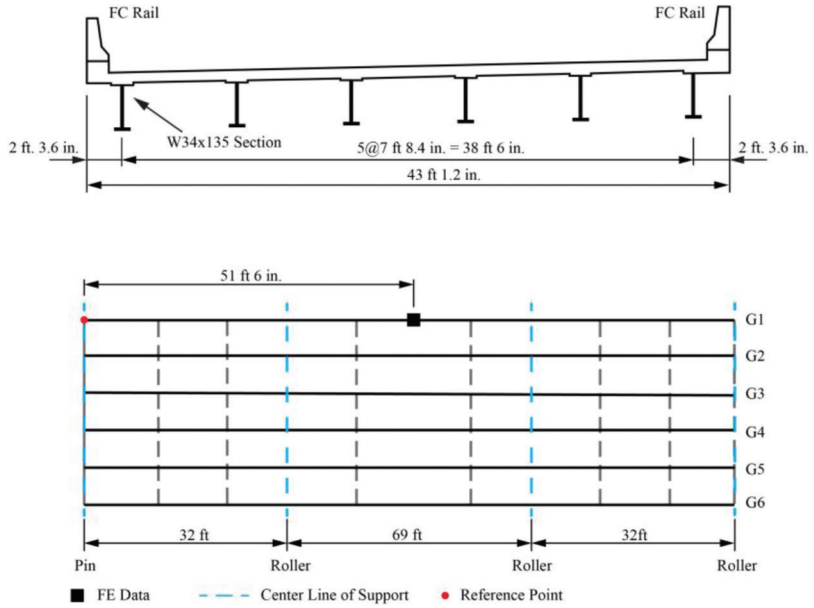

Figure 4.6 Cross-section and frame plan of the modified three-span continuous steel girder bridge.

C.11, Figure C.12, and Figure C.13 (see Appendix C) show the effect of this 30-degree skew angle on a three-span continuous steel girder bridge with the FT, PS-1, and PS-2 rail types, respectively, as compared to the bridge with no skew. For all rail types, there is no significant difference between behavior with a 30-degree skew and zero-degree skew angle in the positive moment region.

4.3 Steel Girder Damaged by Vehicular Collision Parametric Study

The parametric study discussed in Section 4.2 led to valuable findings for undamaged steel girder bridges. This section performs a different parametric study focusing on the behavior of a bridge with an exterior girder that has been damaged by vehicular collision. Note that this study differs from the approach for the undamaged bridges that was discussed in Section 4.1. Specifically, the validated numerical model that was developed for Asset 037-55-05265 is revisited to investigate the effect of varying rail types and rail continuity. The FE model discussed in Section 3.2.3 and validated through comparison in Section 3.4.1 was used. All data is for an FE model in which the composite behavior between the girder and the deck is removed in the damaged region. The transverse location of the rail is the same for all the rail types considered (i.e., FT, FC, PS-1, and PS-2). The applied load is the same truck loading as in the monitoring procedure. Results focus

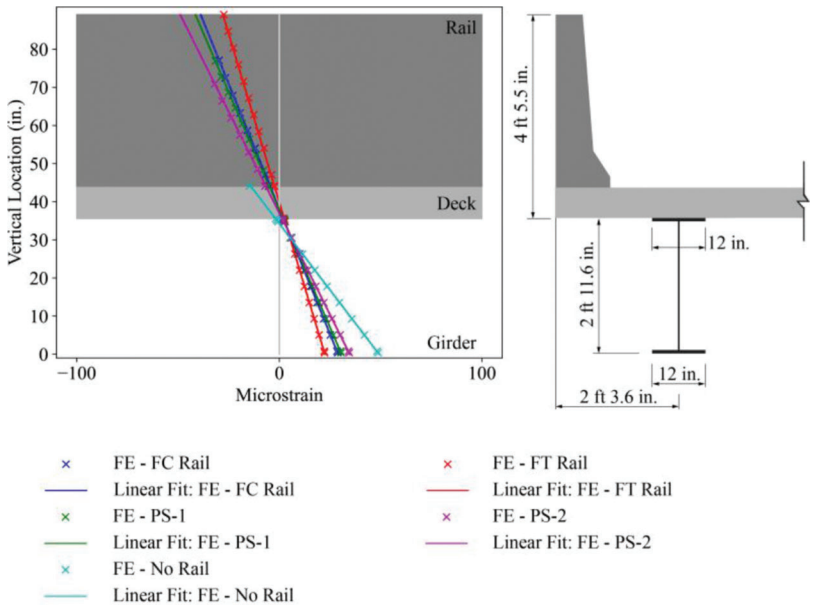

Figure 4.7 Effect of rail type for three-span continuous steel girder bridge: FE predictions for strains at peak positive moment location. Cross-section shows the FT rail as an example.

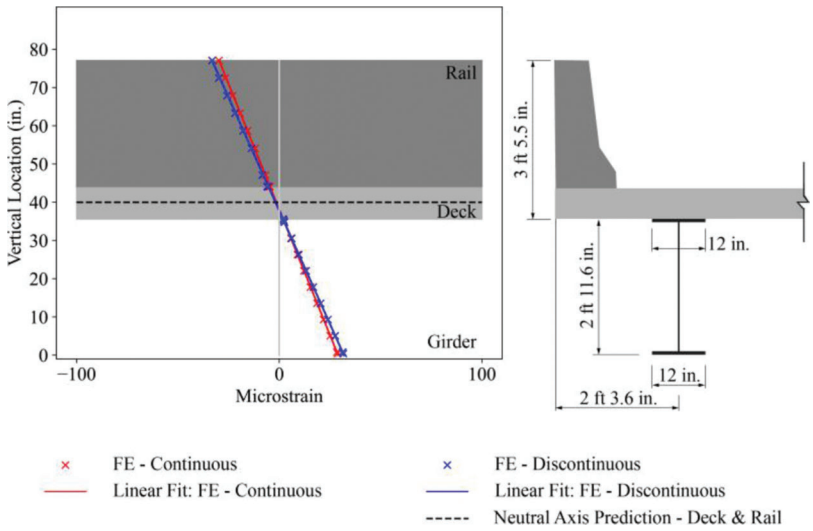

Figure 4.8 Effect of rail discontinuity for three-span continuous steel girder bridge with FC rail: FE predictions for strains at peak positive moment location.

TABLE 4.2
Effect of rail type for three-span continuous steel girder bridge: FE predictions for the curvature and neutral axis location at peak positive moment location

Rail Type	Curvature	% Different from No Rail	Neutral Axis Location	% Different from No Rail
FT	0.57	-60.4	39.8	16.0
FC	0.76	-47.2	38.1	11.1
PS-1	0.81	-43.8	37.9	10.5
PS-2	0.94	-34.7	37.0	7.87
No Rail	1.44	–	34.3	–

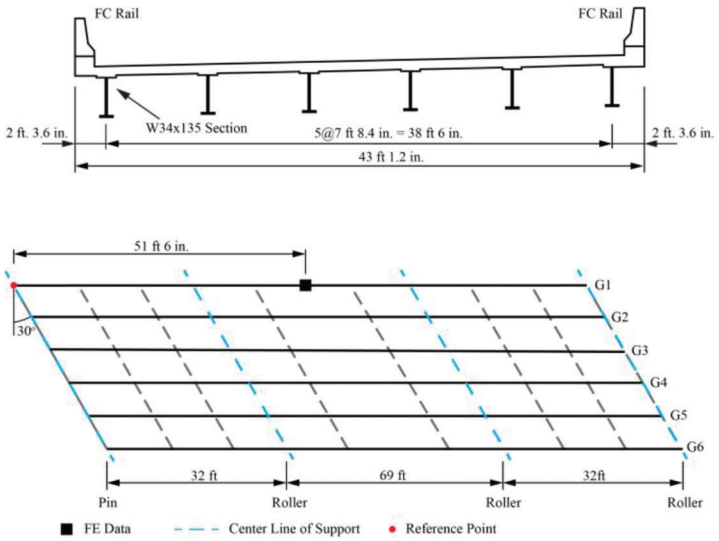

Figure 4.9 Cross-section and frame plan of the modified three-span continuous steel girder bridge with 30-degree skew angle.

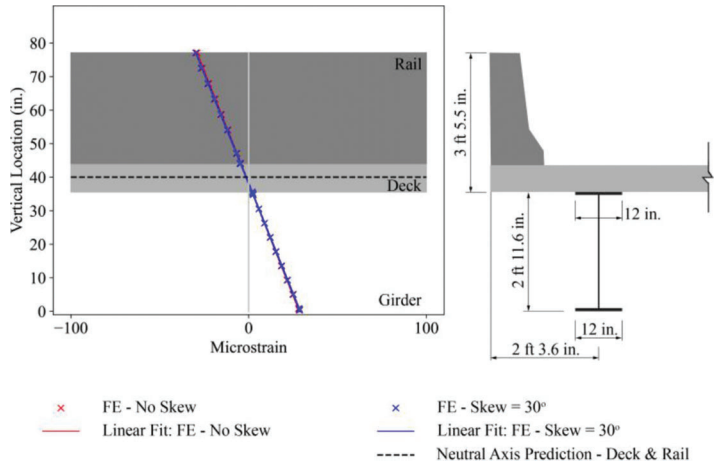

Figure 4.10 Effect of 30-degree skew angle for three-span continuous steel girder bridge with FC rail: FE predictions for strains at peak positive moment location.

on the damaged side of the bridge (Girders 5 and 6), as the behavior of undamaged steel girders was studied in Section 4.2.

As shown in Figure 3.9, Asset 037-55-05265 has an FC rail. Figure 4.11, Figure 4.12, and Figure 4.13, as well as Table 4.3, Table 4.4, and Table 4.5, show the effect of different rail types on the behavior of the exterior damaged girder and adjacent interior girder at Locations M6, D6, and M5, respectively. At all three locations, the FT rail reduces the curvature the most, with decreasing benefits from the other rail types. Similarly, the FT rail increases the neutral axis at all locations, with decreasing benefits from the other rail types. As expected, the rail type has a larger effect on the curvature of the damaged exterior girder than the adjacent interior girder.

Asset 037-55-05265 has a discontinuity in the rail above the pier which is included in the models in Section 3.4.1 by removing the shell elements of the rail at that location. Another version of the model was built where the rail was made continuous. Figure 4.14, Figure 4.15, Figure 4.16 compare the strain profiles for both versions of the FE model at Locations M6 and D6 of the damaged exterior girder and the Location M5 of the adjacent interior girder, respectively. This data indicates that the discontinuity has negligible impact on the behavior of a damaged exterior girder or its adjacent interior girder at these locations.

4.4 Prestressed Concrete Girder Parametric Study

This study assumed that none of the girders have been damaged and that full composite behavior is developed between the top flange of the girder and deck as well as between the deck and the rail.

4.4.1 Two-Span Continuous Prestressed Concrete Girder Bridge Behavior

The two-span continuous prestressed concrete girder prototype bridge structure is based on Asset 641-58-

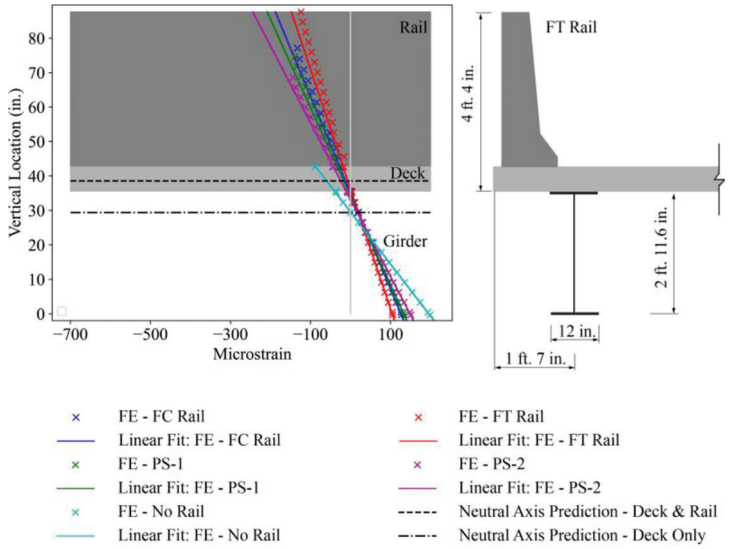

Figure 4.11 Effect of rail type for damaged steel girder bridge (Asset 037-55-05265): FE predictions for strains at Location M6.

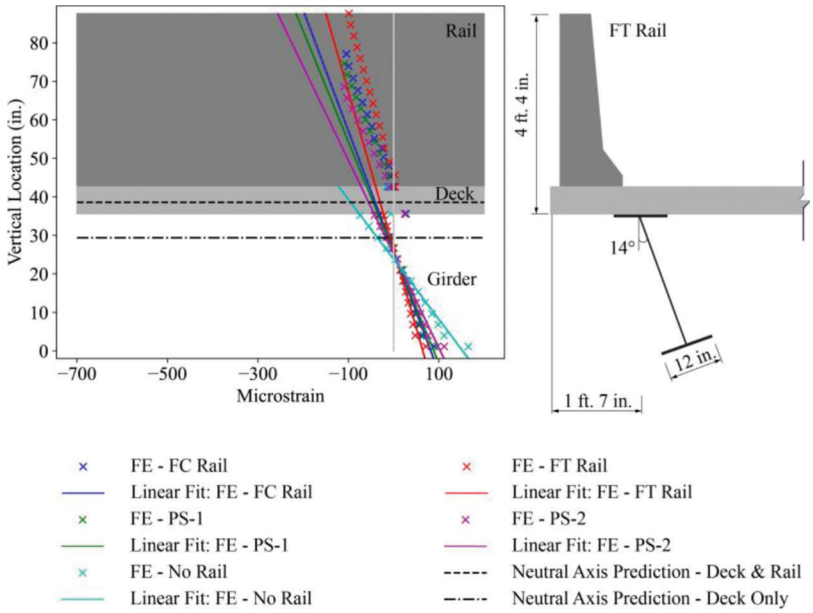

Figure 4.12 Effect of rail type for damaged steel girder bridge (Asset 037-55-05265): FE predictions for strains at Location D6.

9152. This bridge has not been modified. Figure 4.17 shows the plan and cross-section of the prototype structure, and indicates the location where behavior was studied.

Figure 4.18 and Table 4.6 show that all of the rail types decreased the curvature compared to when no rail was modeled. The FT rail provided the greatest benefit, with decreasing benefit from the FC, PS-1, and PS-2 rail types (in order of decreasing benefit). These findings are consistent with those found from the steel girder parametric studies. All of the rails increased the height of the neutral axis compared to the no rail model.

Figure 4.19 shows the effect of rail discontinuity over the pier for the two-span continuous prestressed concrete girder bridge with the FC rail type. Figure C.13, Figure C.14, and Figure C.15 (see Appendix C) show the effect of rail discontinuity over the pier for the two-span continuous prestressed concrete girder bridge with the FT, PS-1, and PS-2 rail types, respectively. Like the steel girder bridges, rail discontinuity over the pier has negligible impact on the behavior in the positive moment region, for any rail type.

Figure 4.20 shows the prototype structure with a 30-degree skew, also indicating the location where behavior was studied. Figure 4.21 shows the effect of this 30-degree skew angle on the behavior of a two-span continuous prestressed concrete girder bridge with the FC rail type, as compared to the bridge with zero-degree skew angle. Figure C.16, Figure C.17, and Figure C.18 (see Appendix C) show the effect of this 30-degree

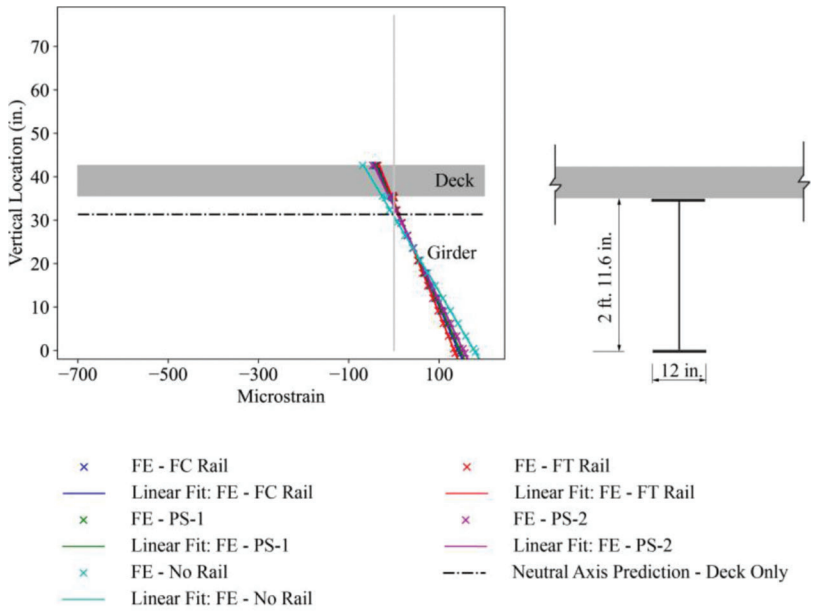

Figure 4.13 Effect of rail type for damaged steel girder bridge (Asset 037-55-05265): FE predictions for strains at Location M5.

TABLE 4.3
Effect of rail type for damaged steel girder bridge (Asset 037-55-05265): FE predictions for the curvature and neutral axis location at Location M6

Rail Type	Curvature	% Different from No Rail	Neutral Axis Location	% Different from No Rail
FT	2.88	-56.5	36.2	22.6
FC	3.58	-45.9	35.1	19.0
PS-1	3.89	-41.2	34.1	15.5
PS-2	4.48	-32.3	33.1	12.2
No Rail	6.62	–	29.5	–

TABLE 4.4
Effect of rail type for damaged steel girder bridge (Asset 037-55-05265): FE predictions for the curvature and neutral axis location at Location D6

Rail Type	Curvature	% Different from No Rail	Neutral Axis Location	% Different from No Rail
FT	2.44	-61.9	26.4	10.9
FC	3.19	-50.3	25.8	8.35
PS-1	3.48	-45.8	25.5	7.36
PS-2	4.10	-36.0	25.1	5.63
No Rail	6.42	–	23.8	–

TABLE 4.5
Effect of rail type for damaged steel girder bridge (Asset 037-55-05265): FE predictions for the curvature and neutral axis location at Location M5

Rail Type	Curvature	% Different from No Rail	Neutral Axis Location	% Different from No Rail
FT	3.89	-32.3	34.3	11.0
FC	4.22	-26.6	33.9	9.59
PS-1	4.37	-24.0	33.6	8.57
PS-2	4.64	-19.1	33.1	7.04
No Rail	5.74	–	30.9	–

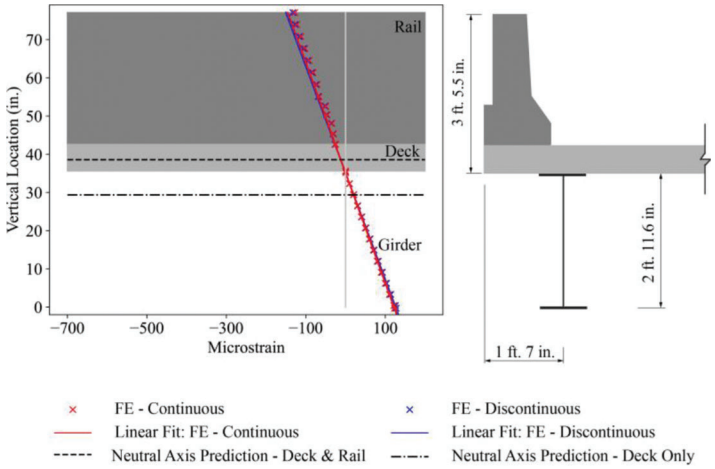

Figure 4.14 Effect of rail discontinuity for damaged steel girder bridge (Asset 037-55-05265): FE predictions for strains at Location M6.

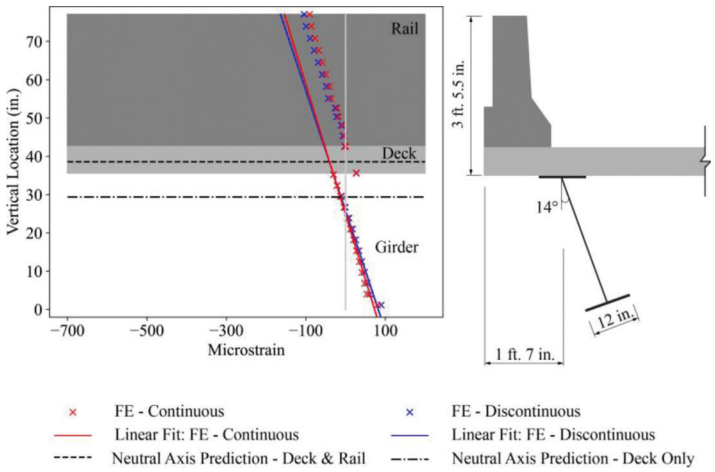

Figure 4.15 Effect of rail discontinuity for damaged steel girder bridge (Asset 037-55-05265): FE predictions for strains at Location D6.

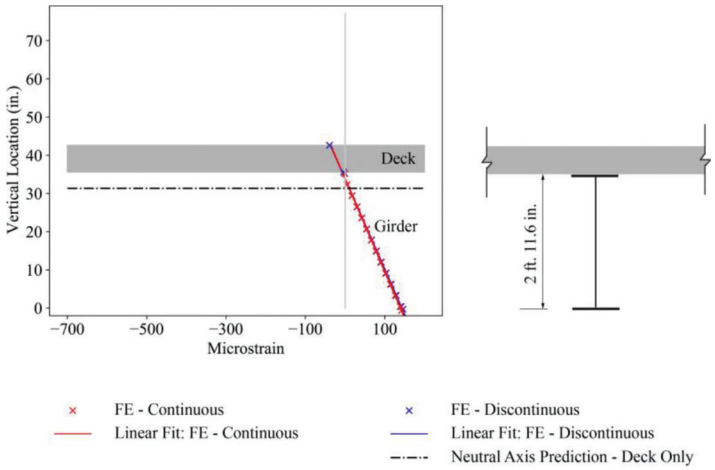

Figure 4.16 Effect of rail discontinuity for damaged steel girder bridge (Asset 037-55-05265): FE predictions for strains at Location M5.

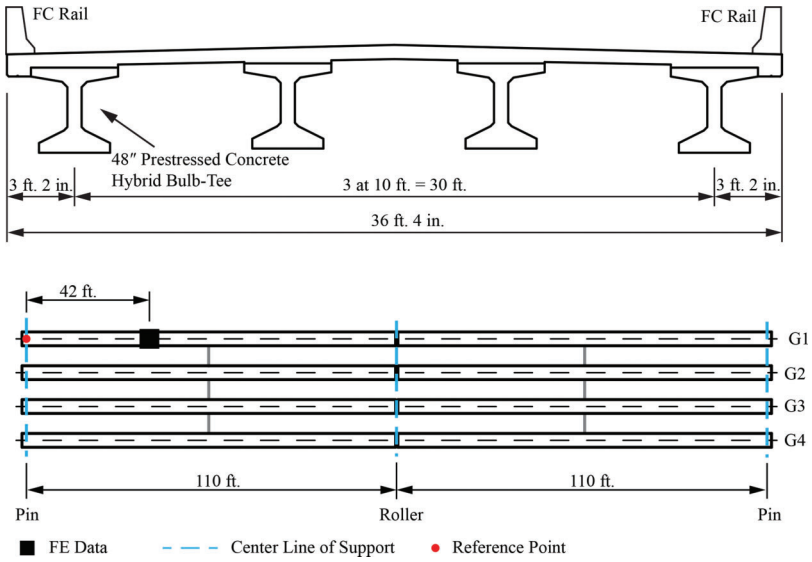

Figure 4.17 Cross-section and frame plan of the two-span continuous prestress girder bridge.

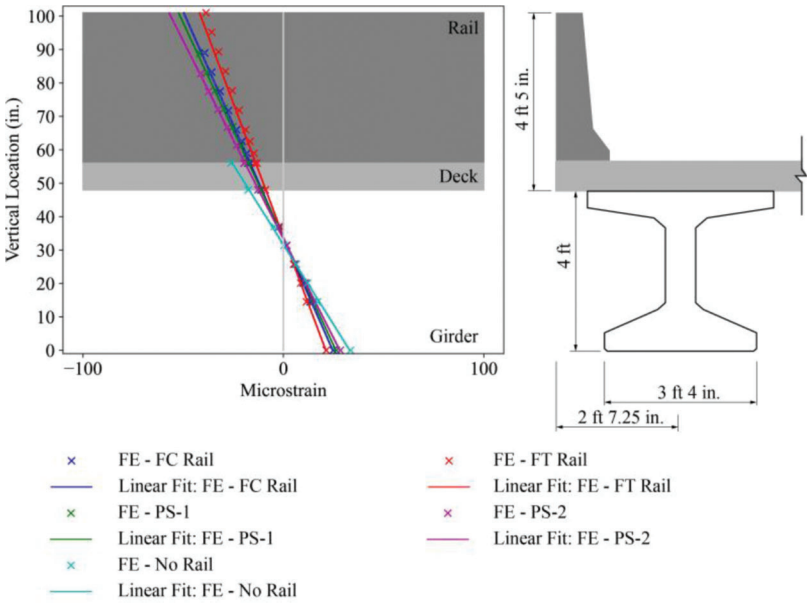

Figure 4.18 Effect of rail type for two-span continuous prestressed concrete girder bridge: FE predictions for strains at peak positive moment location. Cross-section shows the FT rail as an example.

TABLE 4.6
Effect of rail type for two-span continuous prestressed concrete girder bridge: FE predictions for the curvature and neutral axis location at peak positive moment location

Rail Type	Curvature	% Different from No Rail	Neutral Axis Location	% Different from No Rail
FT	0.62	-41.0	33.9	7.28
FC	0.74	-29.5	33.4	5.70
PS-1	0.78	-25.7	33.7	6.65
PS-2	0.84	-20.0	33.3	5.38
No Rail	1.05	–	31.6	–

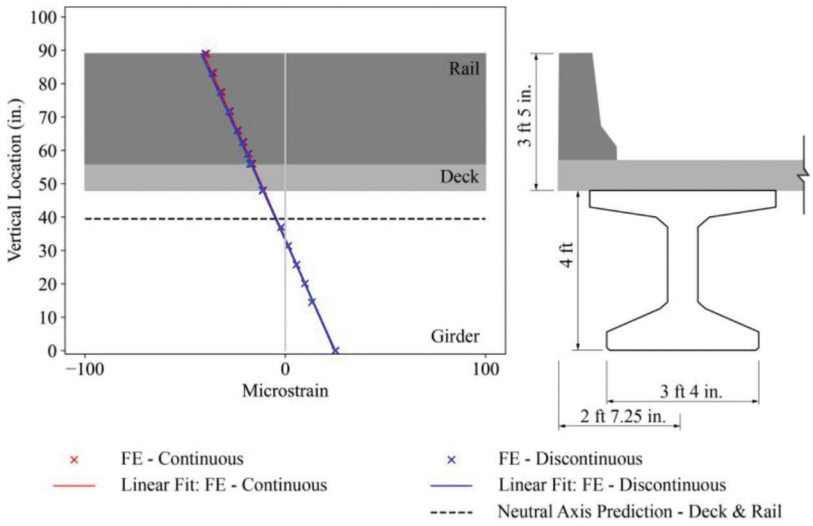

Figure 4.19 Effect of rail discontinuity for two-span continuous prestressed concrete girder bridge with FC rail: FE predictions for strains at peak positive moment location.

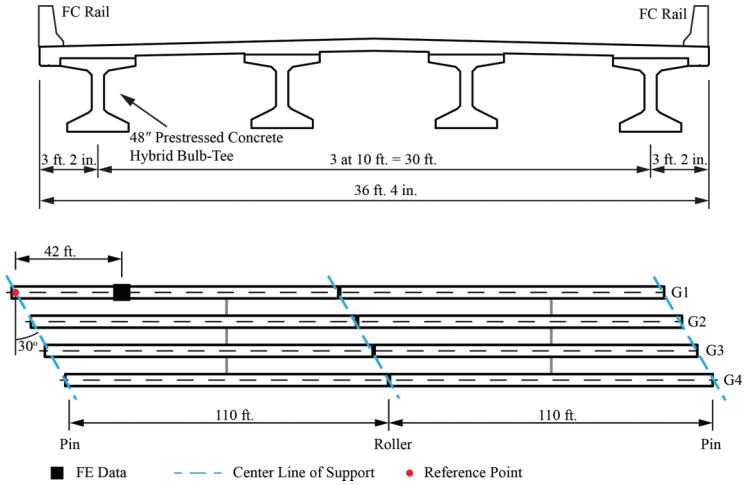

Figure 4.20 Cross-section and frame plan of the two-span continuous prestress girder bridge with 30-degree skew angle.

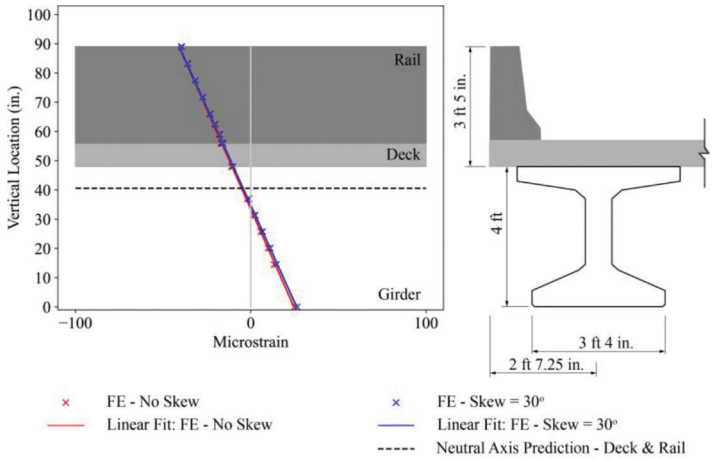

Figure 4.21 Effect of 30-degree skew angle for two-span continuous prestressed concrete girder bridge with FC rail: FE predictions for strains at peak positive moment location.

skew angle on the behavior of a two-span continuous prestressed concrete girder bridge with the FT, PS-1, and PS-2 rail types, respectively, as compared to the bridge with 0-degree skew angle. For all rail types, there is no significant difference between behavior with 30-degree skew and zero-degree skew angle in the positive moment region.

4.4.2 Three-Span Continuous Prestressed Concrete Girder Bridge Behavior

The three-span continuous prestressed concrete girder prototype bridge structure is based on Asset 025-08-08725 SB. It has been modified as follows: symmetry was assumed along the transverse direction of the bridge and a girder spacing of 10 ft. 6 in. was used instead of the original 12 ft. 6 in. Figure 4.22 shows the plan and cross-section of the modified prototype structure with and without skew respectively, and indicates the location where behavior was studied.

As was the case for the other three types of bridges studied, Figure 4.23 and Table 4.7 show that all of the rail types decreased the curvature, with the FT rail providing the greatest benefit and decreasing benefit from the FC, PS-1, and PS-2 rail types (in order of decreasing benefit). Like the two-span continuous prestressed concrete girder bridge, all of the rails increased the height of the neutral axis compared to the no rail model.

Figure 4.24 shows the effect of discontinuity of the rail above the piers for the three-span continuous prestressed concrete girder bridge with the FC rail type. Figure C.19, Figure C.20, and Figure C.21 (see Appendix C) show the effect of discontinuity of the rail above the piers for the three-span continuous prestressed concrete girder bridge with the FT, PS-1, and PS-2 rail types, respectively. As discussed previously, the data show that rail discontinuity at the piers has no significant effect on positive moment behavior for any of the rail types investigated. This has been shown to be consistent for all bridges in this parametric study.

Figure 4.25 shows the modified prototype structure including a 30-degree skew angle. Figure 4.26 shows the effect of this 30-degree skew angle on the behavior of the exterior girder of a three-span continuous prestressed concrete girder bridge with the FC rail type in the positive moment region, as compared to the bridge with no skew. Figure C.22, Figure C.23, and Figure C.24 (see Appendix C) show the effect of this 30-degree skew angle on the behavior of the exterior girder of a three-span continuous prestressed concrete girder bridge with the FT, PS-1, and PS-2 rail types, respectively, in the positive moment region, as compared to the bridge with no skew. The data show that a 30-degree skew angle has negligible impact on the behavior of the exterior girder in the positive moment region for any of the rail types. This trend is consistent among all bridges in the parametric study.

4.5 Summary

For two- and three-span continuous steel and prestressed concrete girder bridges, the bridge rail reduced the curvature (Table 4.8 and Table 4.9), meaning reduced the strain in the girder and deck. The greatest benefit was observed when using the FT rail (Table 4.8), with decreasing benefit corresponding to the rail types that result in composite sections with decreasing moment of inertia of the composite section. Incorporating rail into the models increased the vertical location of the neutral axis for all rail types (Table 4.8 and Table 4.9). For the steel girder bridges, there was a clear trend with the FT rail providing the greatest benefit, with decreasing benefit corresponding to the rail types that result in composite sections with decreasing moment of inertia of the composite section. There was

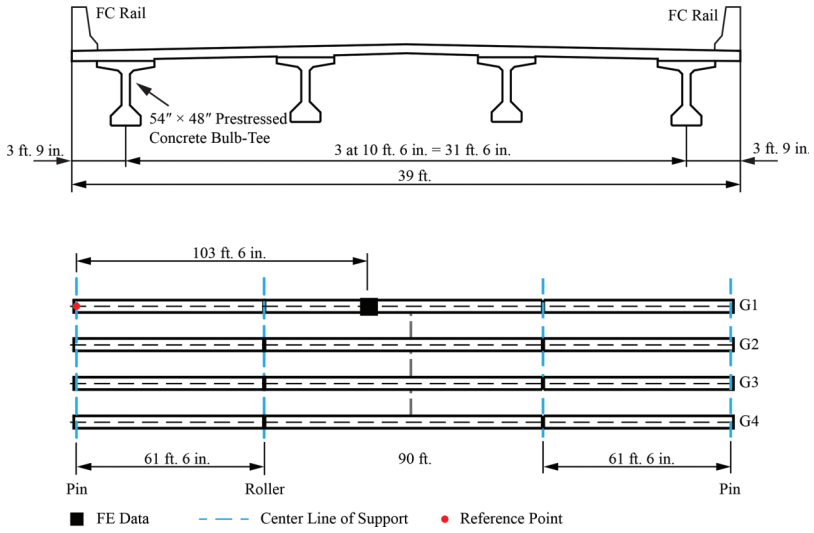

Figure 4.22 Cross-section and frame plan of the modified three-span continuous prestress girder bridge.

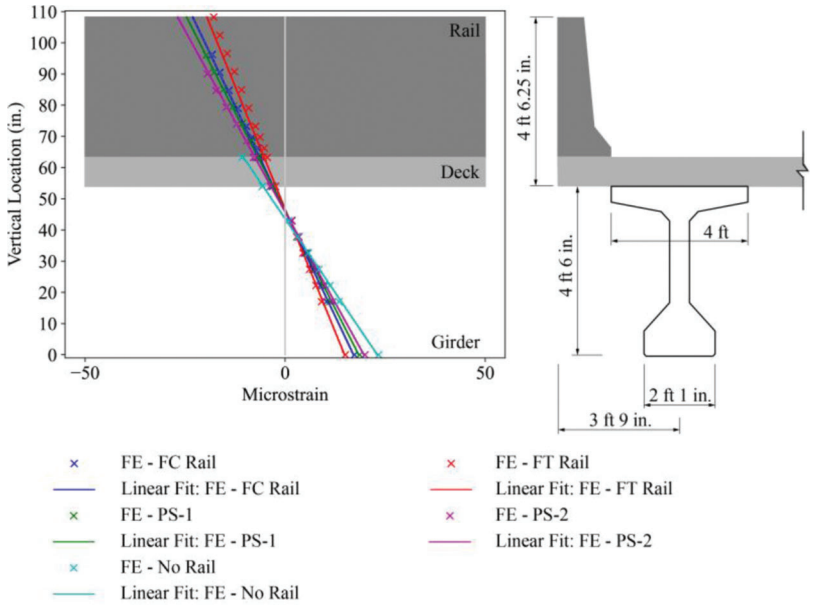

Figure 4.23 Effect of rail type for three-span continuous prestressed concrete girder bridge: FE predictions for strains at peak positive moment location. Cross-section shows the FT rail as an example.

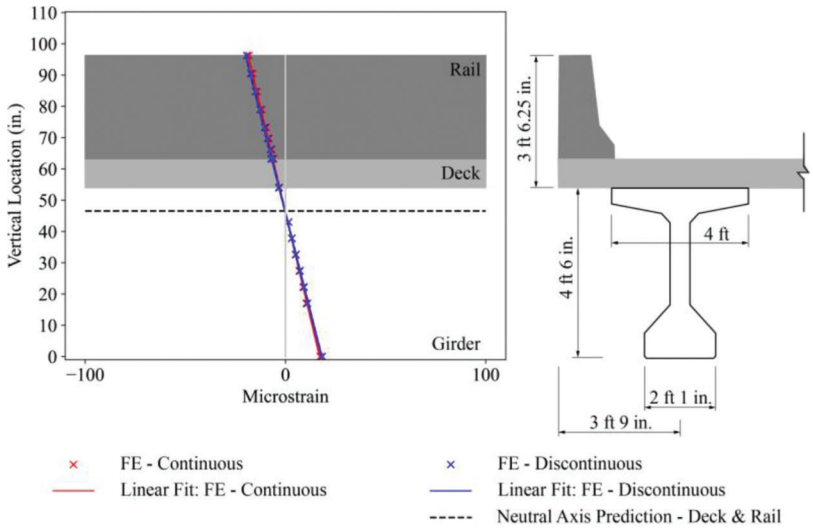

Figure 4.24 Effect of rail discontinuity for three-span continuous prestressed concrete girder bridge with FC rail: FE predictions for strains at peak positive moment location.

TABLE 4.7
Effect of rail type for three-span continuous prestressed concrete girder bridge: FE predictions for the curvature and neutral axis location at peak positive moment location

Rail Type	Curvature	% Different from No Rail	Neutral Axis Location	% Different from No Rail
FT	0.32	-39.6	46.7	7.11
FC	0.37	-30.2	46.0	5.50
PS-1	0.40	-24.5	46.3	6.19
PS-2	0.43	-18.9	45.7	4.82
No Rail	0.53	–	43.6	–

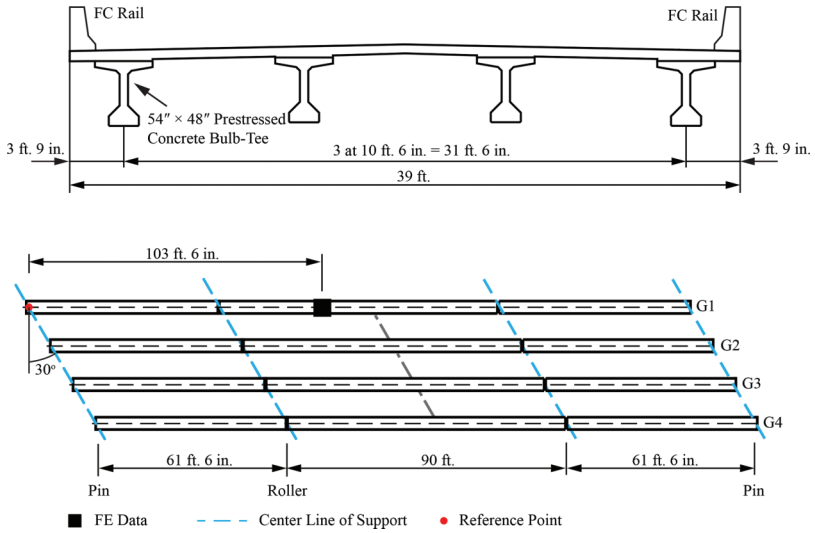

Figure 4.25 Cross-section and frame plan of the modified three-span continuous prestress girder bridge with 30-degree skew angle.

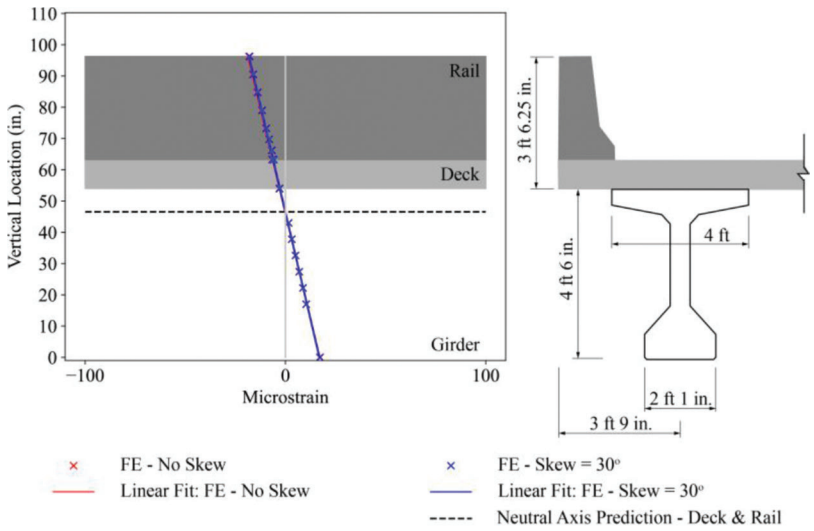

Figure 4.26 Effect of 30-degree skew angle for three-span continuous prestressed concrete girder bridge with FC rail: FE predictions for strains at peak positive moment location.

TABLE 4.8
Effect of FT rail type on the curvature and neutral axis height

Material	Arrangement	% Decrease in Curvature	% Increase in Neutral Axis Height
Steel	2-span	41.5	13.0
	3-span	60.4	16.0
Concrete	2-span	41.0	7.28
	3-span	39.6	7.11

TABLE 4.9
Effect of PS-2 rail type on the curvature and neutral axis height

Material	Arrangement	% Decrease in Curvature	% Increase in Neutral Axis Height
Steel	2-span	20.2	6.28
	3-span	34.7	7.87
Concrete	2-span	20.0	5.38
	3-span	18.9	4.82

no significant trend related to specific rail type for the prestressed concrete girder bridges.

Overall, a discontinuity of the rail at the piers has negligible impact on positive moment behavior for two- and three-span continuous steel and prestressed concrete girder bridges, regardless of rail type.

A steel girder bridge with an exterior girder that has been damaged by vehicular collision follows the above-mentioned behaviors related to rail type and discontinuity of the rail.

5. CONCLUSIONS

5.1 Summary of Research Findings

The main research findings are summarized as follows. These findings are limited to two- or three-span continuous composite, multi-girder steel or prestressed concrete bridges with intact, reinforced concrete rail integral with the deck. Bridges with other rail types (e.g., metal rails) or other structural systems (e.g., girder floorbeam systems) are excluded from these findings. These findings also do not apply in the circumstance where a rail has been damaged or is not integral with the deck. These findings may be limited to the specific bridges monitored in this study and the specific regions that were monitored (e.g., positive moment behavior).

Findings from Measured Data

1. Generally, both FC and PS-1 rail types participate in carrying live load.
2. Neutral axis locations indicate that full composite behavior can be achieved between the girder, deck, and rail.
3. Strains in an exterior girder increase when there is a gap in the rail in the positive moment region.
4. Near abutments, full composite behavior between the girder and deck may not yet developed.
5. When an exterior girder is subjected to Category T damage (i.e., torsion about the longitudinal direction (Avent, 2008)) from a vehicular collision, the shear connection between the deck and girder may be damaged. Live load amplification factors may also be higher due to the damage.

Findings from Numerical Modeling of Monitored Bridges

1. FE numerical models, with the following features, are able to accurately capture rail participation for steel and prestressed concrete girder bridges for which there are no damaged girders:
    a. Components modeled with the following element types:
        i. Rail: Thick shell elements, with changing thickness based on the geometry.
        ii. Deck: Thick shell elements.
        iii. Girders: Frame elements representing the top and bottom flanges, thin shell elements representing the webs for steel girders, thick shell elements representing the webs for prestressed concrete girders.
    b. Composite behavior—implemented by constraining all translational and rotational degrees of freedom of the nodes between the components (i.e., nodes that share the same longitudinal coordinates)—modeled between the rail and deck, as well as the deck and the top flange of the girders.
2. For steel girder bridges where an exterior girder is subjected to Category T damage (i.e., torsion about the longitudinal direction (Avent, 2008)) from a vehicular collision, FE models that remove the composite behavior between the girder and the deck in the region of the damage (by removing the translational and rotational constraints between the top flange of the girder and the deck) can accurately capture behavior. The damaged profile of the girder should be considered.

Findings from Numerical Parametric Investigation

1. When fully composite behavior between the rail, deck, and girder is assumed, the curvature is reduced in the positive moment region, meaning strains in the deck and girder are reduced, as compared to a comparable system where only the deck and girder are composite. The vertical location of the neutral axis is increased (measured from the bottom flange) in the positive moment region as compared to a comparable system where only the deck and girder are composite.
2. FT, FC, PS-1, and PS-2 rail types all contribute to the above-mentioned reduction in curvature. The greatest benefit was observed when using the FT rail, with decreasing benefit corresponding to the rail types that result in composite sections with decreasing moment of inertia.
3. Rail discontinuity at piers has negligible impact on the behavior of the exterior girders in the positive moment region.
4. Skew (up to 30 degrees) has negligible impact on the behavior of the exterior girders in the positive moment region.

Other Findings

1. Through comparisons between measured digital image correlation (DIC) and strain gauge data, DIC is further validated as a technique for field monitoring of bridges.

5.2 Expected Benefits, Deliverables, Implementation, and Cost Saving

This research has contributed to the current INDOT strategic priorities (INDOT, 2019) of safety, asset sustainability, organization and workforce, and innovation and technology (Table 5.1).

The implementation plan for this research includes the following:

1. The *Recommendations for Evaluating the Reserve Strength of Girder Bridges Due to Rail Participation* (Appendix A) to be made available.

TABLE 5.1
Research contributions to INDOT strategic priorities

INDOT Strategic Priority (INDOT, 2019)	Research Contributions
Safety	This research demonstrated that intact, reinforced concrete bridge rail integral with the deck generally participates in carry live load. This may increase the safety of two- or three-span continuous composite, multi-girder steel or prestressed concrete bridges.
Asset Sustainability	Research culminated in recommendations for bridge inspectors and engineers who evaluate the behavior of bridges, thus contributing to long-term asset management.
Organization and Workforce	This research contributed to the education of three graduate students and two undergraduate students, providing them with the opportunity to perform independent research and training them in bridge engineering. All of these students, as well as the Principal Investigator, are women, thereby contributing to increasing the diversity of the field.
Innovation and Technology	Digital Image Correlation (DIC)—the state-of-the-art photographic measurement technology—was used to monitor the behavior of one steel girder bridge. This innovative technology has the potential to provide unprecedented data on bridge behavior and may be a valuable inspection tool in the future. This research demonstrated that strains measured using DIC agree with strain gauge measurements, contributing to the verification of DIC as a tool for field monitoring of bridges.

2. The *Recommendations for Bridge Inspectors for Evaluating Steel Girder Bridges Subjected to Vehicular Damage* (Appendix B) to be included in the *INDOT Bridge Inspection Manual*.
3. Presentation of the results at the 2021 Purdue Road School.
4. A journal paper is currently in preparation and will be submitted for publication.
5. The final report will be made freely available on the Purdue e-Pubs website.

Other deliverables include the following:

PhD Dissertation

- Wang, Y. (2021). *Monitoring the behavior of bridges Using digital image correlation* [Doctoral dissertation, University of Notre Dame]. https://curate.nd.edu/show/6h440r9985m

Peer-Reviewed Journal Paper

- Wang, Y., Tumbeva, M. D., & Thrall, A. P. (n.d.). *Behavior of bridge rails under live load* [Manuscript in preparation].

Presentations

- Wang, Y., Cardona, S., Gasser, C. E., & Thrall, A. P. (2020, February 27). *Evaluating reserve strength of girder bridges due to bridge rail load shedding* [Poster presentation]. Joint Transportation Research Program–Indiana Department of Transportation Poster Session, Indianapolis, Indiana.
- Gonzalez Flores, C., Gasser, C. E., Wang, Y., & Thrall, A. P. (2019, February 13). *Evaluating reserve strength of girder bridges due to bridge rail load shedding* [Poster presentation]. Joint Transportation Research Program–Indiana Department of Transportation, Indianapolis, Indiana.

5.3 Future Studies

Future research could extend this study to also consider the impact of girder depth on the participation of the rail.

This project focused on the behavior of bridge rail under service loads. To provide further understanding, future studies could focus on the ultimate behavior of steel and prestressed concrete girder bridges when the bridge rail is considered. Numerical modeling of the ultimate failure modes should include nonlinear material models, for both the steel and concrete, as well as nonlinear geometry.

REFERENCES

AASHTO. (2020). *AASHTO LRFD bridge design specifications* (9th ed.). American Association of State Highway and Transportation Officials.

AASHTO. (2016). *Manual for assessing safety hardware* (2nd ed.). American Association of State Highway and Transportation Officials.

ABAQUS. (2016). *ABAQUS/standard analysis user's manual version 6.14*. Dassault Systemes. https://130.149.89.49:2080/v6.14/

Akinci, N. O., Liu, J., & Bowman, M. D. (2008). Parapet strength and contribution to live-load response for superload passages. *Journal of Bridge Engineering*, *13*(1), 55–63.

ARAMIS. (2017). *ARAMIS user manual*. GOM.

Avent, R. R. (2008, August). Guide for heat-straightening of damaged steel bridge members (Report No. FHWA-IF-08-999). *Federal Highway Administration*. https://www.fhwa.dot.gov/bridge/steel/heat_guide.pdf

Bakht, B., & Csagoly, P. F. (1979). *Bridge testing* (Report No. 79-SSR-10). Ontario Ministry of Transportation and Communications, Research and Development Division.

Barker, M. G. (2001, July). Quantifying field-test behavior for rating steel girder bridges. *Journal of Bridge Engineering*, *6*(4), 254–261.

Barker, M. G., Imhoff, C. M., McDaniel, W. T., & Frederick, T. L. (1999, May). Field testing and load rating procedures for steel girder bridges (Report No. RDT 99-004). *Missouri Department of Transportation*. https://spexternal.modot.mo.gov/sites/cm/CORDT/RDT99004.pdf

BDI. (2018). *ST350–Strain transducer operations manual, v3.0*. https://bditest.com/wp-content/uploads/2019/01/Manual-Strain-Transducer-ST350-201511-Rev-A-.pdf

BDI. (2014). *STS4-4–Operations manual, v0.7*.

Billing, J. R. (1984, December). Dynamic loading and testing of bridges in Ontario. *Canadian Journal of Civil Engineering*, *11*(4), 833–843. https://doi.org/10.1139/l84-101

Burdette, E. G., & Goodpasture, D. W. (1973, March). Tests of four highway bridges to failure. *Journal of the Structural Division: Proceedings of the American Society of Civil Engineers*, *99*(3), 335–348.

Canna, T. L., & Bowman, M. D. (2001). *Fatigue behavior of beam diaphragm connections with intermittent fillet welds, Part I, Volume 1, field evaluation* (Joint Transportation Research Program Final Report FHWA/IN/JTRP-2001/10-I-1). West Lafayette, IN: Purdue University. https://doi.org/10.5703/1288284313222

Chung, W., Liu, J., & Sotelino, E. D. (2006, March). Influence of secondary elements and deck cracking on the lateral load distribution of steel girder bridges. *Journal of Bridge Engineering*, *11*(2), 178–187. https://ascelibrary.org/doi/abs/10.1061/%28ASCE%291084-0702%282006%2911%3A2%28178%29

Conner, S., & Huo, X. S. (2006, March). Influence of parapets and aspect ratio on live-load distribution. *Journal of Bridge Engineering*, *11*(2), 188–196. https://doi.org/10.1061/(ASCE)1084-0702(2006)11:2(188)

CSiBridge. (2020). *CSiBridge user's manual*. Computers and Structures, Inc.

Eamon, C. D., & Nowak, A. S. (2002). Effects of edge-stiffening elements and diaphragms on bridge resistance and load distribution. *Journal of Bridge Engineering*, *7*(5), 258–266.

Eom, J., & Nowak, A. S. (2001). Live load distribution for steel girder bridges. *Journal of Bridge Engineering*, *6*(6), 489–497. https://doi.org/10.1061/(ASCE)1084-0702(2001)6:6(489)

Fu, C. C., Elhelbawey, M., Sahin, M. A., & Schelling, D. R. (1996, September). Lateral distribution factor from bridge field testing. *Journal of Structural Engineering*, *122*(9), 1106–1109. https://doi.org/10.1061/(asce)0733-9445(1996)122:9(1106)

Geokon. (2019). *Installation manual models 3911/3911A resistance type rebar strain meters*. https://doi.org/www.geokon.com/content/manuals/3911-3911A_Rebar_Strain_Meter.pdf

Ghosn, M., Moses, F., & Gobieski, J. (1986). Evaluation of steel bridges using in-service testing. *Transportation Research Record*, *1072*, 71–78. https:onlinepubs.trb.org/Onlinepubs/trr/1986/1072/1072-010.pdf

Goodpasture, D. W., & Burdette, E. G. (1973). Comparison of bridge stress history results with design-related analyses. *Bridge Evaluation and Analysis*, No. 428, 51–56. https://onlinepubs.trb.org/Onlinepubs/hrr/1973/428/428-005.pdf

INDOT. (2019). *Indiana Department of Transportation 2019 strategic plan*. https://doi.org/www.in.gov/indot/files/INDOTStrategicPlan.pdf

INDOT. (2020). *Indiana Department of Transportation standard drawings: Section 700–Structures*. https://www.in.gov/dot/div/contracts/standards/drawings/sep20/e/sep700.htm

Kim, S., & Nowak, A. S. (1997, August). Load distribution and impact factors for I-girder bridges. *Journal of Bridge Engineering*, *2*(3), 97–104. https://doi.org/10.1061/(ASCE)1084-0702(1997)2:3(97)

Mabsout, M. E., Tarhini, K. M., Frederick, G. R., & Kobrosly, M. (1997, August). Influence of sidewalks and railings on wheel load distribution in steel girder bridges. *Journal of Bridge Engineering*, *2*(3), 88–96.

Maldonado, L. L., & Bowman, M. (2019). *Life-cycle cost analysis for short- and medium-span bridges* (Joint Transportation Research Program Publication No. FHWA/IN/JTRP-2019/09). West Lafayette, IN: Purdue University. https://doi.org/10.5703/1288284316919

Nowak, A. S., Eom, J., & Ferrand, D. (2003, May). *Verification of girder distribution factors for continuous steel girder bridges* (Research Report No. RC-1429). Michigan Department of Transportation Construction and Technology Division. https://www.michigan.gov/documents/mdot_c&t_rc-1429_71596_7.pdf

Rabbat, B. G., & Russell, H. G. (1985, March). Friction coefficient of steel on concrete or grout. *Journal of Structural Engineering*, *111*(3), 505–515. https://10.1061/(ASCE)0733-9445(1985)111:3(505)

Roddenberry, M. R., Chipperfield, J., & Tawfiq, K. S. (2011). Effect of secondary elements on load distribution in prestressed bridge girders. In D. Ames, T. L. Droessler, & M. Hoit (Eds.), *Proceedings of the 2011 Structures Congress* (pp. 215–226). https://doi.org/10.1061/41171(401)20

Ross, H. E., Jr., Sicking, D. L., Zimmer, R. A., & Michie, J. D. (1993). *Recommended procedures for the safety performance evaluation of highway features* (NCHRP Report 350). National Cooperative Highway Research Program. http://onlinepubs.trb.org/onlinepubs/nchrp/nchrp_rpt_350-a.pdf

Smith, K. N., & Mikelsteins, I. (1988, December). Load distribution in edge stiffened slab and slab-on-girder bridge decks. *Canadian Journal of Civil Engineering*, *15*(6), 977–983.

Stallings, J. M., & Yoo, C. H. (1993). Tests and ratings of short-span steel bridges. *Journal of Structural Engineering*, *119*(7), 2150–2168. https://doi.org/10.1061/(ASCE)0733-9445(1993)119:7(2150)

Wang, Y., & Thrall, A. P. (2019). *Assessment of bridges subjected to vehicular collision* (Joint Transportation Research Program Publication No. FHWA/IN/JTRP-2019/01). West Lafayette, IN: Purdue University. https://doi.org/10.5703/1288284316870

Wang, Y., Thrall, A. P., & Zoli, T. P. (2021, February). Behaviour of the Delaware River Bridge during repair. *Journal of Constructional Steel Research*, *177*, 106448. https://doi.org/10.1016/j.jcsr.2020.106448

Wang, Y., Tumbeva, M. D., Thrall, A. P., & Zoli, T. P. (2019, August) Pressure-activated adhesive tape pattern for monitoring the structural condition of steel bridges via digital image correlation. *Structural Control and Health Monitoring*, *26*(8), e2382.

Wood, S. M., Akinci, N. O., Liu, J., & Bowman, M. D. (2007). *Long-term effects of super heavy-weight vehicles on bridges* (Joint Transportation Research Program Final Report FHWA/IN/JTRP-2007/10). West Lafayette, IN: Purdue University. https://10.5703/1288284313355

APPENDICES

Appendix A. Recommendations for Evaluating the Reserve Strength of Girder Bridges Due to Rail Participation

Appendix B. Recommendations for Bridge Inspectors for Evaluating Steel Girder Bridges Subjected to Vehicular Damage

Appendix C. Supporting Data for Parametric Study

APPENDIX A. RECOMMENDATIONS FOR EVALUATING THE RESERVE STRENGTH OF GIRDER BRIDGES DUE TO RAIL PARTICIPATION

Steel and prestressed concrete multi-girder bridges are designed conservatively, resulting in reserve strength. One source of this reserve strength—which is not permitted to be considered when evaluating strength and extreme event limit states per current bridge design code (AASHTO, 2020)—is the participation of the rails in carrying load. In SPR-4119: *Assessment of Bridges Subjected to Vehicular Collision* (Wang & Thrall, 2019), it was found that loads are generally redistributed away from steel girders that have been damaged by vehicular collision, potentially to adjacent girders and/or the rail. These findings from SPR-4119 were the impetus for SPR-4311: *Evaluating Reserve Strength of Girder Bridges due to Bridge Rail Load Shedding* (Wang et al., 2021) which further evaluated the participation of bridge rail in carrying live load by monitoring the behavior of one steel girder bridge (two-span continuous) and one prestressed concrete girder bridge (six-span continuous), as well as a steel girder bridge damaged by vehicular collision (two-span continuous). These bridges were studies under static live load (i.e., two heavily loaded dump trucks) as well as crawl and speed tests. Research also included numerical finite element (FE) modeling.

The following recommendations can be used to evaluate two- or three-span continuous multi-girder composite steel or prestressed concrete bridges with intact reinforced concrete rail integral with the deck. Bridges with other rail types (e.g., metal rails) or other structural systems (e.g., girder floorbeam systems) are excluded from these recommendations and should be evaluated separately. These recommendations also do not apply in the circumstance where a rail has been damaged. The following recommendations should not be used for design. Research focused only on positive moment behavior (i.e., compression on the top of the section, tension on the bottom) and the following recommendations may be limited based on this.

1. Generally, bridge rails participate in carrying live load. However, they should not be relied upon to carry live load.
2. Based on good agreement between measured data and FE numerical predictions, the participation of bridge rails can be captured through FE models. As such, designers can use FE modeling to evaluate the reserve strength of girder bridges.
3. Specific numerical modeling recommendations for evaluating reserve strength include the following.
    a. Bridge components should be modeled using the following element types:
        i. Rail: Thick shell elements, with changing thickness based on the geometry.
        ii. Deck: Thick shell elements.
        iii. Girders: Frame elements representing the top and bottom flanges, thin shell elements representing the webs for steel girders, thick shell elements representing the webs for prestressed concrete girders.
    b. Composite behavior should be assumed between the rail and deck, as well as the deck and the top flange of the girders. This should be implemented by

constraining all translational and rotational degrees of freedom of the nodes between the components (i.e., nodes that share the same longitudinal coordinates).

4. For bridges where an exterior girder is subjected to Category T damage (i.e., torsion about the longitudinal direction (Avent, 2008)) from a vehicular collision, FE models that remove the composite behavior between the girder and the deck in the region of the damage (by removing the translational and rotational constraints between the top flange of the girder and the deck) can accurately capture behavior. The damaged profile of the girder should be considered.
5. If fully composite behavior between the rail, deck, and girder is achieved, the curvature in the positive moment region is reduced, meaning strains in the deck and girder are reduced, as compared to a comparable system where only the deck and girder are composite. The vertical height of the neutral axis in the positive moment region is increased (relative to the bottom flange), as compared to a comparable system where only the deck and girder are composite. All of the rail types that were numerically studied (i.e., Indiana Department of Transportation rail types FC, FT, PS-1 and PS-2 (INDOT, 2020)) contributed to this effect. The rail type that increased the moment of inertia of the composite section the most (i.e., FT) resulted in the greatest decrease in curvature, with decreasing benefit corresponding to decreasing moment of inertia of the composite section.
6. If bridge rail becomes damaged, inspectors should recommend repair or replacement of the rail. Replacement of bridge rail should be with the same rail type or a rail type with increased stiffness to preserve any reserve strength the rail provides.
7. Rail discontinuities above piers have negligible impact on the positive moment behavior of the exterior girders.
8. Bridge skew (up to 30 degrees) has negligible impact on the positive moment behavior of the exterior girders.

References for Appendix A

AASHTO. (2020). *AASHTO LRFD bridge design specifications* (9th edition). American Association of State Highway and Transportation Officials.

Avent, R. R. (2008, August). *Guide for heat-straightening of damaged steel bridge members* (Report No. FHWA-IF-08-999). Federal Highway Administration. https://www.fhwa.dot.gov/bridge/steel/heat_guide.pdf

INDOT. (2020). *Indiana Department of Transportation standard drawings: Section 700 – Structures*. https://www.in.gov/dot/div/contracts/standards/drawings/sep20/e/sep700.htm

Wang, Y., Tumbeva, M. D., & Thrall, A. P. (2021). *Evaluating reserve strength of girder bridges due to bridge rail load shedding* (Joint Transportation Research Program Publication No. TBD). West Lafayette, IN: Purdue University.

Wang, Y., & Thrall, A. P. (2019). *Assessment of bridges subjected to vehicular collision* (Joint Transportation Research Program Publication No. FHWA/IN/JTRP-2019/01). West Lafayette, IN: Purdue University. https://doi.org/10.5703/1288284316870

APPENDIX B. RECOMMENDATIONS FOR BRIDGE INSPECTORS FOR EVALUATING STEEL GIRDER BRIDGES SUBJECTED TO VEHICULAR DAMAGE

In SPR-4119: *Assessment of Bridges Subjected to Vehicular Collision* (Wang & Thrall, 2019), the behavior of four steel girder bridges (one three-span continuous, three two-span continuous) for which an exterior girder has sustained Category T damage (i.e., torsion about the longitudinal direction, as shown for example in Figure B.1 and defined in Figure B.2 (Avent, 2008)) from a vehicular collision were monitored under static live load (i.e., two heavily loaded dump trucks). In SPR-4311: *Evaluating Reserve Strength of Girder Bridges Due to Bridge Rail Load Shedding* (Wang et al., 2021), the behavior of one of the damaged bridges studied in SPR-4119 was monitored, as well as the behavior of one undamaged steel girder bridge (two-span continuous) and one undamaged prestressed concrete girder bridge (six-span continuous). These bridges were studies under static live load (i.e., two heavily loaded dump trucks) as well as crawl and speed tests. Both research studies also include numerical finite element (FE) modeling.

Based on both research projects, bridge inspectors can use the following recommendations to evaluate two- or three-span continuous multi-girder steel bridges for which an exterior girder has sustained Category T damage from a vehicular collision. Other categories of damage (e.g., highly localized damage or cracking) and other structural systems (e.g., girder floorbeam systems) are excluded from these recommendations and should be evaluated separately. These recommendations are limited to bridges with intact reinforced concrete rail integral with the deck. Bridges with other rail types (e.g., metal rails) are excluded from these recommendations and should be evaluated separately. These recommendations also do not apply in the circumstance where a rail has been damaged. Research focused primarily on positive moment behavior (i.e., compression on the top of the section, tension on the bottom) and the following recommendations may be limited based on this.

1. Bridges should always be inspected after a vehicular collision.
2. Live load should always be redirected away from girders with Category T damage (e.g., lane or shoulder closures).
3. Generally, bridge rails participate in carrying live load and can provide a clear benefit to the behavior of steel girder bridges for which an exterior girder has been damaged. However, they should not be relied upon to carry live load.
4. Bridges with open rails, severely cracked or damaged rails, rails with discontinuities in the damaged region, and/or less redundancy (related to number or spacing of girders) require more detailed evaluation.
5. During inspection of composite bridges, special attention should be paid to the shear connection between the girder and deck as this can be damaged during collision and result in higher live load strains in the steel girders.
6. Category T damage in the center of a span with a large angle of deflection of the web, results in the most severe loss of stiffness. Bridges with this type of damage should be prioritized for repair.

7. Girders adjacent to damaged girders may carry live load that is being redistributed away from the damaged girder. While the expected strain in these adjacent girders is still small, they should be inspected.
8. Inspectors should take into account prior heat straightening of damaged girders and its effect on the material properties of the steel when evaluating a girder.
9. Live load amplification factors may be higher when a girder is damaged. Inspectors should take this into consideration.
10. When inspecting a damaged girder, inspectors should measure the peak web rotation angle, α, the location of the start of the damage along the span, D, the length of the damage, l_s, and the relative location of the peak point of damage, x (Figure B.3). These measurements would facilitate deeper evaluation through numerical analysis.

These recommendations are based on measured data and numerical FE model predictions from SPR-4119 and SPR-4311. These recommendations may be limited to the specific bridges monitored in this study.

Figure B.1 Examples of Category T damage (reprinted from Wang & Thrall, 2019).

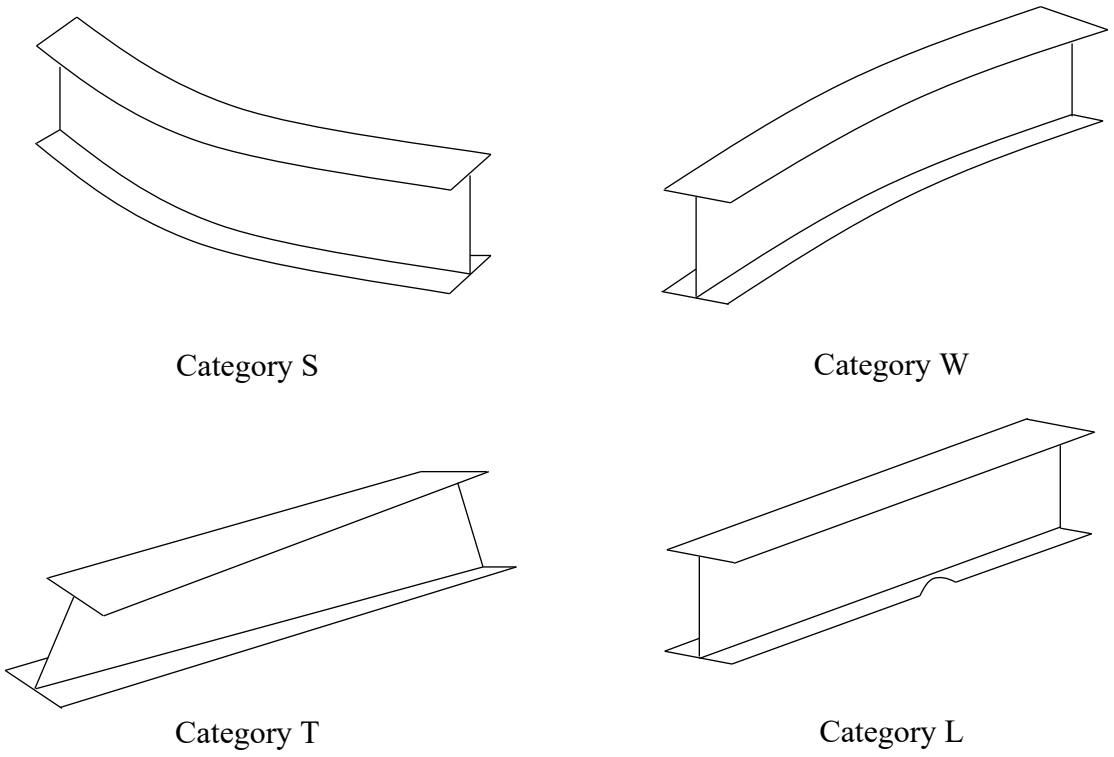

Figure B.2 Categories of damage (adapted from Avent, 2008 and reprinted from Wang & Thrall, 2019), where Category S refers to strong axis bending, Category W refers to weak axis bending, Category T refers to torsion about the longitudinal axis, and Category L refers to local damage (shown for example for a flange deformation).

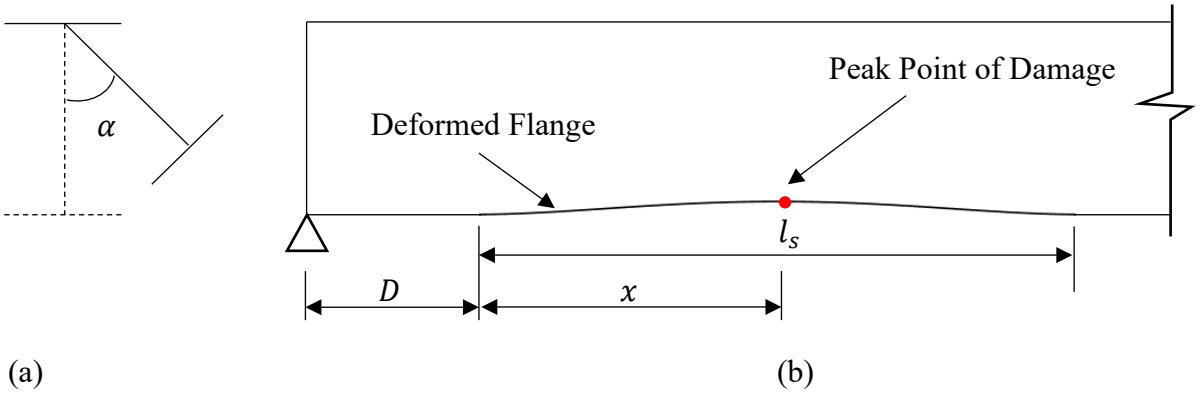

Figure B.3 Category T damage profile in (a) cross-section and (b) elevation (reprinted from Wang & Thrall, 2019).

References for Appendix B

Avent, R. R. (2008, August). *Guide for heat-straightening of damaged steel bridge members* (Report No. FHWA-IF-08-999). Federal Highway Administration. https://www.fhwa.dot.gov/bridge/steel/heat_guide.pdf

Wang, Y., Tumbeva, M. D., & Thrall, A. P. (2021). *Evaluating reserve strength of girder bridges due to bridge rail load shedding* (Joint Transportation Research Program Publication No. TBD). West Lafayette, IN: Purdue University.

Wang, Y., & Thrall, A. P. (2019). *Assessment of bridges subjected to vehicular collision* (Joint Transportation Research Program Publication No. FHWA/IN/JTRP-2019/01). West Lafayette, IN: Purdue University. https://doi.org/10.5703/1288284316870

APPENDIX C. SUPPORTING DATA FOR PARAMETRIC STUDY

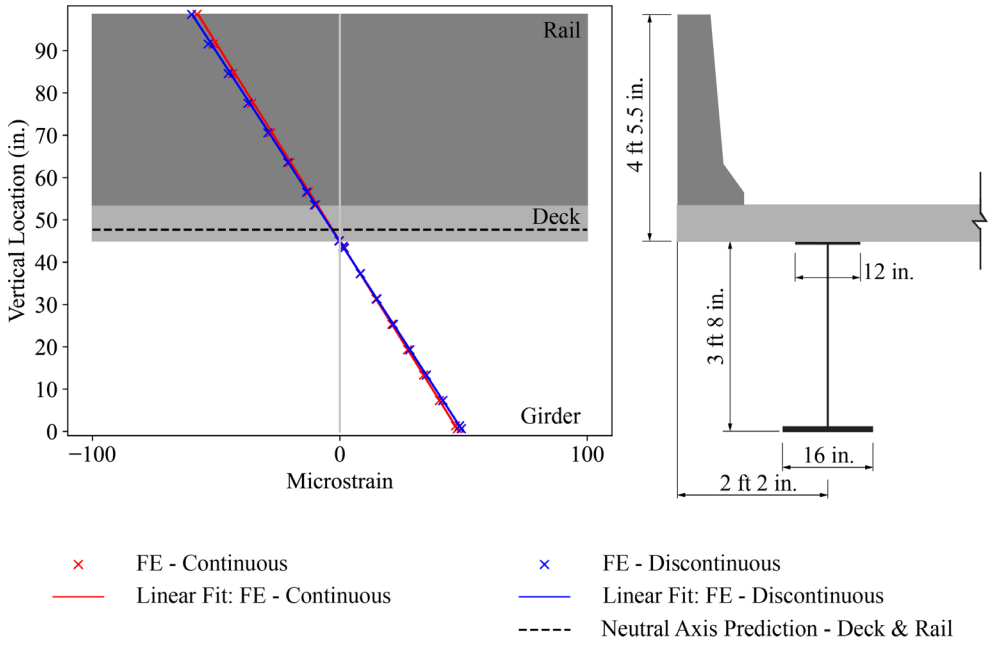

Figure C.1 Effect of rail discontinuity for two-span continuous steel girder bridge with FT rail: FE predictions for strains at peak positive moment location. Cross-section shows the FT rail as an example.

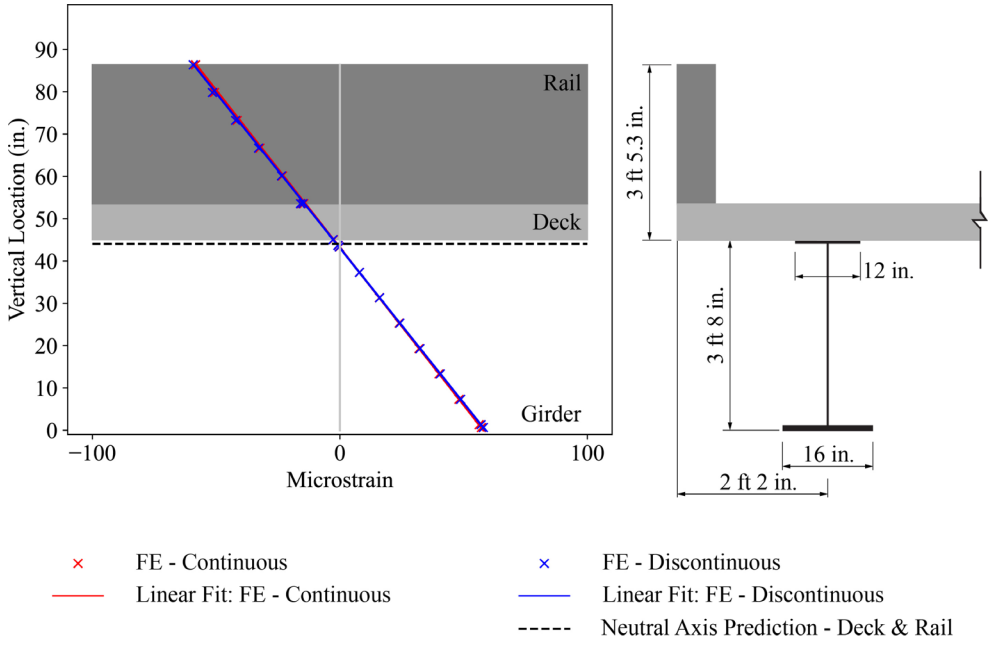

Figure C.2 Effect of rail discontinuity for two-span continuous steel girder bridge with PS-1 rail: FE predictions for strains at peak positive moment location.

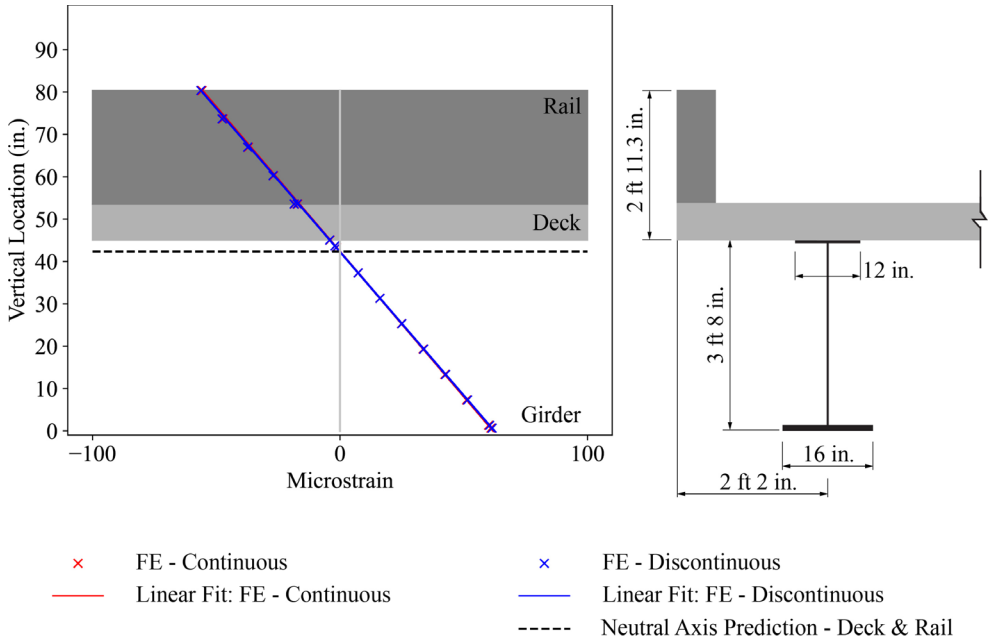

Figure C.3 Effect of rail discontinuity for two-span continuous steel girder bridge with PS-2 rail: FE predictions for strains at peak positive moment location.

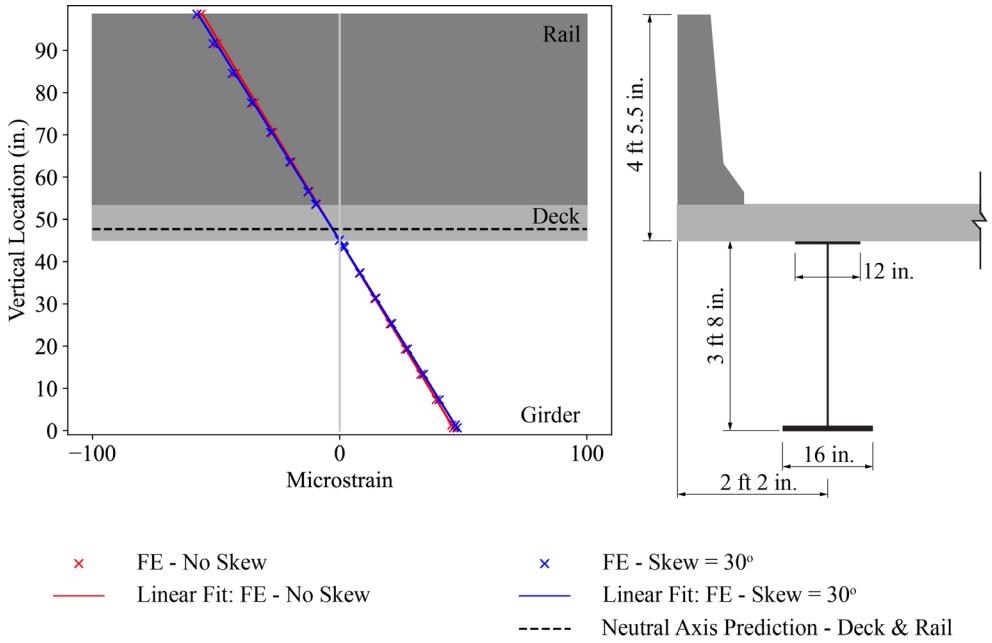

Figure C.4 Effect of 30-degree skew angle for two-span continuous steel girder bridge with FT rail: FE predictions for strains at peak positive moment location.

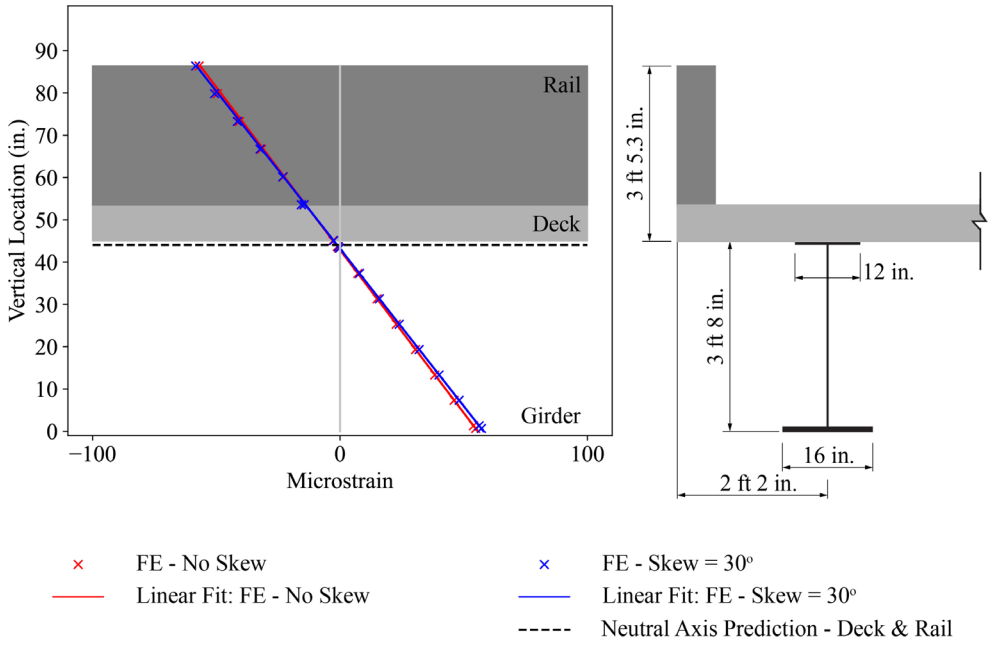

Figure C.5 Effect of 30-degree skew angle for two-span continuous steel girder bridge with PS-1 rail: FE predictions for strains at peak positive moment location.

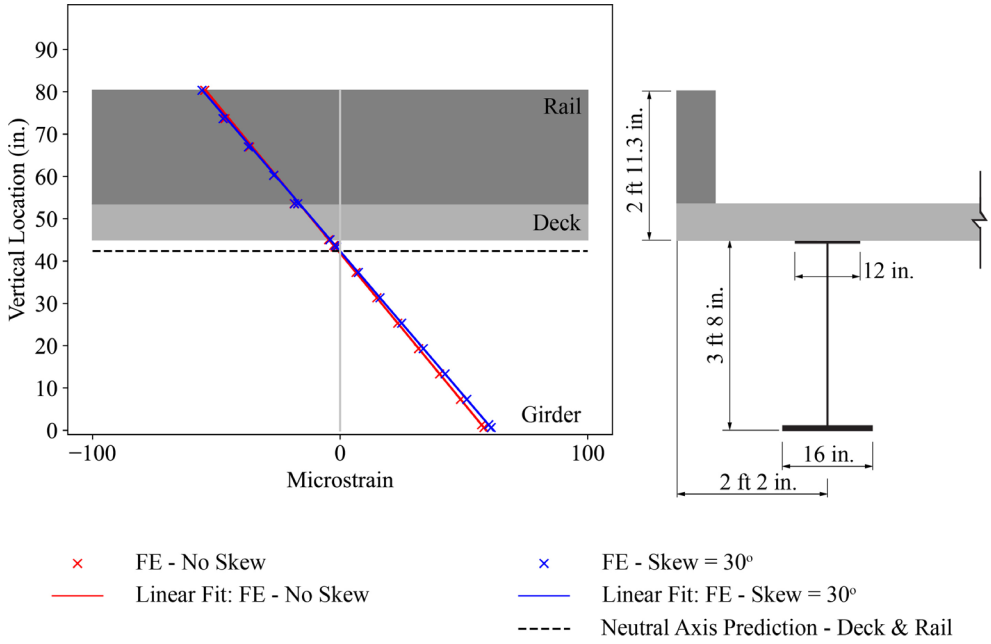

Figure C.6 Effect of 30-degree skew angle for two-span continuous steel girder bridge with PS-2 rail: FE predictions for strains at peak positive moment location.

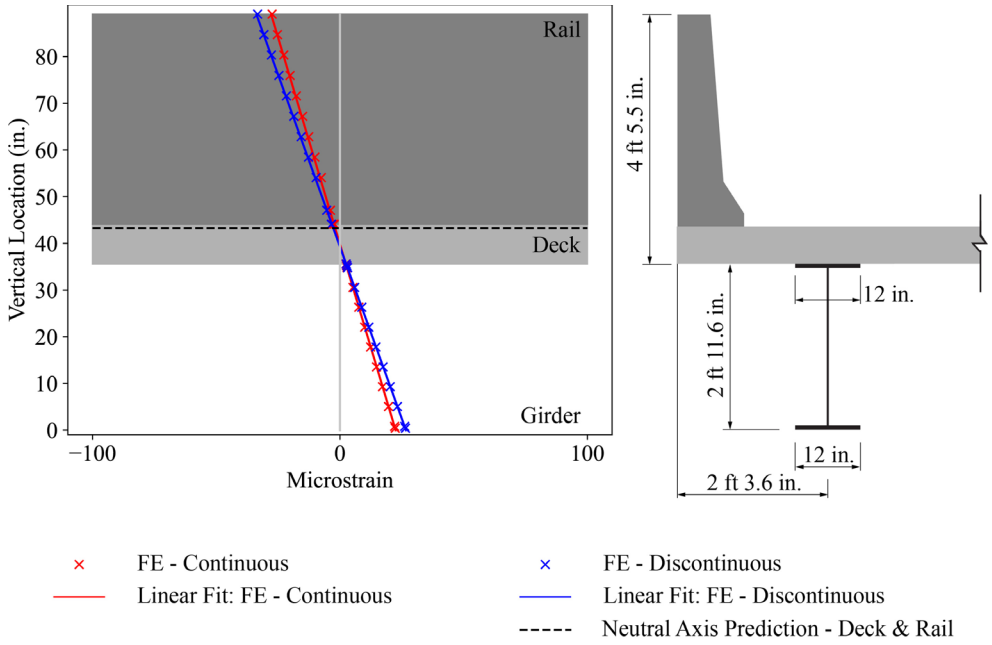

Figure C.7 Effect of rail discontinuity for three-span continuous steel girder bridge with FT rail: FE predictions for strains at peak positive moment location.

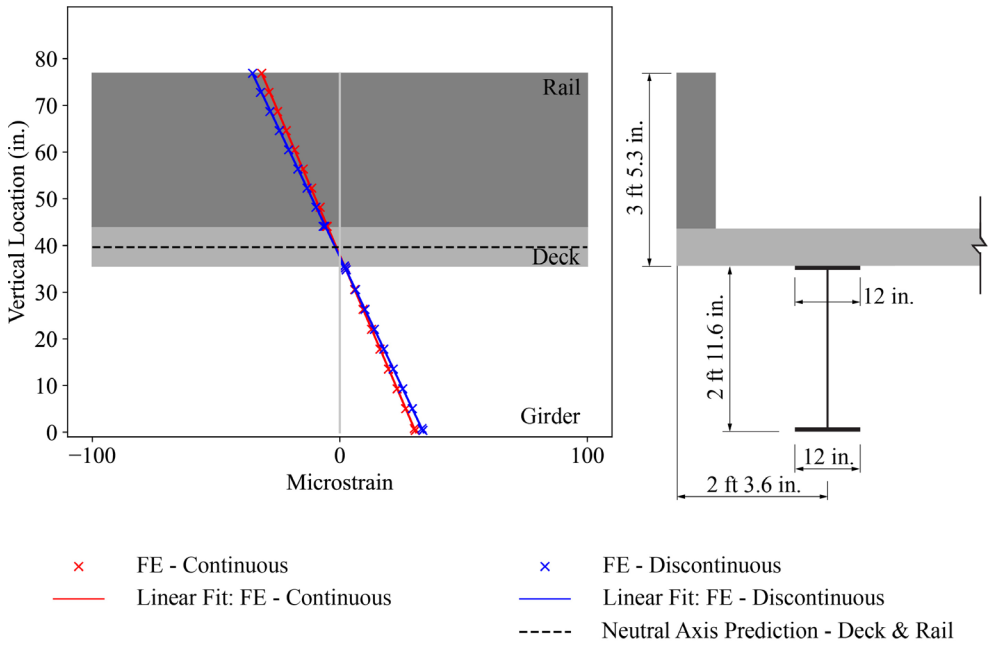

Figure C.8 Effect of rail discontinuity for three-span continuous steel girder bridge with PS-1 rail: FE predictions for strains at peak positive moment location.

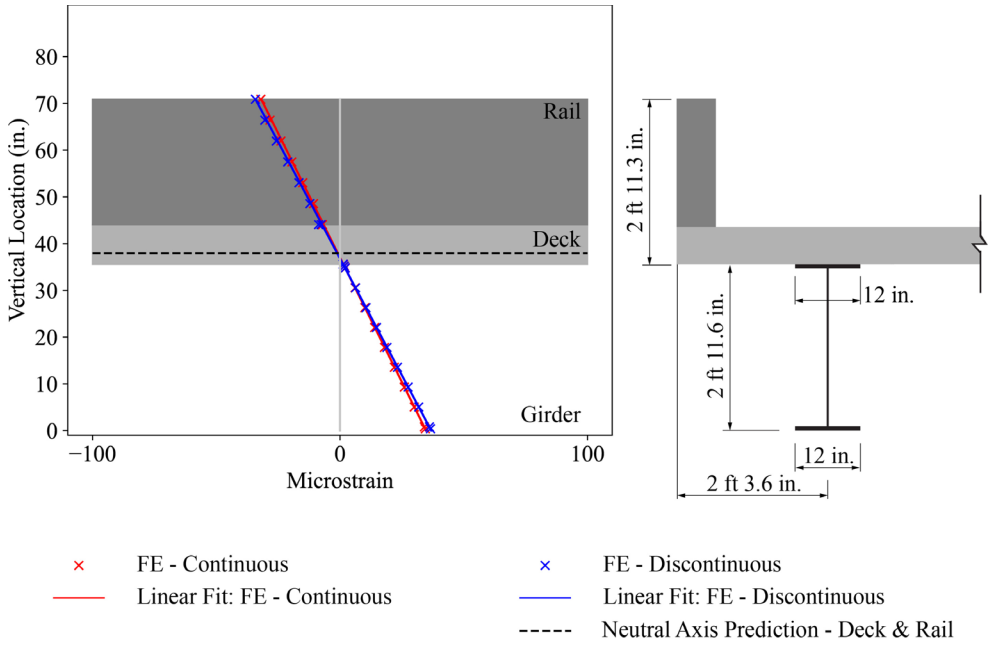

Figure C.9 Effect of rail discontinuity for three-span continuous steel girder bridge with PS-2 rail: FE predictions for strains at peak positive moment location.

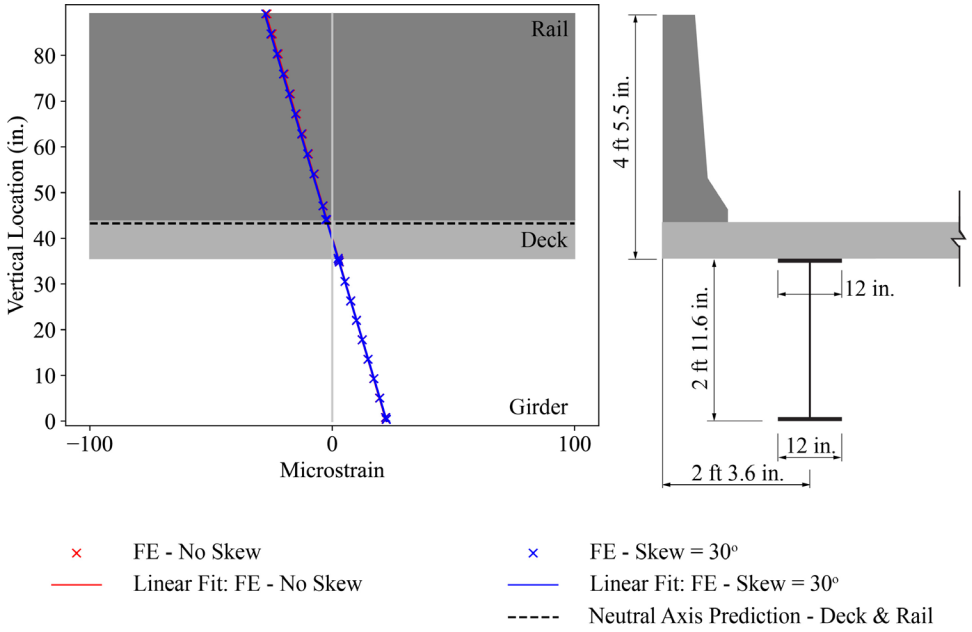

Figure C.10 Effect of 30-degree skew angle for three-span continuous steel girder bridge with FT rail: FE predictions for strains at peak positive moment location.

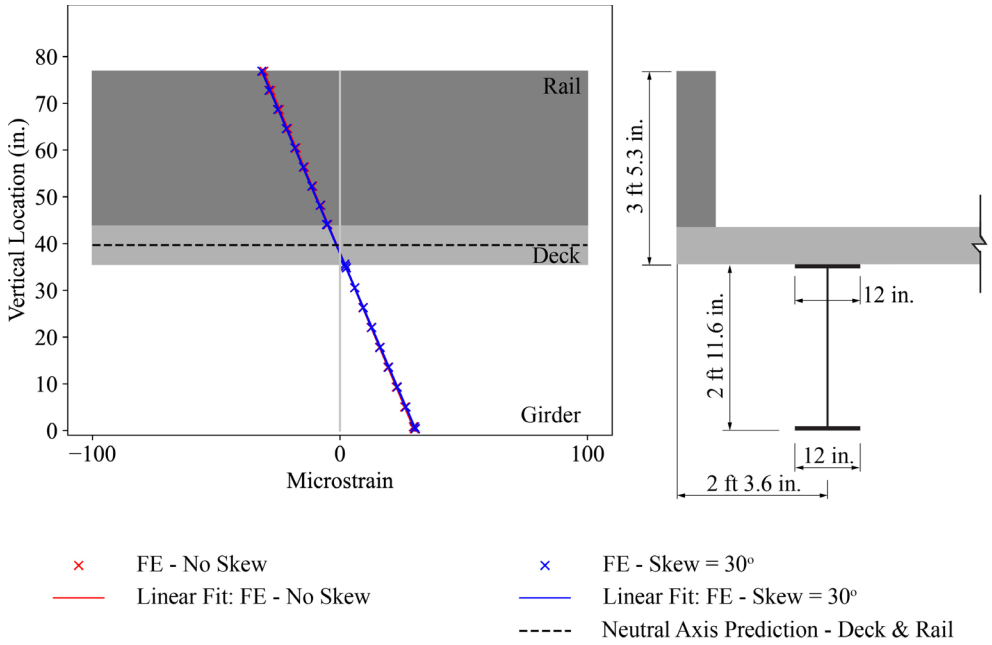

Figure C.11 Effect of 30-degree skew angle for three-span continuous steel girder bridge with PS-1 rail: FE predictions for strains at peak positive moment location.

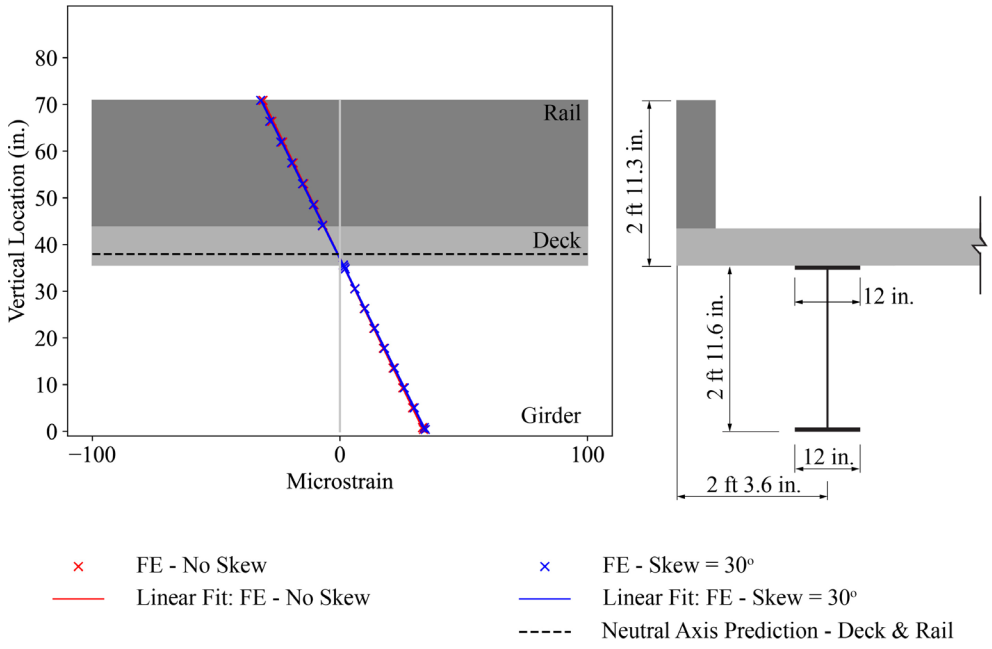

Figure C.12 Effect of 30-degree skew angle for three-span continuous steel girder bridge with PS-2 rail: FE predictions for strains at peak positive moment location.

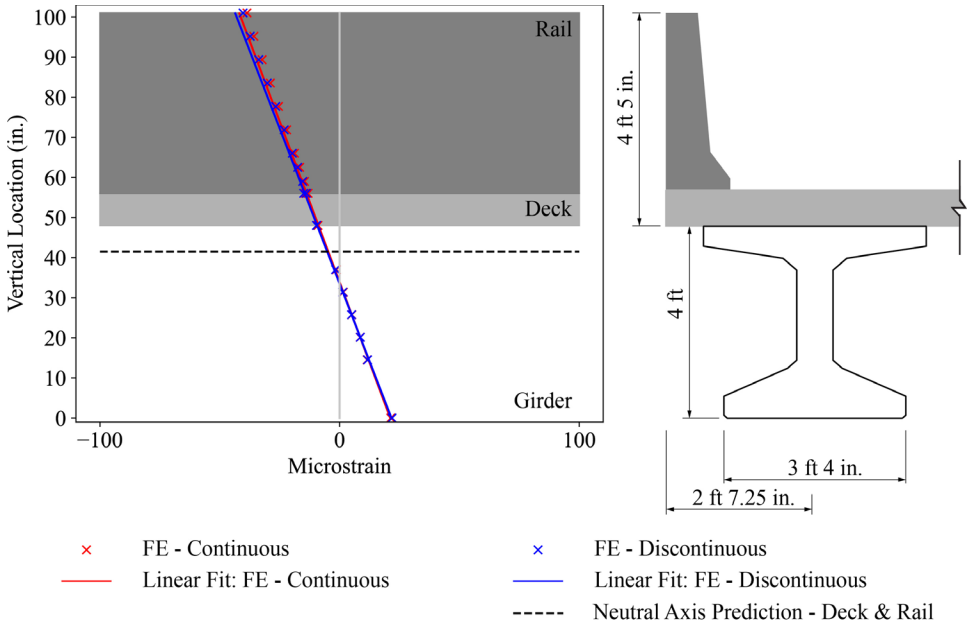

Figure C.13 Effect of rail discontinuity for two-span continuous prestressed concrete girder bridge with FT rail: FE predictions for strains at peak positive moment location.

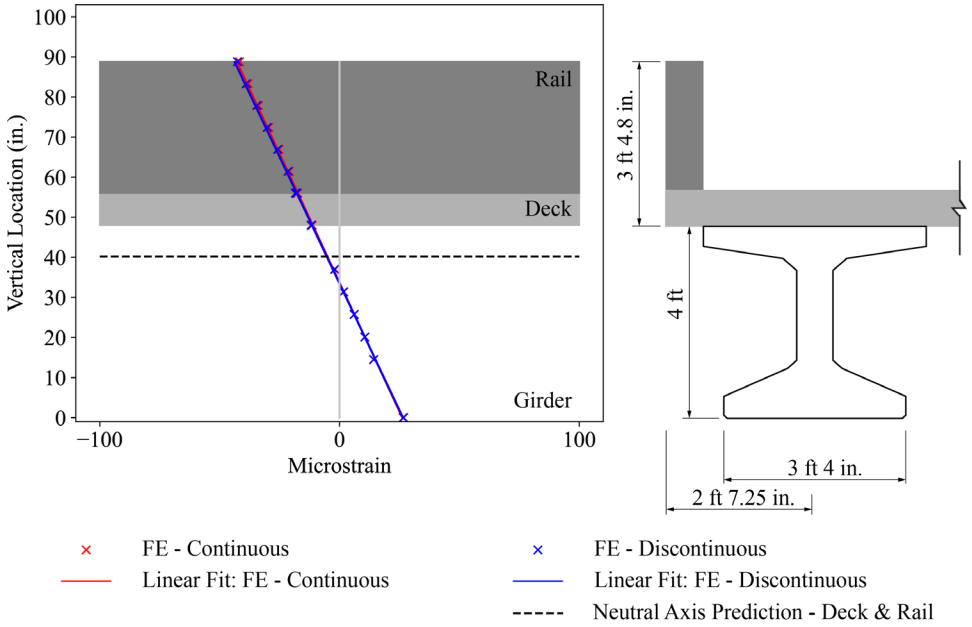

Figure C.14 Effect of rail discontinuity for two-span continuous prestressed concrete girder bridge with PS-1 rail: FE predictions for strains at peak positive moment location.

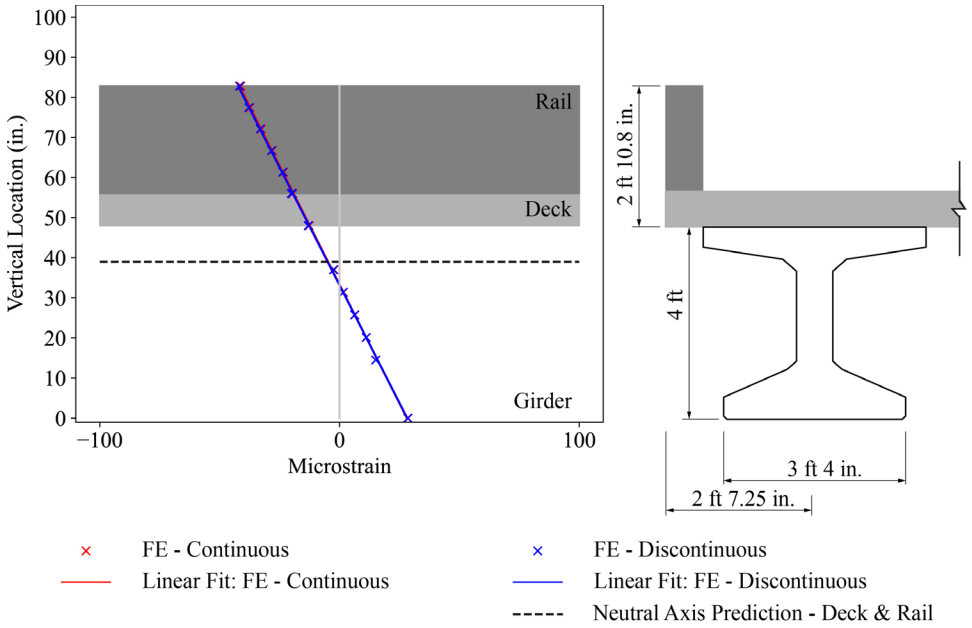

Figure C.15 Effect of rail discontinuity for two-span continuous prestressed concrete girder bridge with PS-2 rail: FE predictions for strains at peak positive moment location.

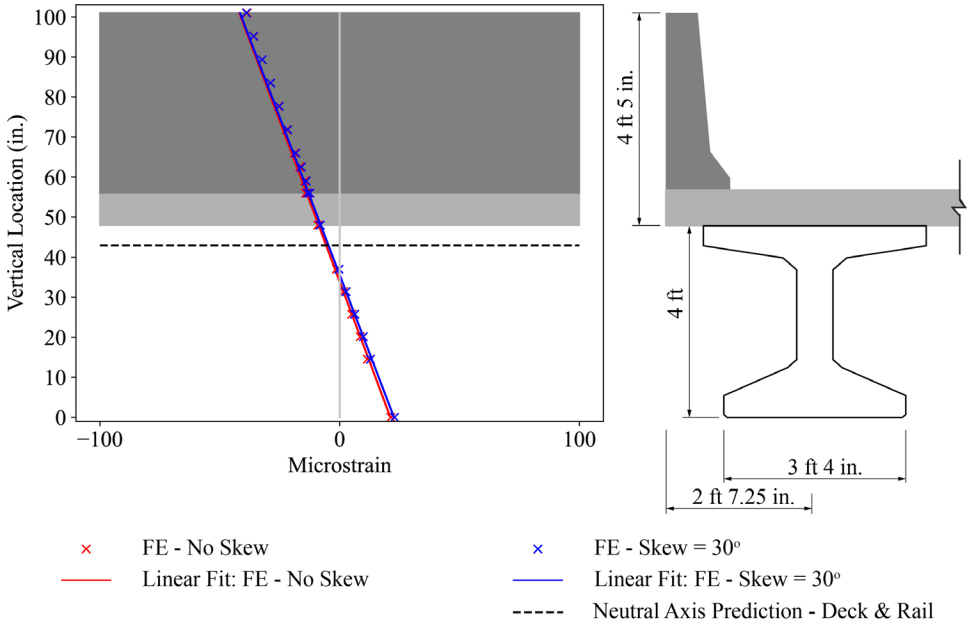

Figure C.16 Effect of 30-degree skew angle for two-span continuous prestressed concrete girder bridge with FT rail: FE predictions for strains at peak positive moment location.

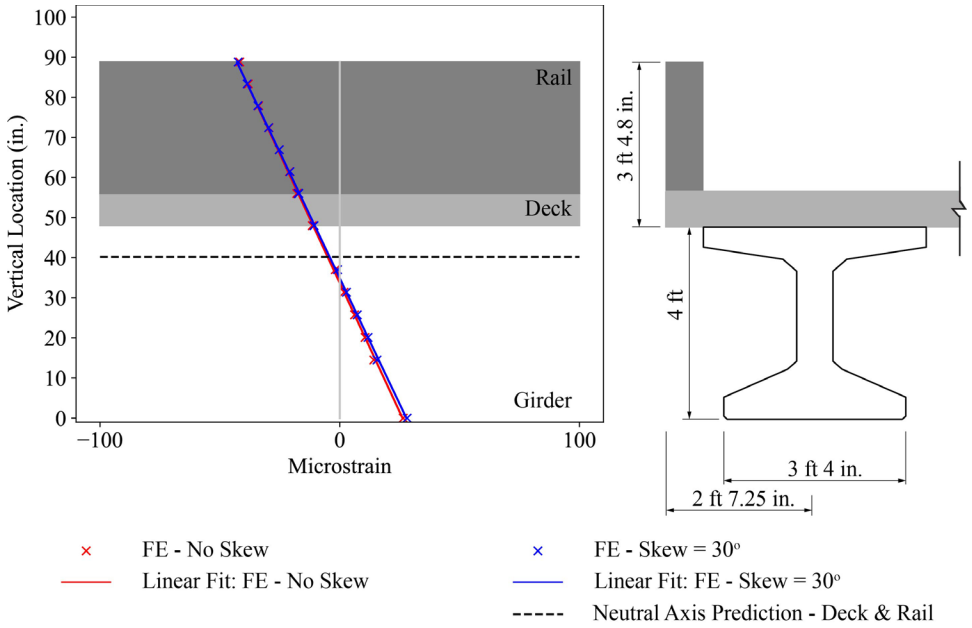

Figure C.17 Effect of 30-degree skew angle for two-span continuous prestressed concrete girder bridge with PS-1 rail: FE predictions for strains at peak positive moment location.

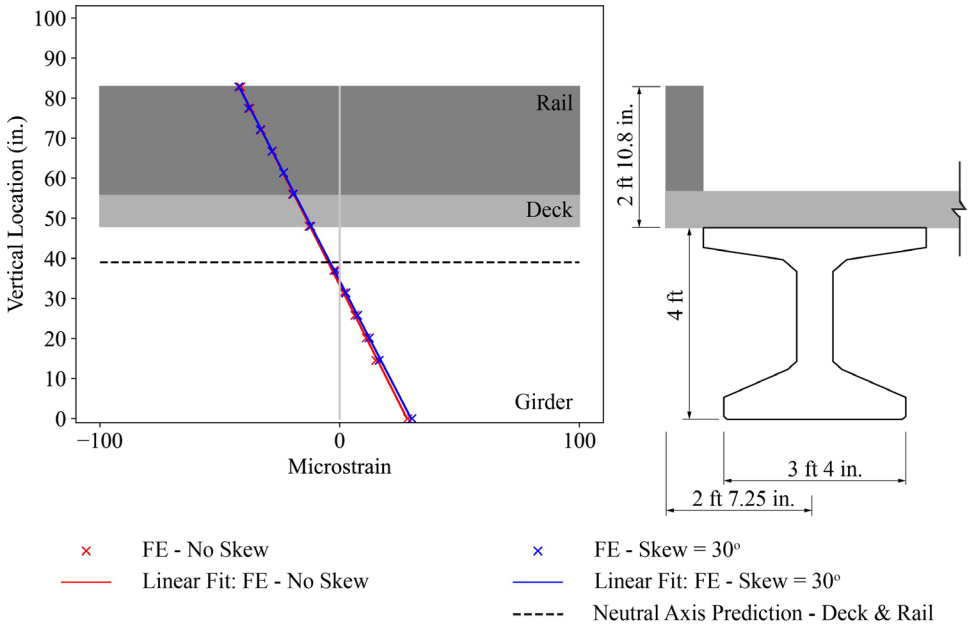

Figure C.18 Effect of 30-degree skew angle for two-span continuous prestressed concrete girder bridge with PS-2 rail: FE predictions for strains at peak positive moment location.

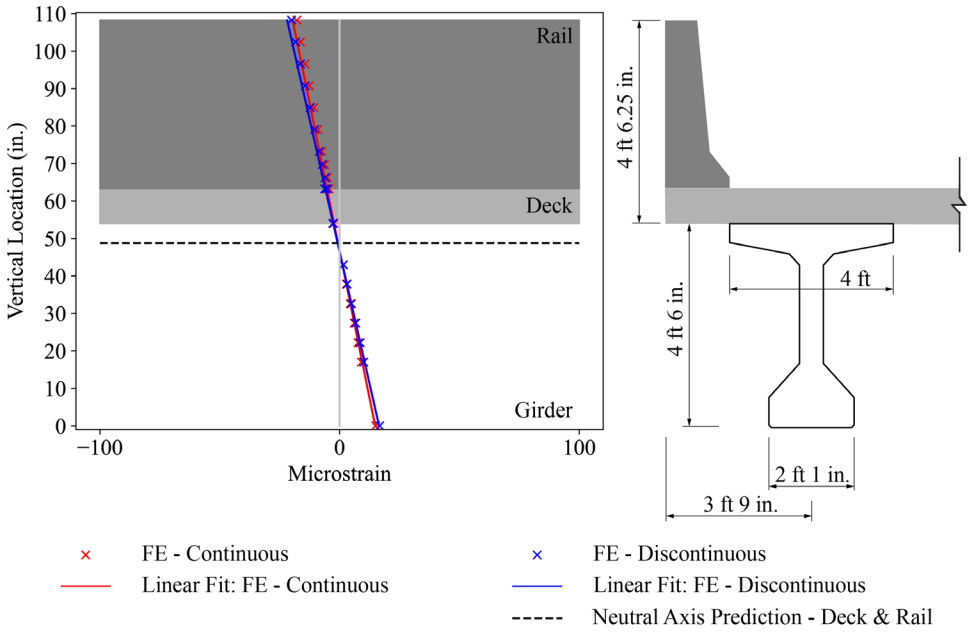

Figure C.19 Effect of rail discontinuity for three-span continuous prestressed concrete girder bridge with FT rail: FE predictions for strains at peak positive moment location.

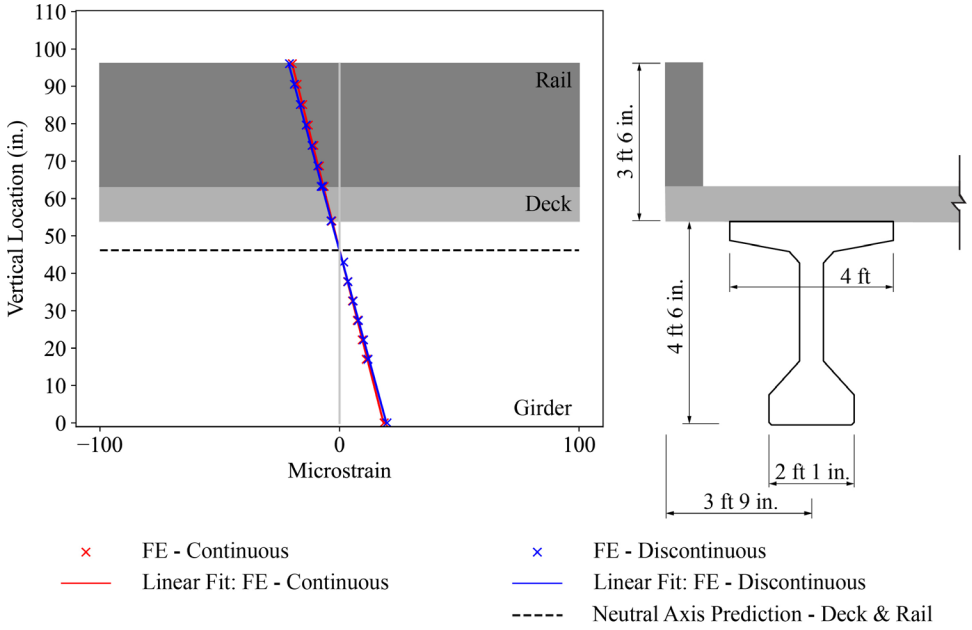

Figure C.20 Effect of rail discontinuity for three-span continuous prestressed concrete girder bridge with PS-1 rail: FE predictions for strains at peak positive moment location.

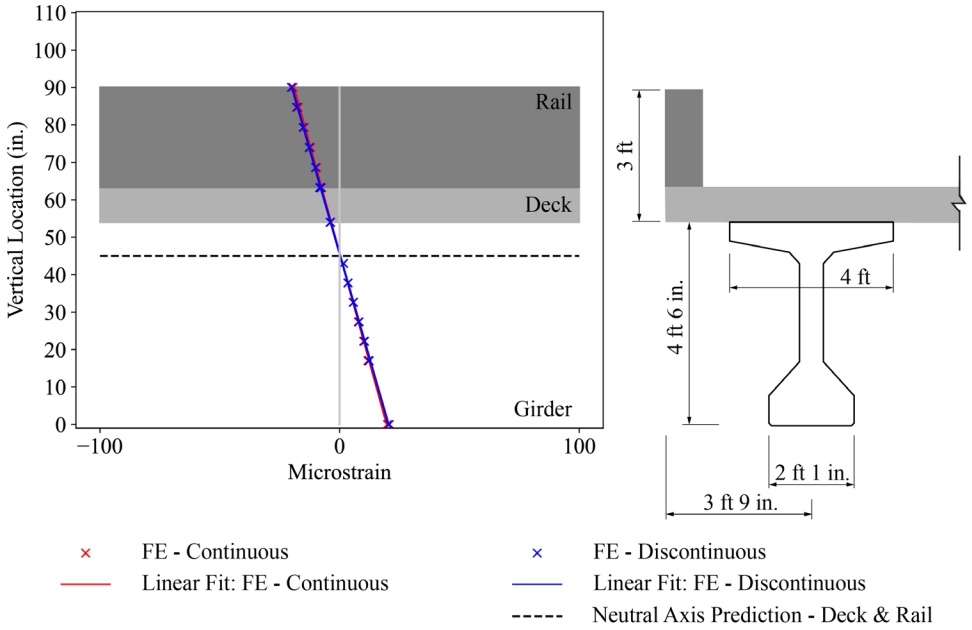

Figure C.21 Effect of rail discontinuity for three-span continuous prestressed concrete girder bridge with PS-2 rail: FE predictions for strains at peak positive moment location.

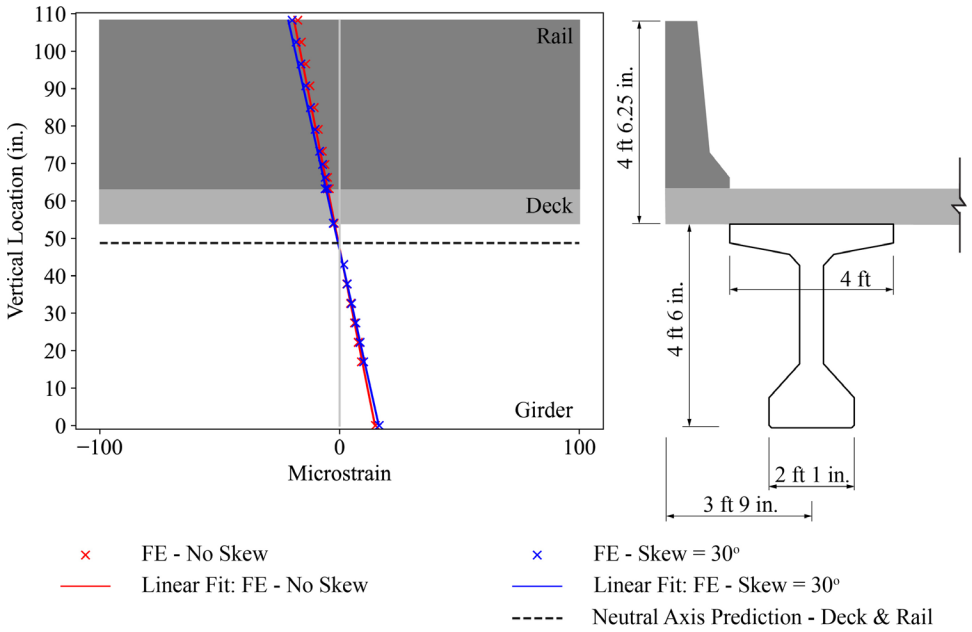

Figure C.22 Effect of 30-degree skew angle for three-span continuous prestressed concrete girder bridge with FT rail: FE predictions for strains at peak positive moment location.

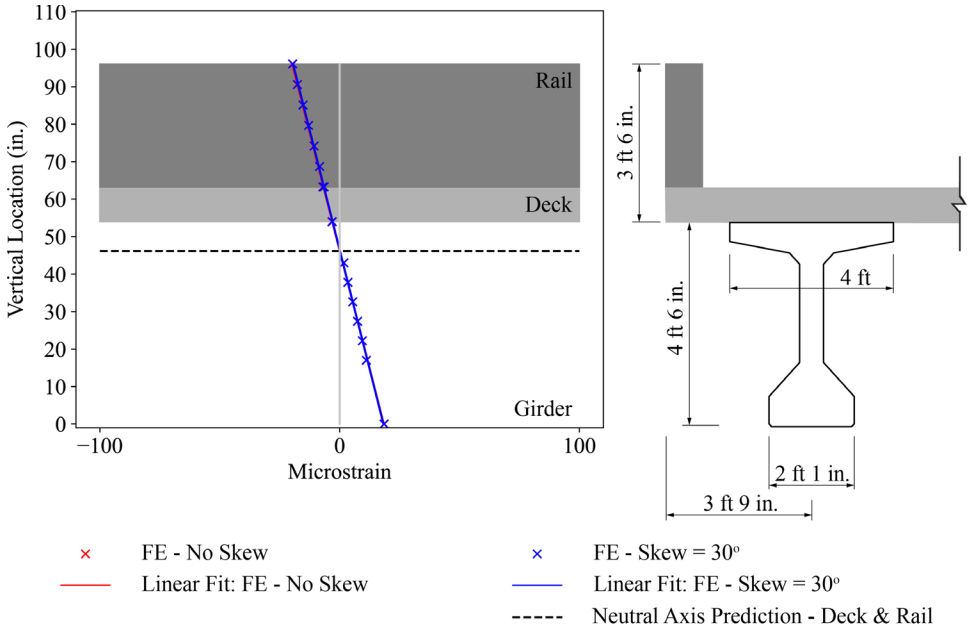

Figure C.23 Effect of 30-degree skew angle for three-span continuous prestressed concrete girder bridge with PS-1 rail: FE predictions for strains at peak positive moment location.

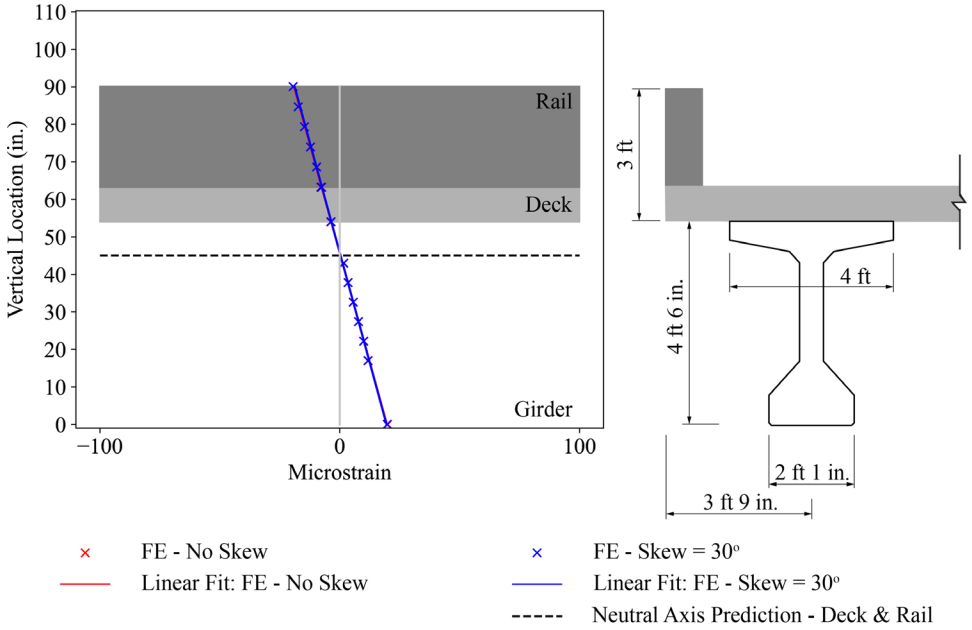

Figure C.24 Effect of 30-degree skew angle for three-span continuous prestressed concrete girder bridge with PS-1 rail: FE predictions for strains at peak positive moment location.

About the Joint Transportation Research Program (JTRP)

On March 11, 1937, the Indiana Legislature passed an act which authorized the Indiana State Highway Commission to cooperate with and assist Purdue University in developing the best methods of improving and maintaining the highways of the state and the respective counties thereof. That collaborative effort was called the Joint Highway Research Project (JHRP). In 1997 the collaborative venture was renamed as the Joint Transportation Research Program (JTRP) to reflect the state and national efforts to integrate the management and operation of various transportation modes.

The first studies of JHRP were concerned with Test Road No. 1—evaluation of the weathering characteristics of stabilized materials. After World War II, the JHRP program grew substantially and was regularly producing technical reports. Over 1,600 technical reports are now available, published as part of the JHRP and subsequently JTRP collaborative venture between Purdue University and what is now the Indiana Department of Transportation.

Free online access to all reports is provided through a unique collaboration between JTRP and Purdue Libraries. These are available at http://docs.lib.purdue.edu/jtrp.

Further information about JTRP and its current research program is available at http://www.purdue.edu/jtrp.

About This Report

An open access version of this publication is available online. See the URL in the citation below.

Wang, Y., Tumbeva, M. D., & Thrall, A. P. (2021). *Evaluating reserve strength of girder bridges due to bridge rail load shedding* (Joint Transportation Research Program Publication No. FHWA/IN/JTRP-2021/08). West Lafayette, IN: Purdue University. https://doi.org/10.5703/1288284317308